TEPHROCHRONOLOGY AND STRATIGRAPHY OF EOCENE AND OLIGOCENE VOLCANIC ASHES OF EAST AND CENTRAL TEXAS

A Thesis

by

MINDI HEINTZ

Submitted to the Office of Graduate Studies and Professional Studies of
Texas A&M University
in partial fulfillment of the requirements for the degree of

MASTER OF SCIENCE

Chair of Committee,	Thomas E. Yancey
Co-Chair of Committee,	Brent V. Miller
Committee Member	Deborah J. Thomas
Head of Department,	John R. Giardino

December 2013

Major Subject: Geology

ABSTRACT

Sedimentary formations of east and central Texas contain many Eocene to Oligocene volcanic ash beds, with some of the younger ash layers containing hydrated but otherwise unaltered glass shards. This study analyzed samples of 15 volcanic ash beds using neutron activation analysis (NAA) of bulk ash and glass shards, inductively coupled plasma mass spectrometry (ICPMS) of bulk ash, and electron microprobe analysis of both apatite phenocrysts and glass shards to characterize their geochemistry.

$^{40}Ar/^{39}Ar$ dating of single sanidine phenocrysts gives an age of 30.64 ±0.03 Ma for the youngest (Sam Rayburn) sample to 41.79 ±0.02 Ma for the oldest (Hurricane Bayou) sample. The nine radiometric dates obtained by this study serve to better constrain the ages of the Claiborne and Jackson Groups and the Catahoula Formation of Texas with the Conquista and Hurricane Bayou ash beds being possible calibration points for the Eocene/Oligocene and Lutetian/Bartonian boundaries, respectively.

Geochemical fingerprinting, particularly apatite phenocryst chemistry, supports the correlation of the Little Brazos volcanic ash in Brazos County to volcanic ash deposits in Houston County, Texas, and provides supporting evidence for equivalence to the St. Johns bentonite in Louisiana. Geochemical fingerprinting also suggests equivalence of the Caddell (Koppe Bridge) volcanic ash to deposits within the Gonzales County bentonite mines of south-central Texas.

Major element electron microprobe data from seven samples of volcanic glass shards indicate the ash was produced from sub-alkaline rhyolitic volcanism and the

trace-element characteristics of all 15 ashes are consistent with subduction-related sources. Rare earth element (REE) data indicates light rare earth element (LREE) enrichment with a moderate Europium anomaly. The Sierra Madre Occidental of Mexico is the likely source area, but the Trans-Pecos of Texas and Mogollon-Datil of New Mexico cannot be definitively ruled out as possible eruptive source regions.

DEDICATION

I would like to dedicate this work to my loving husband, Colby Kreft, who put up with geologic journal papers being scattered all over the house for two years and to my family and friends for being so supportive.

ACKNOWLEDGEMENTS

I would like to thank my committee chair, Dr. Yancey, and my committee co-chair, Dr. Miller, and member, Dr. Thomas for their guidance and support throughout the course of this research. Dr. Yancey's vision of the project and Devon Energy's funding for graduate student support are what made this research and my master's degree possible. I would also like to thank Dr. Guillemette for his expertise on the electron microprobe that made my apatite analysis a success. Thanks also go to my friends and colleagues and the department faculty and staff for making my time at Texas A&M University a great experience. I would also like to acknowledge all the geologists that have helped me along the way, especially, Dr. Christopher Baldwin, Dr. Brian Cooper and Dr. David James. Finally, thanks to my mother and father for their encouragement and to my husband for his patience and support.

TABLE OF CONTENTS

Page

ABSTRACT ii

DEDICATION iv

ACKNOWLEDGEMENTS v

TABLE OF CONTENTS vi

LIST OF FIGURES viii

LIST OF TABLES x

INTRODUCTION 1

PALEOGENE VOLCANIC ASH DEPOSITS OF EAST AND CENTRAL TEXAS 7

METHODS 14

$^{40}Ar/^{39}Ar$ Dating 14
Neutron Activation Analysis (NAA) 15
Electron Microprobe Analysis of Volcanic Glass Shards 15
Electron Microprobe Analysis of Apatite Phenocrysts 16
Inductively Coupled Plasma Mass Spectrometry (ICPMS) Analysis 17

RESULTS 19

Elemental Chemistry of Volcanic Ash Deposits 19
Bulk Volcanic Ash Chemistry 19
Volcanic Glass Shard Chemistry 29
Apatite Phenocryst Chemistry 37
$^{40}Ar/^{39}Ar$ Dating 39

DISCUSSION 42

$^{40}Ar/^{39}Ar$ Dating 42
Correlation of Volcanic Ash Beds 43
Patterns of Volcanic Ash Alteration 51
Possible Source of Volcanic Ash 56

Page

CONCLUSIONS 60

REFERENCES 62

APPENDIX A 70

LIST OF FIGURES

Page

Figure 1. Location of volcanic ash samples 2

Figure 2. Stratigraphy for the study location showing the position of the volcanic ash beds studied in this report 3

Figure 3. Silicic volcanism trend running from Mexico into the western United States that makes up the Sierra Madre Occidental, Trans-Pecos Volcanic Province and Mogollon-Datil Volcanic Field 5

Figure 4. Examples of volcanic ash deposits 8

Figure 5. TAS diagram showing $Na_2O + K_2O$ versus SiO_2 data from the ICPMS bulk volcanic ash analysis 24

Figure 6. Trace element data from ICPMS analysis of bulk volcanic ash samples 25

Figure 7. REE data from ICPMS analysis of bulk volcanic ash 26

Figure 8. Plot of La/Yb versus Yb showing the measure of the degree of REE fractionation with changing REE content in bulk volcanic ash data from ICPMS analysis 27

Figure 9. Plot of La/Sm versus Sm showing the degree of LREE fractionation with changing REE content in bulk volcanic ash from ICPMS analysis 28

Figure 10. BSE images showing the South Somerville, Conquista and Tarball Quarry volcanic glass separates 30

Figure 11. Alkali data plotted versus total wt % for the South Somerville and Tarball Quarry individual glass shard analyses 31

Figure 12. TAS diagram showing $Na_2O + K_2O$ versus SiO_2 data from the seven glass bearing volcanic ashes 33

Figure 13. Trace element data from NAA of volcanic glass shards 35

Figure 14. REE data from NAA of volcanic glass shards 36

Page

Figure 15. Plot of Mg versus Mn versus Cl from individual apatite microprobe analysis 38

Figure 16. Summary of age probability data presented in stratigraphic order from youngest to oldest 41

Figure 17. REE data from ICPMS analysis of the South Somerville volcanic ash in Brazos County and Plum volcanic ash in Fayette County 44

Figure 18. REE data from ICPMS analysis of the Koppe Bridge volcanic ash sample in Brazos County in comparison with the McBA (R5) volcanic ash sample from Gonzales County 45

Figure 19. Trace element data from ICPMS analysis of bulk volcanic ash 47

Figure 20. REE data from ICPMS analysis of bulk volcanic ash 47

Figure 21. Plot of Fe versus Mg versus Mn from individual apatite microprobe analysis 48

Figure 22. Plot of Ce versus Y from microprobe analysis of individual apatite phenocrysts 49

Figure 23. Comparison of ICPMS bulk volcanic ash data of Crockett and Cook Mountain Formation (JGIC) ash beds 50

Figure 24. Total Alkali versus Silica diagram showing $Na_2O + K_2O$ versus SiO_2 in wt % 53

Figure 25. Relative enrichment or depletion of selected elements from NAA in bulk volcanic ash compared to volcanic glass shard data 55

Figure 26. A/CNK-A/NK plot showing $Al_2O_3/CaO+Na_2O+K_2O$ versus Al_2O_3/Na_2O+K_2O 58

LIST OF TABLES

Page

Table 1. Characteristics of volcanic ash samples included in this study.....9

Table 2. Standards used in apatite microprobe analysis.....17

Table 3. Raw ICPMS data from bulk volcanic ash analysis.....20

Table 4. Raw NAA data from bulk volcanic ash analysis.....22

Table 5. Electron microprobe data in wt % from the analysis of individual volcanic glass shards.....29

Table 6. Raw NAA data of volcanic glass shards.....34

Table 7. Raw data shown as average wt % from microprobe analysis of individual apatite phenocrysts.....37

Table 8. Summary table of $^{40}Ar/^{39}Ar$ dating of individual sanidine phenocrysts.....39

Table 9. Chemical Index of Alteration values of raw bulk volcanic ash ICPMS data and microprobe glass shard analysis.....52

Table 10. CIPW Norm calculations done using GDCkit software for the volcanic glass shard analyses.....57

INTRODUCTION

The occurrence of volcanic ash deposits in the Eocene and Oligocene strata of the Texas Gulf Coast has been reported by many studies, but little work has been done on them to characterize the geochemistry and provide radiometric dating to obtain age determination of the formations containing the ash beds (Ledger 1988; Roberson 1964; Stenzel 1940; Guillemette and Yancey 1996; Yancey and Guillemette 1998). Paleocene and Early Eocene strata lack recognizable volcanic ash beds, although sands with grains of probable volcanic origin, including bipyramidal euhedral quartz crystals and small lithic grains, are recognized in latest Paleocene and Eocene sandstones (Callender and Folk 1958). Middle to Late Eocene strata contain many thin or thick volcanic ash deposits (Figure 1). The oldest known coastal plain Eocene volcanic ash occurs in the Crockett Formation (Stenzel 1940; Gimbrede 1951).

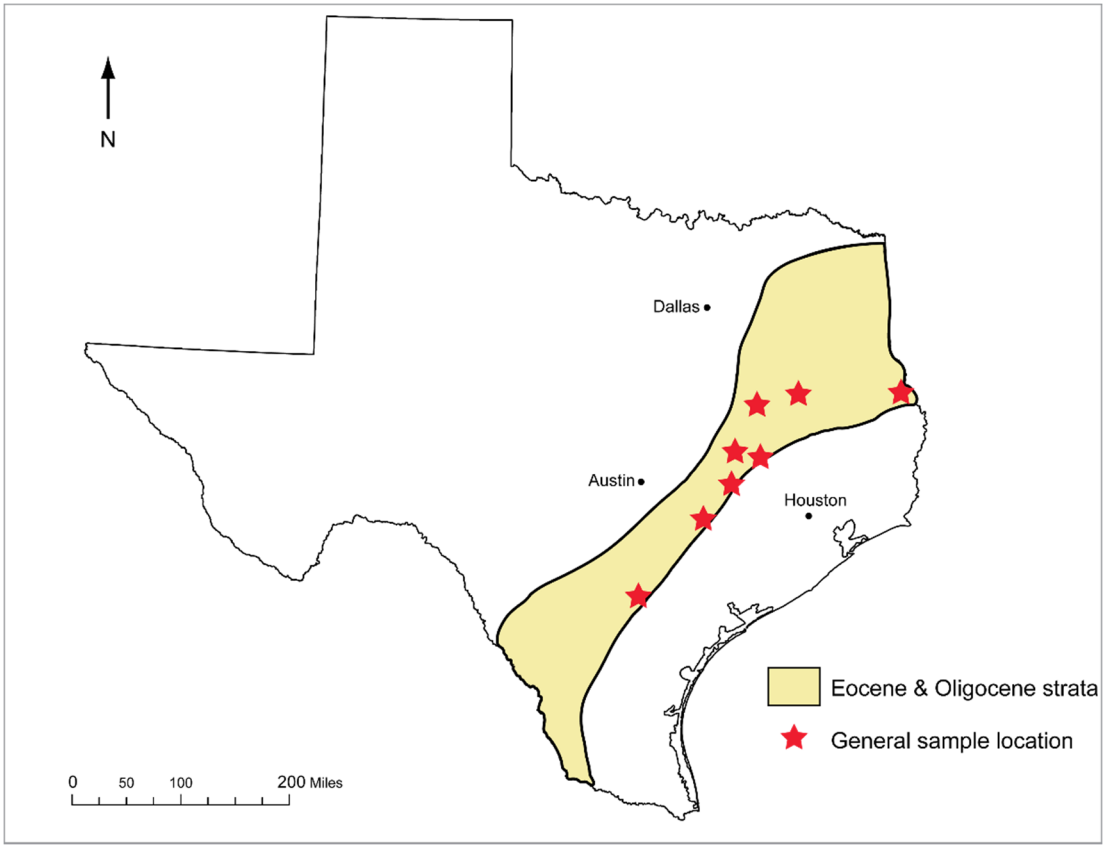

Figure 1. Location of volcanic ash samples.

This study documents 15 volcanic ash layers within the Eocene Claiborne and Jackson Groups and the Oligocene Catahoula Formation of Texas (Figure 2). Volcanic ashes of rhyolitic composition become more common in an upward succession in the Middle to Late Eocene and Oligocene stratigraphic section of the Texas coastal plain, with volcaniclastic materials forming most of the volume of Oligocene deposits in the central and south Texas outcrop belt. Strata in south Texas are closer to the source of the volcanism and therefore contain significantly more volcanic ash deposits than the eastern section (Roberson 1964; McBride et al. 1968; Gowan 1985; Grigsby and Dennis 1991).

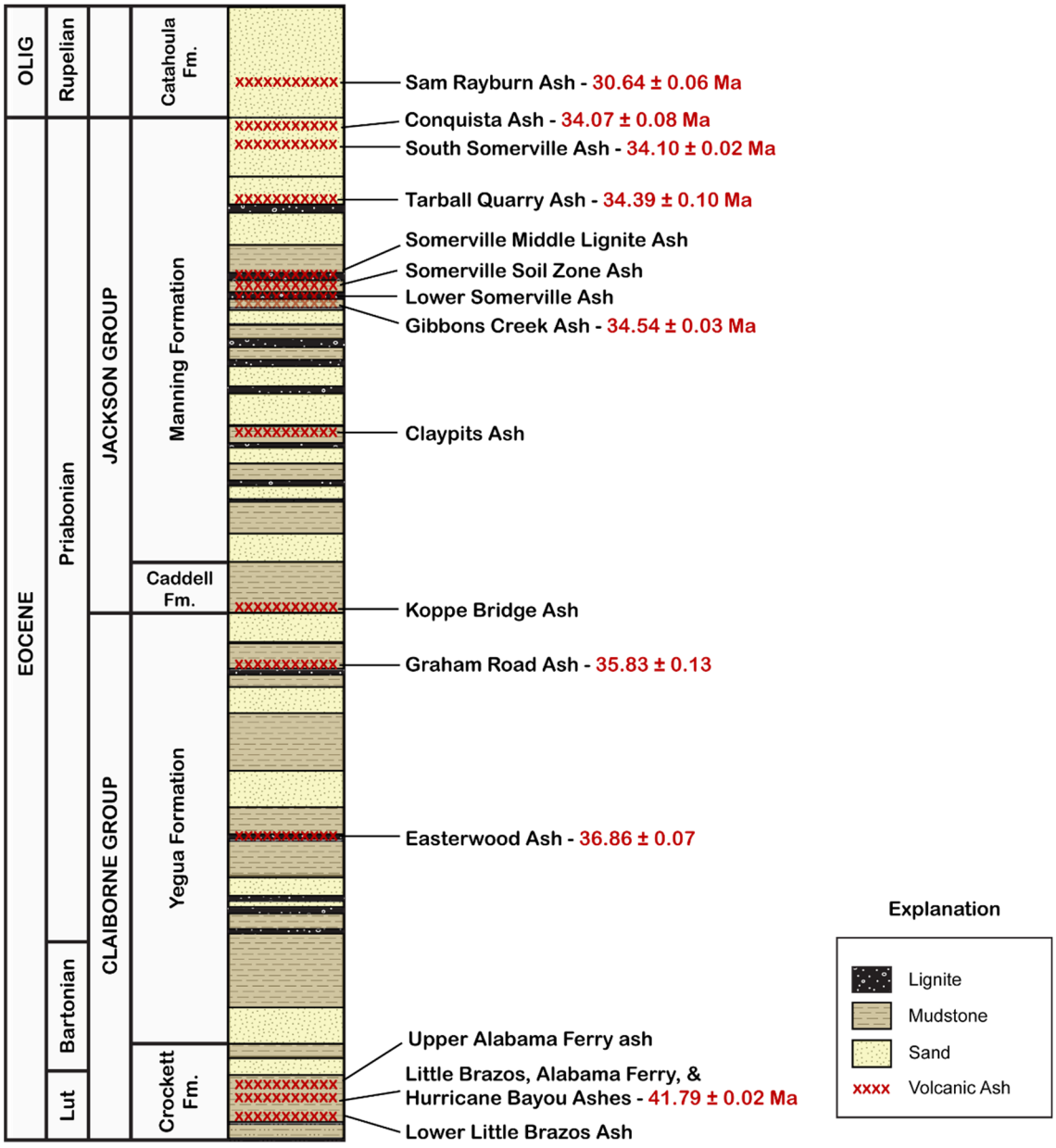

Figure 2. Stratigraphy for the study location showing the position of the volcanic ash beds studied in this report. Modified from Guillemette and Yancey (1996).

Volcanic ash beds can provide numerical age dates of the enclosing strata, be used to determine composition of the volcanic source and establish time horizons by correlation of geographically separated sections. An ash bed that can be unambiguously identified is usable as a regional marker in the stratigraphic section. Volcanic ash beds occur in Eocene and Oligocene Gulf of Mexico coastal plain deposits as far east as Louisiana, Mississippi and Alabama, indicating that volcanic ashes may be correlatable throughout the northern Gulf Coast (Obradovich et al. 1993; Grigsby 1999). An Eocene age volcanic ash is also present in North Carolina that may be an eastern extension of the northern Gulf volcanic ash bed (Harris and Fullagar 1989). These volcanic ashes are the product of middle Cenozoic explosive rhyolitic volcanism along the southwestern margin of North America (Henry et al. 1991; McDowell and Mauger 1994) (Figure 3). The location of local eruptive centers producing these volcanic ashes is not determined, but the volcanic ash beds probably have multiple sources in the many eruptive centers along the subduction-generated volcanic trend of western Mexico (Guillemette and Yancey 1996; Grigsby 1999; Michealides 2011).

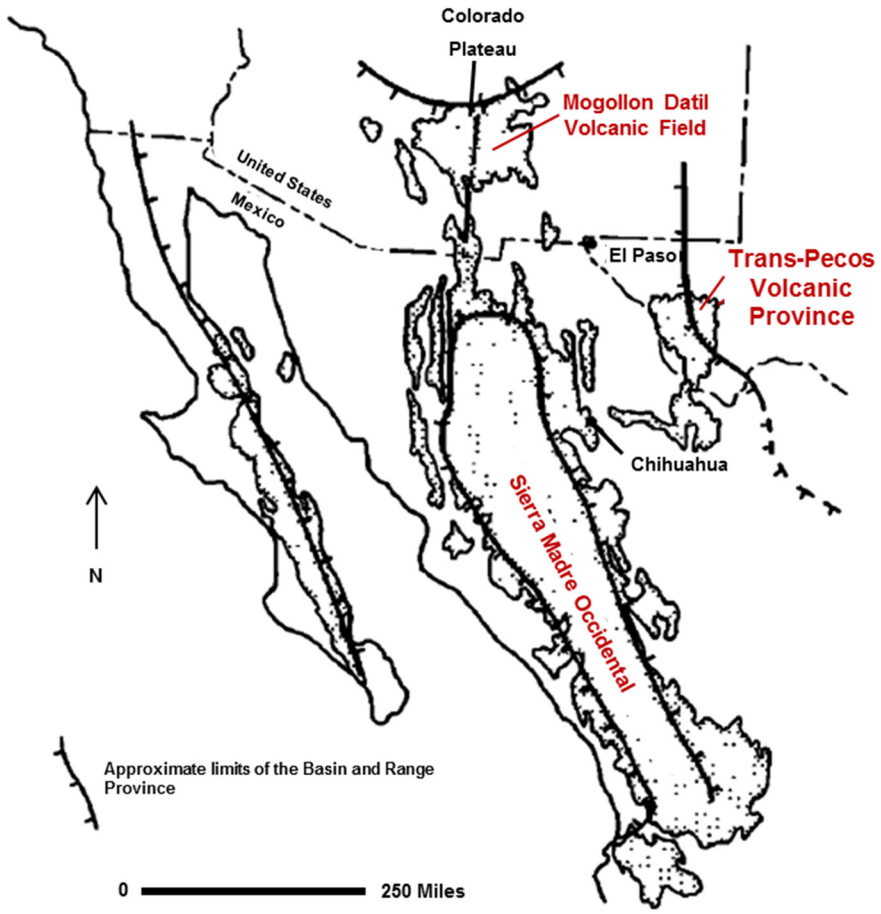

Figure 3. Silicic volcanism trend running from Mexico into the western United States that makes up the Sierra Madre Occidental, Trans-Pecos Volcanic Province and Mogollon-Datil Volcanic Field. (Modified from Henry and Price, 1991)

This study utilizes six different types of analysis to characterize the volcanic ash deposits. Radiometric age dating is obtained by $^{40}Ar/^{39}Ar$ dating of sanidine phenocrysts contained in the ash. However, radiometric age dates are calculated as an age range (e.g. 41.79 ±0.02 Ma) and when the ashes are close in age, ash bed geochemistry is needed to further constrain the geochronologic framework. Bulk rock composition of the volcanic ash samples is determined by Neutron Activation Analysis (NAA) and by Inductively

Coupled Plasma Mass Spectrometry (ICPMS) analysis that includes the full set of rare earth elements (REE). Bulk analysis of volcanic ash is an effective tool for constraining the geochemical fingerprint of the ash, but it is more difficult to obtain reliable data because alteration of the ash can mobilize elements and alter the elemental composition. Elemental analysis of unaltered volcanic glass shards is a more reliable indicator of the original ash bed geochemistry, but glass shards are preserved only in younger volcanic ash that was deposited in primarily non-marine depositional environments.

Apatite phenocrysts analyzed by electron microprobe provide data on single components of volcanic ash beds where the volcanic glass has been altered to clay. Apatite is a stable mineral, has the capacity to include many elements into its crystal structure, and has been proven to be a useful correlation tool for highly altered volcanic ash beds (Carey et al. 2009; Sell and Samson 2011 and references therein).

PALEOGENE VOLCANIC ASH DEPOSITS OF EAST AND CENTRAL TEXAS

Volcanic ash of Eocene and Oligocene age in central and east Texas has a silicic composition and originated as vitric ash with small amounts of phenocrysts and few lithic grains (Roberson 1964; Senkayi et. al 1984; Ledger 1988). Phenocrysts consist of quartz and lesser amounts of feldspar with accessory minerals biotite, apatite and zircon in varying amounts. From this original composition, three types of volcanic ash beds have formed from diagenetic change in different depositional environments. All Paleogene volcanic ash deposited in an open marine environment has total alteration of glass shards, producing dark green to black bentonite beds composed of smectite clay (Figure 4). In some deposits like the Alabama Ferry ash, the outlines of shards are recognizable in the clay matrix. When disaggregated, these ash beds yield concentrations of phenocrysts that are usually dominated by biotite with apatite present. Apatite phenocrysts in the Little Brazos, Alabama Ferry and Hurricane Bayou samples are euhedral and are approximately 200 μm in size. Apatites found in the Lower Little Brazos volcanic ash bed are also euhedral, but are approximately 100 μm in size.

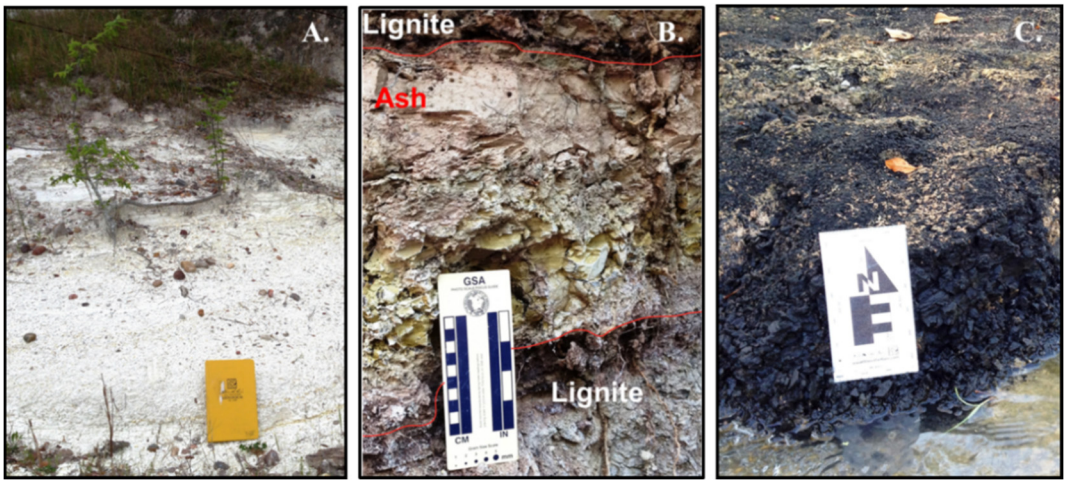

Figure 4. Examples of volcanic ash deposits. A. Claypits volcanic ash outcrop, fresh/brackish body of water depositional setting. B. Easterwood volcanic ash outcrop, swamp depositional setting. C. Little Brazos volcanic ash outcrop, open marine depositional setting.

Volcanic ash beds deposited in a non-marine environment (fluvial, lake or land) tend to alter to kaolinite or be preserved where the smallest glass shards are altered to kaolinite or smectite (Figure 4). Larger (>50 µm) shards are preserved as hydrated but otherwise unaltered glass. Unaltered glass shards occur in the Late Eocene Manning Formation and the Oligocene Catahoula Formation. Volcanic glass shards are made up of mainly bubble wall fragments with some micro-pumice fragments (Guillemette and Yancey 1996). The volcanic glass shard fragments range in size from 400 µm in the coarser deposits to 50 µm in the finer deposits.

Volcanic ash beds deposited in a swamp environment undergo complete alteration to kaolinite and it is common for large vermiform crystals of kaolinite to develop (Figure 4). Samples of the Easterwood and Gibbons Creek ash beds are dominated by large diameter kaolinite vermiforms that reach lengths of several

millimeters. These develop commonly in tonsteins (a light-colored volcanic ash bed contained within a lignite or coal) like the Gibbons Creek ash, but also in ash deposited in standing water carbonaceous sediment like that containing the Easterwood ash (Ross and Kerr 1930). Sample locations, depositional setting and mineralogical aspects are presented in Table 1.

Ash Bed	Location	Thickness	Aspect	Glass	Accessory minerals*	Secondary Minerals*
Sam Rayburn	31.062366°, -- 94.108534°	20-60 cm	White ash in fluvial channel	Abundant, fine size	Quartz, sanidine, zircon, magnetite	Kaolinite
South Somerville	30.291262°, -96.524058°	10-20 cm	White ash in lignite (tonstein)	Abundant, coarse	Quartz, sanidine, zircon, biotite, hornblende, magnetite	Kaolinite
Conquista	28.876347°, -98.101288°	3 m	White ash	Abundant, medium size	Quartz, sanidine, zircon, biotite	Kaolinite
Tarball Quarry	30.300803°, -96.520110°	5-10 cm	White ash in lignite (tonstein)	Abundant, fine size	Quartz, sanidine, zircon, hornblende	Kaolinite
Somerville Soil Zone	30.317799°, -96.517152°	80 cm	White ash in soil zone	Common	Quartz, sanidine, zircon, hornblende	Kaolinite, soil minerals
Gibbons Creek	30.570702°, -96.054297°	20 cm	White ash in lignite (tonstein)	None	Quartz, sanidine, biotite, zircon	Kaolinite, pyrite
Seale Ranch	29.833333°, -97.029167°	1 m	White ash	Abundant, fine size	Quartz, sanidine, zircon, hornblende	Kaolinite, sponge spicules
Claypits	30.489718°, -96.312718°	1.5 m	White ash in shallow marine	Abundant, medium size	Quartz, sanidine, biotite, zircon	Kaolinite
Plum	29.935115°, -96.979841°	1 m	White ash	None	Quartz, sanidine, zircon, magnetite	Kaolinite
Koppe Bridge	30.509068°, -96.354858°	12 cm	White ash in shallow marine	None	Quartz, sanidine, zircon	Kaolinite
Graham Road	30.552001°, -96.328746°	8 cm	White ash in shallow marine	None	Quartz, sanidine, zircon	Kaolinite, pyrite
Easterwood	30.590192°, -96.349734°	15 cm	White ash in shallow marine	None	Quartz, sanidine, zircon,	Kaolinite, gypsum, jarosite
Hurricane Bayou	31.358546°, -95.431536°	80 cm	Dark, waxy ash in open marine (bentonite)	None	Quartz, sanidine, biotite, apatite, zircon, hornblende	Smectite, pyrite
Alabama Ferry	31.225576°, -95.727310°	1 m	Dark, waxy ash in open marine (bentonite)	None	Quartz, sanidine, biotite, apatite, zircon, hornblende	Smectite, pyrite
Little Brazos	30.642296°, -96.520528°	25 cm	Dark, waxy ash in open marine (bentonite)	None	Quartz, sanidine, biotite, apatite, zircon, hornblende	Smectite, pyrite
Lower Little Brazos	30.642296°, -96.520528°	6 cm	Dark, waxy ash in open marine (bentonite)	None	Quartz, sanidine, biotite, apatite, zircon, hornblende	Smectite, pyrite

Table 1. Characteristics of volcanic ash samples included in this study. *Minerals identified – volcanic ash beds could contain other minerals not noted.

Outcrops of a thick volcanic ash occur within the Crockett Formation (Late Middle Eocene) in several places between the Little Brazos River and Hurricane Bayou near Crockett, Texas. This is a dark green/black bentonite that thickens from 25 cm at Little Brazos to 0.7 m in Leon County (Stenzel 1938; Gimbrede 1951) and 1 m at Alabama Ferry on the Trinity River (Stenzel 1940; Gray 1953), and is 0.7 m thick at Hurricane Bayou on the east end of the outcrops (Gray 1953). At the Little Brazos site the volcanic ash was measured on a vertical cut through the bed and it has sharp, well defined upper and lower boundaries, with minimal bioturbation on the upper boundary. A thin (6 cm) volcanic ash layer occurs 1 m below the main volcanic ash bed at Little Brazos and extends over the same outcrop belt. Another thin volcanic ash bed occurs 3 m above the main bed at Alabama Ferry. These occur in the so-called Hurricane "Lentil" of Stenzel (1940), a lithologic and biostratigraphically distinct zone in the Crockett Formation. Gray (1953) noted the presence of two additional thin volcanic ash beds in the underlying Wheelock Member strata. These five volcanic ash beds occur in a 20 m interval of fine-grained marine deposits. The thickest volcanic ash bed of the Crockett Formation has been correlated with volcanic ash deposits in Louisiana (Grigsby 1999). The Crockett Formation contains sediments deposited in an open marine environment that were deposited during a major marine transgression (Renick 1936; Stenzel 1940).

The Yegua Formation contains two or more volcanic ash beds in Brazos County. The middle Easterwood Member of the Yegua Formation is composed of bentonitic clays that produce unstable soils in the county (Berg 1970), indicating a high volcanic

ash content in the sediments. Samples were collected from a 25 cm thick bed in the Easterwood Member (Senkayi et al. 1984) and an 8 cm thick ash layer in the upper part of the formation. Both were deposited in standing water environments in during times of high rates of sediment deposition. The overlying Caddell Formation at the base of the Jackson Group contains a thin (12 cm) volcanic ash bed, located about 1 m above the Yegua-Caddell formation boundary in Brazos County. The Caddell contains sediments deposited in an open marine environment that were deposited during a major marine transgression (Atlee et al. 1967).

Many volcanic ash beds occur in strata of the Jackson group. Volcanic ash is a common component of sediments in the upper part of the Manning Formation and occurs as layers of air fall deposit or as redeposited layers of ash. The Claypits volcanic ash bed of Brazos County is a 1.5 m thick unit in lower part of the Manning Formation that was mined commercially for kaolin in a series of pits along strike of the ash bed (Yancey and Guillemette 1998). The Somerville spillway section (Guillemette and Yancey 1996; Yancey 1997) contains two thick deposits of redeposited volcanic ash and a 0.8 m thick ash deposited onto a land surface and weathered in-place to an ash-rich soil, as well as two thin tonstein ash layers deposited within lignite beds. Three of the volcanic ash beds sampled for this study are from lignite bed tonsteins in the upper part of the Manning Formation. The South Somerville ash bed, a tonstein deposit at the top of the Manning Formation, is distinct from other Manning volcanic ashes in containing larger glass shards and phenocrysts than in underlying volcanic ash beds.

Volcanic ash is a major component of the Catahoula Formation (Renick 1936) in central and east Texas and its lateral equivalent Gueydan Formation in south Texas (Bailey 1926; McBride et al. 1968). Ash deposition occurred on non-marine surfaces and is mostly reworked into channels or weathered in-place to ash-rich soils. The Catahoula volcanic ash used in this study was deposited in a small channel filled with volcanic ash (Ledger 1988) and similar lenticular masses of ash occur elsewhere in Oligocene deposits (McBride et al. 1968). The Catahoula Formation was deposited during a time of major volcanic eruptive activity that spread volcanic ash widely across the southern part of North America.

Volcanic ash in Paleogene strata of central and east Texas was all delivered to the area by air fall deposition, but is preserved in variable condition. Volcanic ash deposited in low energy marine environments and in peat swamps is preserved with minimal disturbance after the ash fall. This is the best condition for age dating because there is minimal or no admixing with other sediment and all of the ash is from one time of ash fall. Ash beds preserved in standing water environments usually have sharp, well defined lower and upper boundaries. In marine deposits, burrowing may mix some mud sediment into the volcanic ash, but these can be recognized and removed before preparing the sample for analysis. In peat swamps where volcanic ash is encased in peat (a tonstein), the ash layer usually has more irregular boundaries due to compaction of fluid-rich peat and from plant root penetration. However, mixing is limited to inclusion of plant bioclasts and possibly some clay mud.

Evidence for transport and reworking of volcanic ash comes from sedimentary structures that reveal sediment movement by water currents. An example of this is the presence of cross bedding in the lower parts of the Claypits volcanic ash, an indicator of strong wave and sustained current activity at the time of deposition. The presence of good sorting and a minor upward-fining grain size trend in the Conquista ash deposit is evidence of transport and redeposition. In both of these volcanic ash deposits the absence of other types of sediment particles is taken as an indication that there was no mixing with other sediment in samples collected for study. The deposits are judged to be from a single air fall event. Volcanic ash beds with extensive cross bedding and/or evidence of deposition in shoreline environments are clearly reworked and are less suitable for radiometric age dating. A 1.3 m sand bed composed entirely of volcanic ash in the Somerville spillway section is not sampled for this study because of the evidence of deposition in a high energy shorezone environment and possibility of mixing with other volcanic materials.

METHODS

Samples weighing one to two kilograms were collected from outcrop with a putty knife after removing surface zones of weathered and crumbly sediment. Blocks of sample were examined in the field and in the lab to remove sediment crusts present on fracture surfaces and where volcanic ash layers contain burrows, the burrow fill was removed before preparing the sample for chemical analysis. Cleaned samples were then oven dried for at least 12 hours at 75°C. A 500 gm bulk sample was set aside for later analysis and one kilogram was disaggregated and concentrated for phenocrysts following procedure outlined in Guillemette and Yancey (1996). Samples then underwent secondary processing, if needed, for different types of analysis.

$^{40}Ar/^{39}Ar$ Dating

For radiometric age dating, samples were disaggregated and the sediment fraction < 62 μm was removed. The magnetic materials of the coarse fraction were removed using a hand magnet, and then heavy liquid separation was performed using lithium heteropolytungstate (LST) in a separatory funnel to split the heavy and light mineral fractions. The amount of light density minerals (<2.85 g/mL) sent for analysis was dependent on the makeup of the volcanic ash. Clay rich volcanic ashes contained the least amount of phenocrysts, so there was less sample available to send. At least two grams (more if available) of the light density separate was sent to the New Mexico Bureau of Geology and Mineral Resources geochronology laboratory for $^{40}Ar/^{39}Ar$ radiometric dating. Radiometric age dates were made on sanidine phenocrysts extracted

from the separates. All sanidine separation and laboratory procedures for radiometric dating were completed at the New Mexico lab and are detailed in Appendix A.

Neutron Activation Analysis (NAA)

For NAA, a two gram bulk rock split of each volcanic ash sample was powdered using a ceramic ring mill. The samples were powdered to a condition that at least 95 % of the powder was 106 μm or less. After each sample was powdered, the ceramic ring mill was cleaned by powdering agate and then washed out to avoid contamination from preceding samples. The powdered samples were submitted to the Elemental Analysis Laboratory at Texas A&M University for NAA to obtain trace element and rare earth element (REE) data. For the five volcanic ash deposits with preserved glass shards, NAA was also performed on separates of glass shards. A 50 mg portion of volcanic glass shards was hand-picked from the low density fraction of the heavy liquid separation and submitted for NAA. Two grams of sample is preferred, but due to the small size of the glass shards the hand-picking process was too extensive to collect over 50 mg. The Somerville Soil Zone and Seale Ranch samples did not have adequate glass shards for NAA.

Electron Microprobe Analysis of Volcanic Glass Shards

A 50 mg portion of washed glass shards was submitted for electron microprobe analysis on a Cameca SX50 electron microprobe at Texas A&M University. These samples supplement previous geochemical characterization of Texas volcanic glass shards reported by Guillemette and Yancey (1996) and a portion of the Sam Rayburn

(Catahoula) volcanic ash was reanalyzed to calibrate the different times of analysis and determine the reproducibility of analyses.

Electron Microprobe Analysis of Apatite Phenocrysts

Apatites from the high density fraction of four Crockett Formation samples were selected for elemental characterization, following the procedures of Carey and others (2009). They were analyzed at Texas A&M University on a Cameca SX50 electron microprobe. Quantitative compositional analyses for the elements of F, Ca, P, Cl, Fe, Mg, Mn, Sr, La, Ce, Nd and Y were targeted for analysis carried out on a four-spectrometer Cameca SX50 electron microprobe, using an accelerating voltage of 15 kV at beam currents of 20 to 200 nA with a beam size of 20 μm. Major elements were analyzed at 20 nA while minor and trace elements were analyzed 200 nA for improved sensitivity. All quantitative work employed wavelength-dispersive spectrometers (WDS). Analyses were carried out after standardization using very well characterized compounds or pure elements (Table 2). Great care was taken to avoid interfering spectral lines from other elements when selecting analytical conditions and off-peak background positions. Qualitative EDS analyses (spectra) were obtained with an Imix Princeton Gamma Tech (PGT) energy dispersive system (EDS) using an ultra-thin window detector.

Typical WDS quantitative accuracy for major elements (> 10 wt %) is about equal to ±1 to 2 % of the amount present; the uncertainty at low concentrations increases as the concentration decreases, with the uncertainty reaching 100 % at the lower limit of detection (LLD). The lower limit of detection for most elements under typical

conditions is about 0.05 to 0.10 wt %, but could be reduced to as low as the 0.001 wt % range by using high beam currents and long counting times. Statistical LLD's were calculated for all analyses.

Element	Standard	Standard Description
Ca	5apatite	CMT apatite standard
P	5apatite	CMT apatite standard
F	5CaF_2	CMT fluorite standard
Cl	5NaCl	CMT sodium chloride standard
Y	6YPO_4	NMNH single crystal yttrium phosphate standard (1)
La	6$LaPO_4$	NMNH single crystal lanthanum phosphate standard (1)
Ce	6$CePO_4$	NMNH single crystal cerium phosphate standard (1)
Nd	6$NdPO_4$	NMNH single crystal neodymium phosphate standard (1)
Sr	3strontia	NMNH strontianite standard (2)
Mg	5olivine	CMT olivine standard
Fe	3siderite	NMNH siderite standard (3)
Mn	5spessart	CMT spessartine garnet standard

Table 2. Standards used in apatite microprobe analysis. CMT = Charles M. Taylor Corporation, 289 Leota Avenue, Sunnyvale, CA 94086. NMNH: National Museum of Natural History (Smithsonian, NIST), Washington, DC, (1) Jarosewich, 1991, (2) Jarosewich and White, 1987, (3) Jarosewich and McIntyre, 1983.

Inductively Coupled Plasma Mass Spectrometry (ICPMS) Analysis

For ICPMS analysis, seven gram bulk samples were powdered using a ceramic ring mill. The samples were powdered to a condition that at least 95 % of the powder was 106 μm or less. After each sample was powdered, the ceramic ring mill was cleaned by powdering agate and then washed out to avoid contamination from previous samples. Powdered volcanic ash was then submitted to a commercial lab (Actlabs) for ICPMS analysis to obtain major element, trace element and REE data. Each sample was fused into a glass disk, then analyzed with a Perkin Elmer Sciex ELAN 6000, 6100 or

9000 ICP/MS (Actlabs, personal communication). Three blanks and five controls (three before sample group and two after) were analyzed per group of samples. Duplicates are fused and analyzed every 15 samples and the instrument is recalibrated every 40 samples.

RESULTS

Elemental Chemistry of Volcanic Ash Deposits

Bulk Volcanic Ash Chemistry

Chemical characterization of the volcanic ash beds is documented by analysis of bulk volcanic ash samples with Neutron Activation Analysis (NAA) or Inductively Coupled Plasma Mass Spectrometry (ICPMS) analysis. This is used in conjunction with mineral composition of the volcanic ash beds to compare volcanic ash layers for purposes of identification and correlation of geographically separated occurrences. Both methods provide quantitative abundance data on a wide range of elements, with ICPMS reporting major element data as wt % oxides and trace element plus rare earth element (REE) in parts per million (ppm). NAA does not provide data on some elements reported in ICPMS analysis and can have lower levels of precision depending upon the element. Both types of analysis have been done in this study to characterize the volcanic ash beds and to be able to compare data from these beds to other ashes previously analyzed by either method. Major element, trace element and REE data from ICPMS analysis is presented in Table 3. Trace element and REE data from NAA is presented in Table 4. All plots and tables list the volcanic ash samples in stratigraphic order from youngest (Sam Rayburn) to oldest (Lower Little Brazos). Values reported by the two methods are similar, indicating that comparison of composition made by different methods will yield useful information.

Element	DL*	Sam Rayburn	Conquista	South Somerville	Tarball Quarry	Somerville Soil Zone	Gibbons Creek	Claypits
SiO_2	0.01	70.12	56.86	70.21	68.02	67.71	55.05	63.38
Al_2O_3	0.01	13.7	18.85	11.92	13.98	14.12	26.02	15.41
Fe_2O_3(T)	0.01	0.89	1.68	1.19	0.66	2.79	0.66	1.32
MnO	0.001	0.052	0.02	0.023	0.051	0.036	0.033	0.073
MgO	0.01	0.34	2.98	0.08	0.18	0.63	0.49	0.76
CaO	0.01	0.46	2.12	0.35	0.35	0.72	0.71	0.92
Na_2O	0.01	1.25	0.58	0.85	1.17	1.1	0.88	1.63
K_2O	0.01	3.53	0.63	2.76	2.8	2.21	0.92	2.98
TiO_2	0.001	0.114	0.122	0.121	0.13	0.45	0.262	0.147
P_2O_5	0.01	0.02	0.02	0.26	0.09		0.02	
LOI		8.46	16.75	12.02	12.84	9.56	14.75	11.58
Total	0.01	98.93	100.6	99.79	100.3	99.35	99.79	98.19
Sc	1	5	3	3	4	6	3	5
Be	20	3	3	4	4	3	1	5
V	10	8	< 5	9	10	49	11	8
Cr	30	< 20	< 20	< 20	< 20	20	< 20	< 20
Co	1	< 1	< 1	< 1	1	4	1	< 1
Ni	0.5	< 20	< 20	< 20	< 20	< 20	< 20	< 20
Cu	5	10	< 10	< 10	< 10	< 10	< 10	< 10
Zn	1	30	50	< 30	40	60	< 30	50
Ga	2	18	25	12	17	19	37	19
Ge	0.5	1.7	0.9	1	1.6	1.2	1	1.3
As	1	5	< 5	6	< 5	< 5	< 5	< 5
Rb	0.2	212	19	169	207	171	37	165
Sr	2	54	158	41	36	95	75	65
Zr	0.1	82	195	129	131	180	131	160
Nb	1	12.2	38.9	14.3	15.3	18.9	32.2	13.5
Mo	0.2	2	12	3	< 2	3	2	< 2
Ag	0.1	0.8	0.8	1.1	1.2	1.6	0.7	0.9
In	3	< 0.1	< 0.1	< 0.1	< 0.1	< 0.1	< 0.1	< 0.1
Sn	0.05	1	6	< 1	< 1	2	2	2
Sb	0.05	0.3	0.6	0.3	< 0.2	0.5	2.2	1.1
Cs	0.01	5.2	0.5	5.3	7.2	8.8	2	4.9
Ba	0.05	897	15	230	88	296	254	186
Hf	5	3.6	8.8	6	6.5	5.9	5.5	6
Ta	0.1	1.06	3.98	2.94	1.4	1.37	4.63	1.6
W	0.05	< 0.5	< 0.5	< 0.5	< 0.5	0.8	< 0.5	< 0.5
Tl	0.01	1.1	0.08	1.25	2.36	0.87	0.17	0.46
Pb		23	30	49	29	20	53	15
Bi		0.3	2.7	0.8	0.5	1.5	< 0.1	0.6
Th		16.1	55	14.9	14.9	13	19	25.1
U		6.27	78.8	6.56	5.9	4.63	7.46	6.27
La	0.01	33	24.1	44.1	28.6	20	18.1	27.3
Ce	0.005	64.8	58.7	96	68.4	33.9	33.2	55.4
Pr	0.01	7.65	6.66	12.5	8.8	3.61	3.21	7.04
Nd	0.01	27.7	23.2	47.5	33	11.9	10.2	25.6
Sm	0.01	6.06	5.12	10.8	8.36	2.34	1.57	5.26
Eu	0.01	0.672	0.207	1.34	1.01	0.329	0.304	0.563
Gd	0.01	5.97	4.1	9.12	7.18	2.23	1.51	4.89
Tb	0.005	1.06	0.66	1.43	1.23	0.41	0.27	0.89
Dy	0.01	6.73	3.49	7.99	7.5	2.63	1.52	5.22
Ho	0.002	1.4	0.61	1.57	1.51	0.58	0.29	1.01
Er	0.1	4.22	1.55	4.53	4.56	1.88	0.85	2.99
Tm	0.01	0.649	0.212	0.691	0.691	0.314	0.134	0.484
Yb	0.5	4.47	1.37	4.63	4.76	2.23	0.94	3.35
Lu	0.05	0.73	0.218	0.747	0.78	0.383	0.168	0.608
Y	0.5	39.1	12.4	36.7	35.7	16.7	7.7	27.3

Table 3. Raw ICPMS data from bulk volcanic ash analysis. Oxides shown in wt % all other elements in ppm. LOI = loss on ignition during fusing to make disc. *<Number = less than detection limit (DL).

Element	DL*	Plum	Koppe Bridge	Graham Road	Easter wood	Alabama Ferry	Hurricane Bayou	Little Brazos	Lower Little Brazos
SiO_2	0.01	60.82	55.34	55.52	52.77	52.47	48.14	50.29	38.52
Al_2O_3	0.01	15.08	20.82	18.5	24.79	17.49	16.93	16.06	17.51
Fe_2O_3(T)	0.01	1.08	2.5	6.05	1.56	7.85	7.98	7.07	20.98
MnO	0.001	0.01	0.007	0.022	0.008	0.01	0.008	0.019	0.011
MgO	0.01	1.46	2	1.68	0.74	3.99	3.52	4.16	3.42
CaO	0.01	1.59	1.31	0.28	1.26	2.44	2.52	1.76	1.37
Na_2O	0.01	0.05	0.37	0.94	1.02	0.07	0.2	0.07	0.11
K_2O	0.01	0.05	0.25	0.66	1	0.26	0.24	0.16	0.25
TiO_2	0.001	0.359	0.322	0.266	0.364	0.279	0.284	0.251	0.326
P_2O_5	0.01	0.02	0.04	0.03	0.02	0.13	0.1	0.1	0.1
LOI		17.53	16.51	14.98	14.37	14.95	19.22	18.95	17.97
Total	0.01	98.04	99.48	98.95	97.9	99.94	99.14	98.88	100.6
Sc	1	8	7	6	5	3	3	3	11
Be	20	1	< 1	2	3	1	< 1	1	1
V	10	15	15	27	24	27	19	18	80
Cr	30	< 20	< 20	< 20	< 20	< 20	< 20	< 20	< 20
Co	1	< 1	< 1	24	2	3	2	2	9
Ni	0.5	< 20	< 20	20	40	< 20	< 20	< 20	40
Cu	5	< 10	< 10	< 10	< 10	< 10	< 10	< 10	< 10
Zn	1	< 30	< 30	150	40	40	50	30	100
Ga	2	19	25	24	31	18	17	17	16
Ge	0.5	< 0.5	< 0.5	< 0.5	1.9	0.7	< 0.5	< 0.5	< 0.5
As	1	< 5	< 5	34	< 5	< 5	19	< 5	23
Rb	0.2	3	10	11	21	8	8	5	7
Sr	2	87	45	49	174	427	152	176	85
Zr	0.1	228	203	97	187	145	155	149	184
Nb	1	13	3.1	2	14.6	4.5	6.2	11	3.7
Mo	0.2	< 2	< 2	23	< 2	< 2	< 2	< 2	< 2
Ag	0.1	1.7	1.3	< 0.5	1	0.9	1	0.6	1.6
In	3	< 0.1	< 0.1	< 0.1	< 0.1	< 0.1	< 0.1	< 0.1	< 0.1
Sn	0.05	2	2	3	3	1	< 1	1	3
Sb	0.05	0.3	1.2	10.3	1.2	< 0.2	1.2	0.5	0.7
Cs	0.01	0.9	0.4	0.4	0.6	< 0.1	< 0.1	< 0.1	0.2
Ba	0.05	91	141	259	621	103	123	82	61
Hf	5	6.9	8.2	4.7	8.1	4.1	4.6	4.7	8.1
Ta	0.1	1.22	1.67	2.25	2.99	1.59	1.53	1.36	1.78
W	0.05	< 0.5	< 0.5	0.7	< 0.5	< 0.5	< 0.5	3.3	< 0.5
Tl	0.01	0.08	< 0.05	0.84	0.07	< 0.05	0.13	< 0.05	< 0.05
Pb		< 5	6	40	17	28	29	14	39
Bi		0.8	1.7	1.4	1.2	1.4	1.5	1.1	1.7
Th		18.3	18.8	26.8	21.9	35.3	35.7	34.5	31.1
U		4.16	2.33	9.56	4.68	9.44	8.33	7.48	3.55
La	0.01	55.8	36.7	50.1	27.1	36.1	37.5	41.4	32.4
Ce	0.005	89.6	84.4	115	48.7	69.6	71.2	66.1	77
Pr	0.01	12.8	9.47	13.5	5.37	6.91	6.97	7.5	8.9
Nd	0.01	48.5	37.7	47.8	18.6	22.8	24.5	25.2	32.7
Sm	0.01	9.39	6.59	8.76	3.3	3.94	4.61	4.38	6.41
Eu	0.01	1.28	1.04	1.71	0.731	0.709	0.742	0.667	1.03
Gd	0.01	8.6	5.79	7.58	2.91	3.19	4.12	3.28	5.23
Tb	0.005	1.34	0.87	1.19	0.46	0.52	0.6	0.5	0.81
Dy	0.01	7.57	4.65	6.45	2.45	2.8	3.26	2.84	4.38
Ho	0.002	1.43	0.85	1.24	0.47	0.53	0.57	0.54	0.77
Er	0.1	3.93	2.36	3.62	1.3	1.43	1.55	1.51	2.02
Tm	0.01	0.553	0.338	0.544	0.193	0.206	0.227	0.23	0.269
Yb	0.5	3.54	2.27	3.74	1.28	1.33	1.49	1.56	1.64
Lu	0.05	0.546	0.37	0.636	0.206	0.205	0.238	0.259	0.248
Y	0.5	36.4	21.8	34.8	12.7	13.9	12.8	14	16.9

Table 3 Continued

Element	Sam Rayburn	South Somerville	Conquista	Tarball Quarry	Somerville Soil Zone	Gibbons Creek	Claypits	Plum
Na	9608.76	6222.16	4298.16	8909.54	8353.38	6390.81	11643.49	421.01
Al	71192.12	63773.68	97899.73	71599.28	71252.32	138250.10	82531.97	80832.54
K	34424.92	27250.80	4922.18	23941.83	0.00	7454.18	23937.26	0.00
Ca	3051.73	2148.20	15899.54	2716.74	4745.81	3755.14	5904.59	10926.76
Sc	4.79	3.02	3.00	4.24	5.92	2.45	5.27	8.38
Ti	801.80	353.53	512.97	787.83	2470.10	1694.50	851.09	2188.29
V	4.72	3.77	2.31	5.76	2470.10	4.17	0.00	2188.29
Cr	12.55	1.91	0.00	3.04	18.66	1.60	0.00	0.73
Mn	392.06	164.04	140.29	372.01	266.48	237.22	549.35	66.08
Fe	6306.51	10799.54	12190.63	4474.31	18466.12	4788.56	9677.72	7698.63
Co	0.64	0.95	0.00	1.22	3.96	1.23	0.22	0.10
Zn	75.66	57.28	92.24	48.47	56.88	35.05	81.29	10.89
As	5.40	5.37	4.82	5.55	2.19	1.71	3.71	0.00
Rb	217.59	184.80	16.29	210.39	149.06	33.39	154.56	2.21
Sr	0.00	0.00	252.69	0.00	71.13	107.09	0.00	99.38
Zr	161.41	90.30	1077.89	175.44	147.63	209.94	169.50	204.45
Sb	0.82	0.82	0.62	0.45	0.92	1.41	0.79	0.61
Cs	5.60	5.88	0.46	7.78	8.58	1.98	5.04	1.02
Ba	958.91	318.62	918.07	32.06	288.72	282.96	222.04	110.96
Hf	4.43	6.86	10.67	7.25	6.41	5.32	6.68	8.51
Ta	1.28	3.31	4.24	1.72	1.55	3.95	1.52	1.13
Th	16.25	16.51	57.16	14.83	12.15	15.45	25.83	18.81
U	7.48	6.80	85.95	6.00	0.00	7.12	6.40	0.00
La	33.69	46.64	26.67	27.87	18.32	14.40	25.30	57.54
Ce	77.33	120.28	87.97	76.25	32.21	31.99	60.07	91.35
Nd	19.47	55.54	50.75	19.99	10.49	16.11	25.18	45.07
Sm	6.58	12.13	10.79	8.45	2.70	2.02	5.49	9.78
Eu	0.68	1.44	0.20	1.00	0.29	0.28	0.58	1.32
Tb	0.82	1.23	0.58	0.88	0.37	0.13	0.45	1.42
Dy	6.05	8.12	3.41	6.85	2.53	0.62	4.42	7.83
Yb	4.39	4.88	1.42	4.98	0.00	0.90	3.06	0.00
Lu	0.71	0.76	0.18	0.75	0.39	0.11	0.43	0.60

Table 4. Raw NAA data from bulk volcanic ash analysis. All elements are ppm. Detection limits were not given for NAA.

Element	Koppe Bridge	Graham Road	Easterwood	Alabama Ferry	Hurricane Bayou	Little Brazos	Lower Little Brazos
Na	2847.35	7536.44	7687.80	504.35	534.70	1587.39	835.79
Al	108310.80	101056.60	132683.80	89588.29	84558.23	89377.84	92336.09
K	0.00	0.00	7684.31	0.00	0.00	0.00	0.00
Ca	9453.02	2806.59	9154.15	18209.11	13221.58	18746.19	9534.42
Sc	6.60	6.20	4.52	3.19	2.89	3.14	11.11
Ti	2062.45	1622.70	2115.92	1335.78	1263.49	1674.98	2026.16
V	9.78	23.43	17.97	15.57	11.71	16.14	2026.16
Cr	4.17	0.00	6.48	2.75	2.24	1.64	5.99
Mn	42.94	162.36	164.36	45.55	128.04	44.53	60.47
Fe	17381.83	43164.95	10866.30	56221.45	51382.16	55545.75	146398.30
Co	0.98	23.94	2.93	2.63	2.17	2.38	9.14
Zn	21.03	294.94	71.25	75.29	50.10	69.36	98.49
As	1.99	43.60	1.59	1.25	0.83	18.04	20.11
Rb	10.29	15.95	19.51	0.00	0.00	0.00	0.00
Sr	0.00	0.00	339.66	787.54	269.19	173.59	42.27
Zr	196.81	207.75	266.33	207.81	236.71	143.39	130.68
Sb	1.20	10.36	0.75	1.05	0.43	0.97	1.12
Cs	0.18	0.25	0.64	0.00	0.00	0.00	0.00
Ba	137.72	336.50	652.66	173.48	157.65	213.44	81.18
Hf	9.41	5.80	8.89	5.95	5.17	5.38	9.31
Ta	1.41	2.18	2.43	1.42	1.44	1.34	1.90
Th	17.59	24.57	20.67	35.94	34.67	31.85	31.26
U	2.29	12.64	4.43	10.03	7.56	8.81	0.00
La	36.17	56.22	24.91	37.29	39.96	36.63	32.11
Ce	85.57	124.11	45.18	70.88	73.18	70.32	77.55
Nd	53.04	62.99	31.62	33.41	41.78	31.24	28.75
Sm	6.86	9.96	3.50	4.76	4.47	4.74	6.54
Eu	1.12	1.39	0.67	0.70	0.70	0.71	1.00
Tb	0.68	0.90	0.29	0.39	0.38	0.23	0.72
Dy	4.00	6.31	1.95	3.29	2.91	2.62	4.31
Yb	2.18	3.69	1.27	1.62	1.53	1.34	0.00
Lu	0.31	0.46	0.16	0.21	0.22	0.19	0.33

Table 4. Continued

The bulk volcanic ash ICPMS data was corrected for loss on ignition (LOI) and is plotted on a total alkali versus silica (TAS) diagram (Figure 5). These volcanic ash samples show a range of alkali ($Na_2O + K_2O$) content and silica (SiO_2) content, but the composition reflects combined composition of voclanic ash components and alteration products. Voclanic ash composition occurs in two clusters, with one plotting in the rhyolite field and the other in the dacite field.

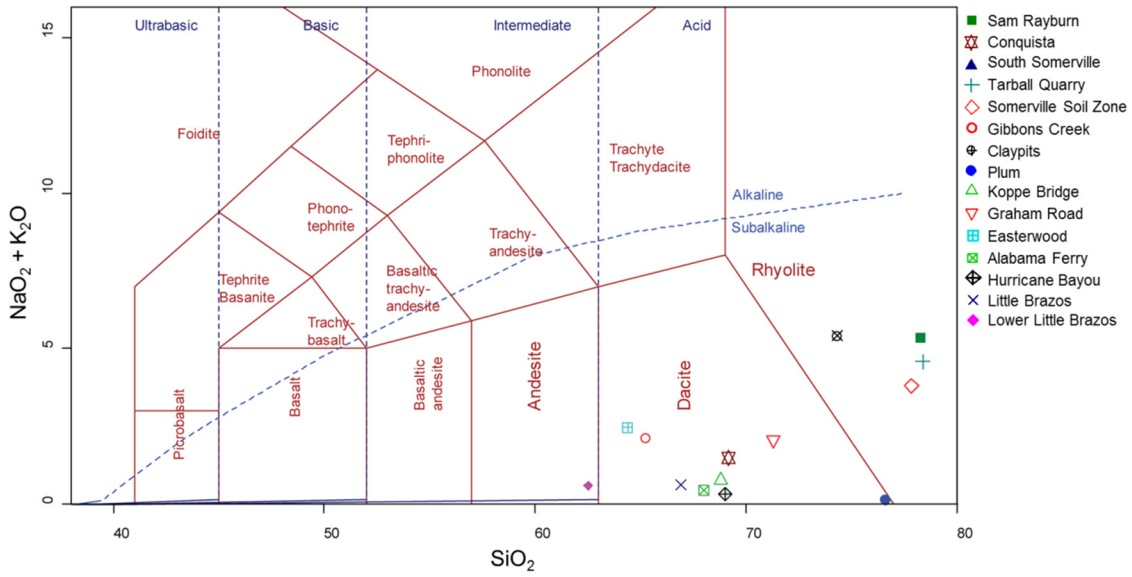

Figure 5. TAS diagram (Le Bas 1986) showing $Na_2O + K_2O$ versus SiO_2 data from the ICPMS bulk volcanic ash analysis. Data is corrected for LOI and is in wt %. Plotted with GCDkit (Janoušek et al. 2006).

The ICPMS trace element data is plotted in Figure 6 in a form normalized to primitive mantle values of McDonough and Sun (1995). Trace element compositions for all samples are similar with some variation in Rb, Ba, Nb, K, Sr and P. Elements plotted to the left of La are more abundant than those to the right except for Nb. All of the samples are depleted in Nb, P and Ti. The samples dominated by volcanic glass shards, Sam Rayburn, Conquista, South Somerville, Tarball Quarry and Claypits can be identified by their lower level (600-800 ppm) of Ti (Table 3). The Conquista volcanic ash stands out with noticeably higher level of U, slightly higher Th and a lower level of Ba.

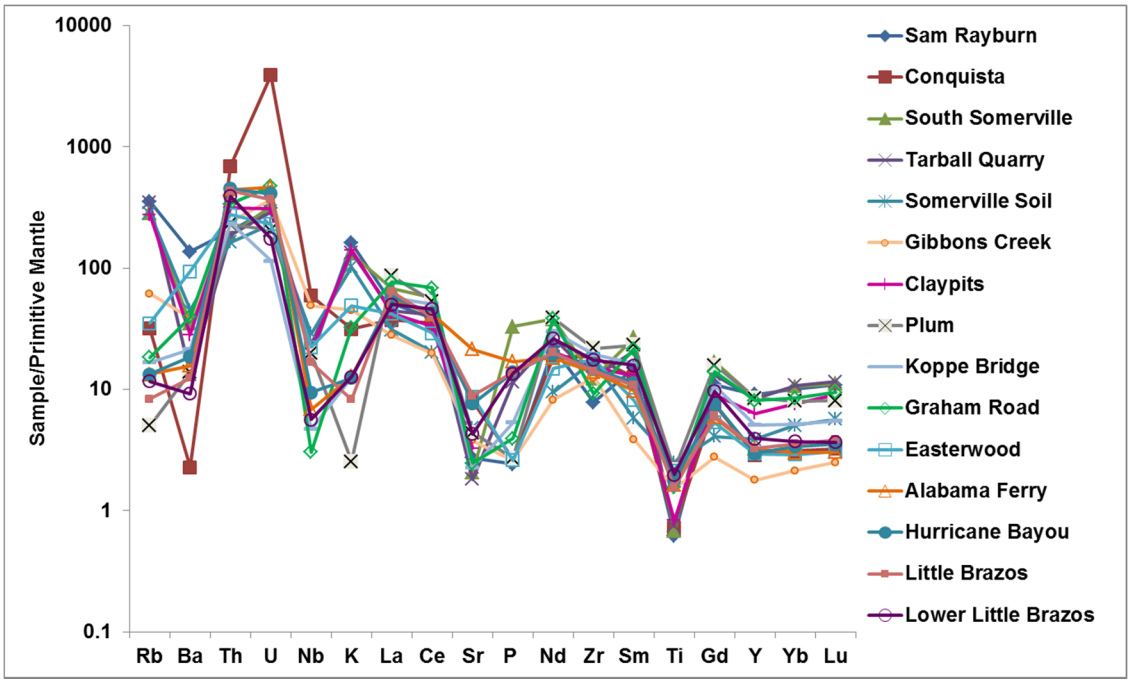

Figure 6. Trace element data from ICPMS analysis of bulk volcanic ash samples. Values are in ppm and normalized to the primitive mantle values of McDonough and Sun (1995).

The REE data was collected from ICPMS analysis of bulk volcanic ash is plotted in Figure 7 in a form normalized to chondrite values of McDonough and Sun (1995). The REE composition is generally the same with all bulk volcanic ash samples, exhibiting enrichment in light rare earth elements (LREE) and very similar values for all heavy rare earth elements (HREE). The HREE have a flat or slightly concave-up trace on the diagram. The Conquista ash has a greater Eu anomaly compared to other samples and the Gibbons Creek ash has the lowest REE values of all the samples.

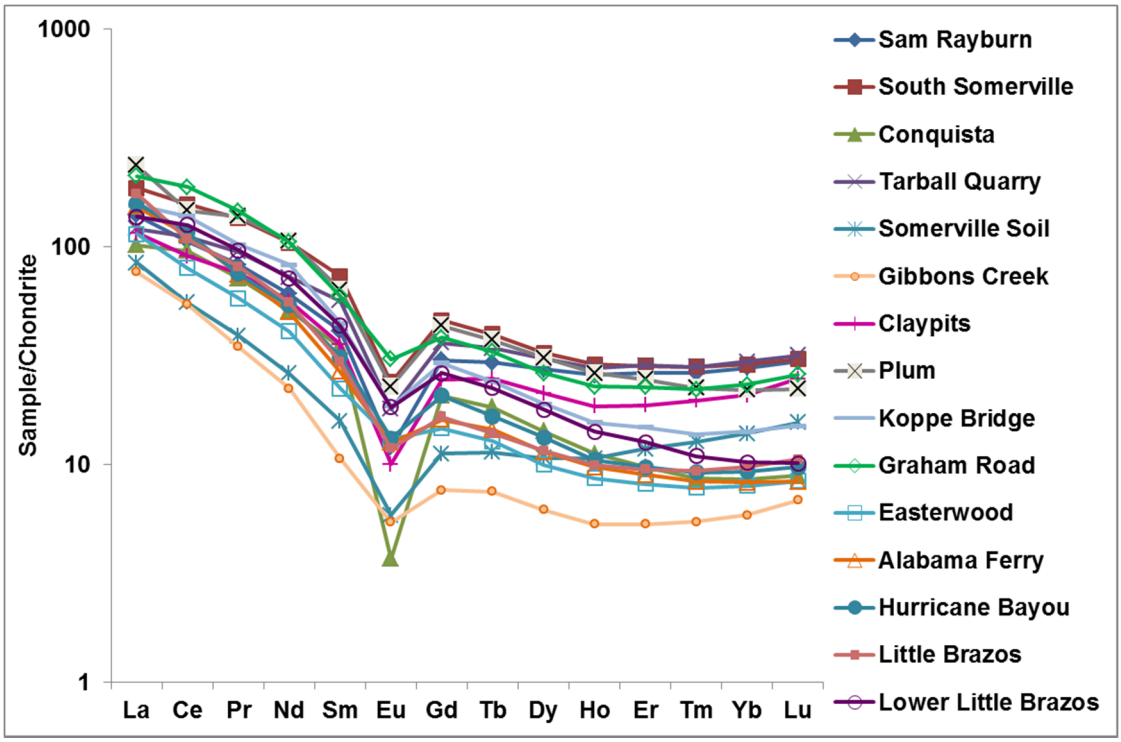

Figure 7. REE data from ICPMS analysis of bulk volcanic ash. All values are in ppm and normalized to the chondrite values of McDonough and Sun (1995).

La/Yb ratios show the degree of fractionation in the light and heavy REE and can be used to characterize the volcanic ash samples. The glass-dominated Tarball Quarry, Sam Rayburn, South Somerville, Claypits, and Somerville Soil Zone samples exhibit lower levels of fractionation with La/Yb ratios between 4 and 8, excluding the Conquista ash outlier that is closer to 12 (Figure 8). The Graham Road, Plum, Koppe Bridge, Conquista, Gibbons Creek, Easterwood, Lower Little Brazos, Little Brazos, Alabama Ferry and Hurricane Bayou samples all have La/Yb ratios from 9 to 19.

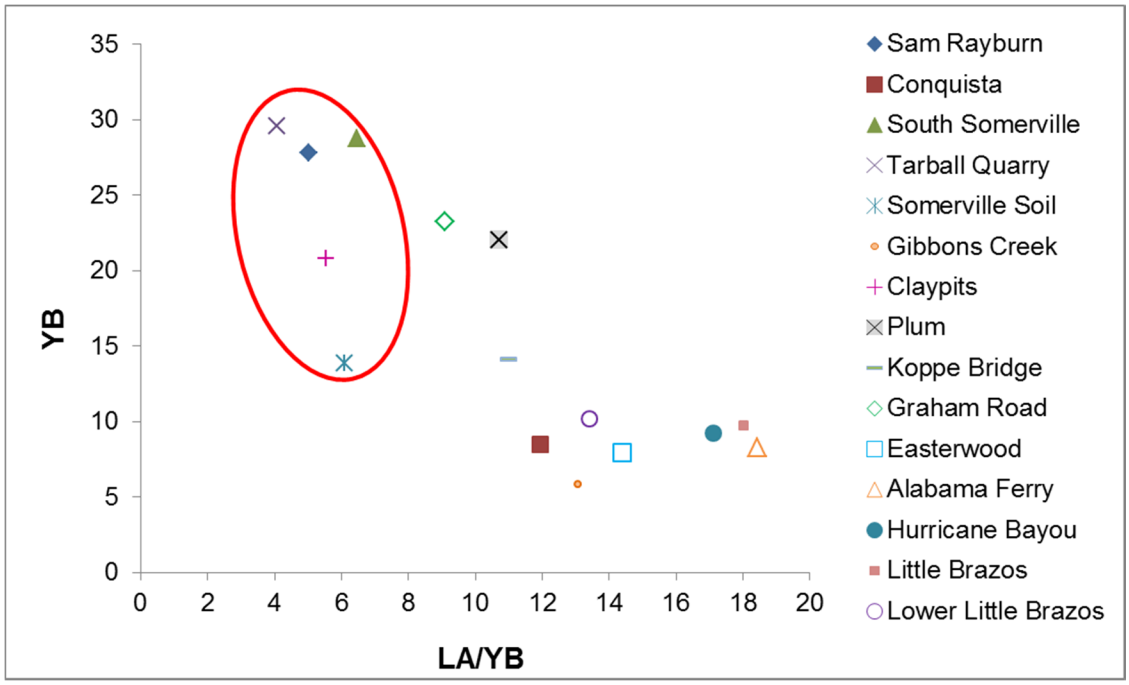

Figure 8. Plot of La/Yb versus Yb showing the measure of the degree of REE fractionation with changing REE content in bulk volcanic ash data from ICPMS analysis. Glass-dominated samples are circled. Values are in ppm and normalized to the chondrite values of McDonough and Sun (1995).

La/Sm ratios can be used to distinguish the volcanic ash samples into two groups by the level of LREE fractionation. The Easterwood, Hurricane Bayou, Alabama Ferry, Somerville Soil Zone, and Gibbons Creek samples show higher levels of LREE fractionation with La/Sm ratios between 5 and 7.5 (Figure 9). The South Somerville, Tarball Quarry, Plum, Graham Road, Koppe Bridge, Sam Rayburn, Lower Little Brazos, Claypits, and Conquista samples exhibit lower levels of LREE fractionation with La/Sm ratios from 2 to 4.

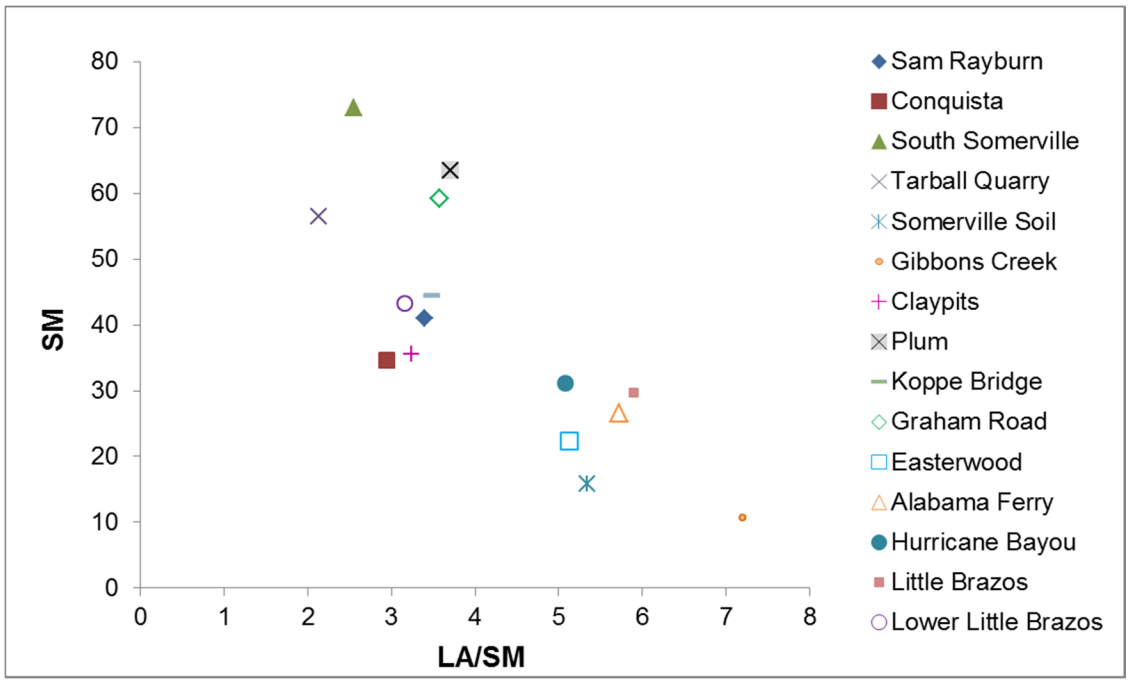

Figure 9. Plot of La/Sm versus Sm showing the degree of LREE fractionation with changing REE content in bulk volcanic ash from ICPMS analysis. Values are in ppm and normalized to chondrite values of McDonough and Sun (1995).

Volcanic Glass Shard Chemistry

Major element data from microprobe analysis of individual volcanic glass shards is available from seven ash beds in the Late Eocene Manning Formation and the Early Oligocene Catahoula Formation (Table 5). All plots and tables list the volcanic ash samples in stratigraphic order from youngest (Sam Rayburn) to oldest (Claypits). Results from the Claypits, Sam Rayburn and Seale Ranch (Muldoon average) volcanic ashes previously analyzed by Yancey and Guillemette (1998) are shown for comparison. Analysis of the Sam Rayburn volcanic glass is repeated in this study with the original volcanic glass shards used by Yancey and Guillemette (1998) and showed good reproducibility between the two analyses. The South Somerville volcanic glass shard sample is equivalent to the Top Jackson volcanic glass shard sample from Yancey and Guillemette (1998) and the two analyses also show good reproducibility even though they were collected at different times.

Element	Sam Rayburn	Conquista	South Somerville	Tarball	Somerville Soil Zone	Seale Ranch	Claypits
Number Analyses	63	37	37	20	82	56	33
SiO_2	74.40 (0.50)	72.63 (0.36)	72.05 (0.32)	72.13 (0.29)	73.40 (0.50)	73.95 (0.60)	72.80 (0.30)
Al_2O_3	12.00 (0.10)	11.37 (0.10)	11.49 (0.15)	11.77 (0.13)	11.80 (0.10)	11.90 (0.30)	11.60 (0.10)
K_2O	4.30 (0.30)	5.89 (0.09)	6.09 (0.13)	6.27 (0.13)	5.80 (0.40)	4.50 (0.35)	5.20 (0.10)
CaO	0.39 (0.50)	0.33 (0.02)	0.38 (0.03)	0.36 (0.02)	0.41 (0.06)	0.39 (0.17)	0.30 (0.02)
Na_2O	1.60 (0.08)	2.52 (0.12)	2.32 (0.27)	2.10 (0.12)	2.13 (0.30)	2.10 (0.30)	2.70 (0.10)
FeO	0.58 (0.12)	0.79 (0.06)	0.93 (0.06)	0.64 (0.05)	0.72 (0.10)	0.83 (0.18)	0.53 (0.05)
Total wt%	93.48 (0.38)	93.73 (0.57)	93.53 (0.40)	93.55 (0.39)	94.38 (0.96)	93.95 (0.90)	93.36 (0.37)

Table 5. Electron microprobe data in wt % from the analysis of individual volcanic glass shards. Data is shown as an average of analyses with total wt % over 93 %. Values in parentheses are one standard deviation. Results from the Claypits, Sam Rayburn and Seale Ranch (Muldoon average) volcanic ashes are from Yancey and Guillemette (1998).

Backscatter electron (BSE) images taken from the volcanic glass shard separates prior to analysis show cuspate volcanic glass shards with some shards containing bubbles (Figure 10). Volcanic glass shards within the South Somerville, Conquista and Tarball Quarry samples range from 400 to 100 µm with the South Somerville containing the coarsest glass shards.

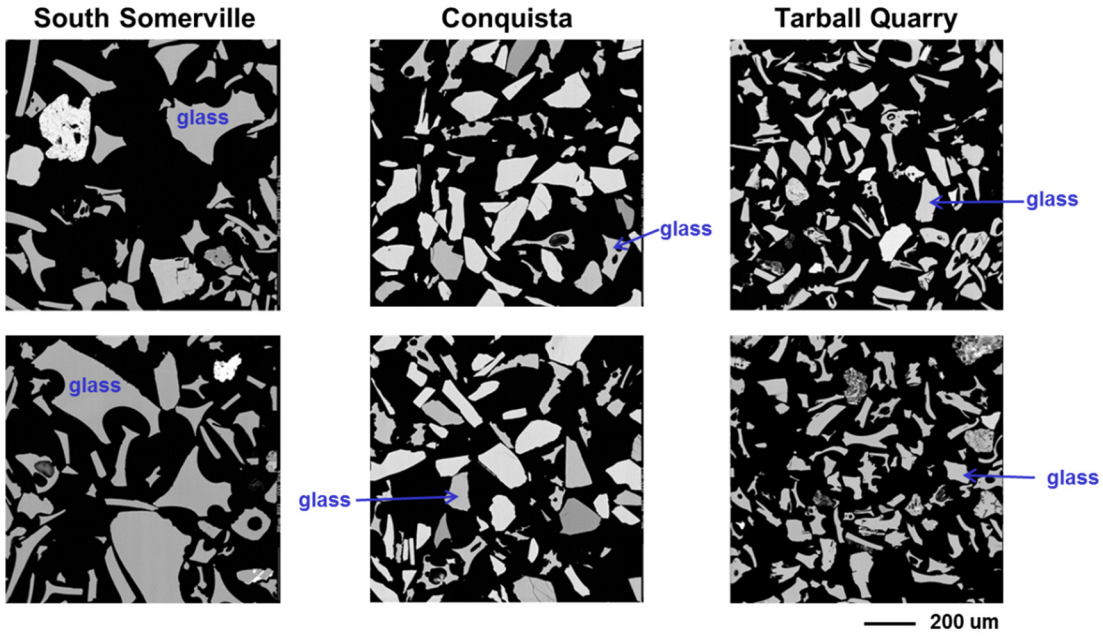

Figure 10. BSE images showing the South Somerville, Conquista and Tarball Quarry volcanic glass separates. Examples of glass are given for each sample.

Many of the glass shards give analytical totals substantially below 100 %. Following the procedures of Yancey and Guillemette (1998), shards with totals less than 93 % are considered too altered to be a good representation of the original chemistry and are not discussed. The devitrification of volcanic glass shards is an alteration process that involves a loss of the more mobile elements and subsequent hydration. Na and K are more mobile than Ca and Si, with Al and Fe being the least mobile during alteration of the major elements. The lower wt % total corresponds to lower levels of Na and K in most of the glass analyses. This decrease in alkali corresponding with total wt % is present in the South Somerville sample, but is more pronounced in the Tarball Quarry sample that contains the smallest glass shards (Figure 11).

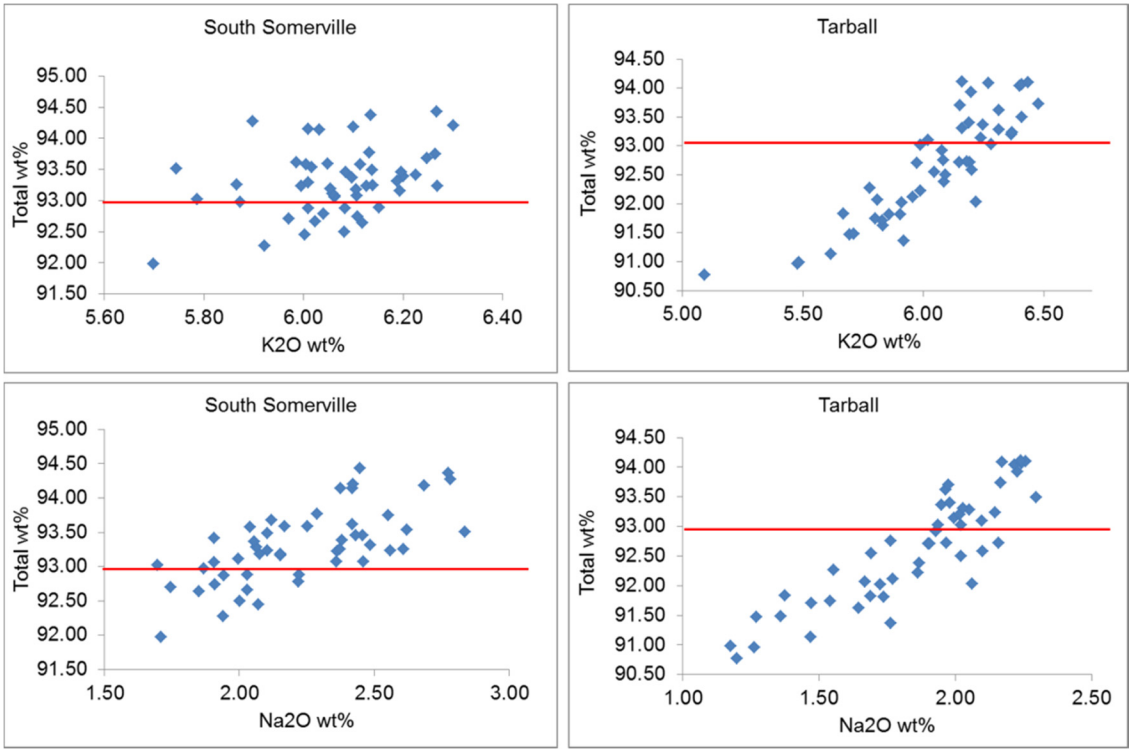

Figure 11. Alkali data plotted versus total wt % for the South Somerville and Tarball Quarry individual glass shard analyses. The 93 total wt % cut off from Yancey and Guillemette (1998) is shown.

Major element data is fairly consistent in the volcanic ash samples with preserved glass shards. The seven samples containing glass shards all carry a geochemical fingerprint corresponding to sub-alkaline (<10 % alkali) rhyolitic magma on a TAS diagram (Figure 12). The volcanic glass shards have variable total alkali content with samples from the Conquista, South Somerville, Claypits, Tarball Quarry and Somerville Soil Zone being comparable to each other in Na, K and Si composition, but the Seale Ranch and Sam Rayburn samples have lower alkali content. The Na_2O content of the Sam Rayburn volcanic glass shards is significantly lower (72% of the average) than other samples, and it also has the highest SiO_2 content. The largest variation in the major elements is in FeO content, but FeO is less than one percent in all samples.

Comparison of bulk volcanic ash ICMPS data to the microprobe glass shard data from the Sam Rayburn, Conquista, South Somerville, Tarball Quarry, Somerville Soil Zone and Claypits samples show differences in the major element values between the two data sets. All of the samples show a loss of Na_2O, K_2O, and SiO_2 with a subsequent gain in Al_2O_3, FeO, and CaO in the bulk volcanic ash data (Table 3; Table 5).

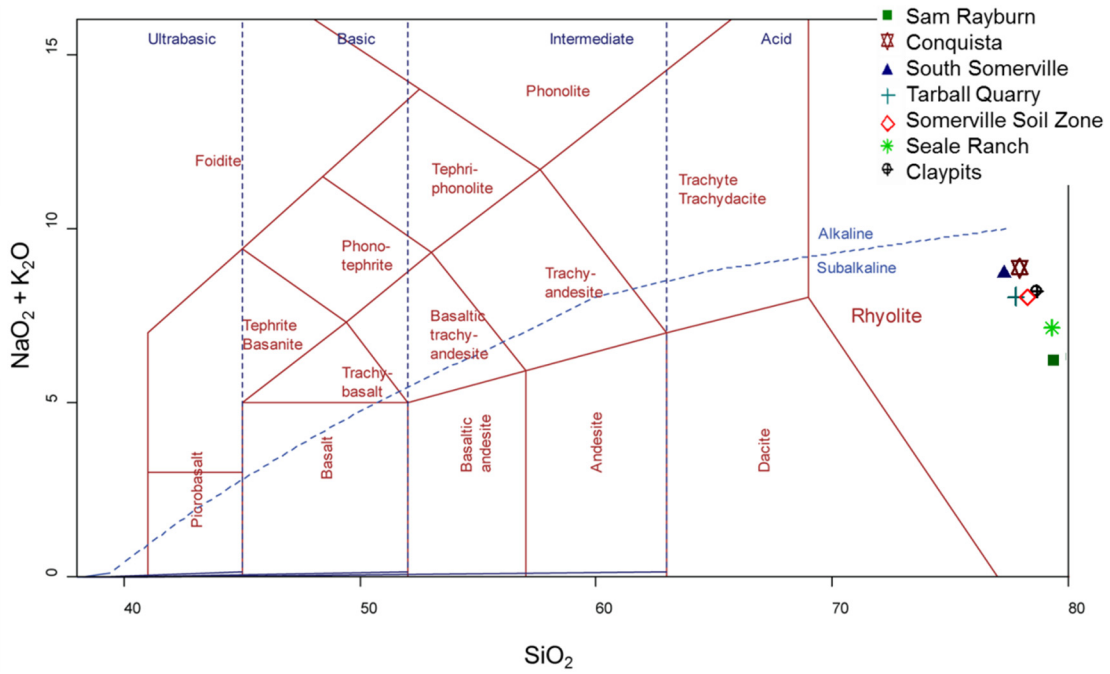

Figure 12. TAS diagram (Le Bas 1986) showing $Na_2O + K_2O$ versus SiO_2 data from the seven glass bearing volcanic ashes. Data is normalized to 100 wt %. Claypits, Somerville Soil Zone and Seale Ranch data are from Guillemette and Yancey (1998). Plotted using GCDkit software (Janoušek et al. 2006).

Trace element and REE data obtained from NAA of volcanic glass shards is presented in Table 6 in ppm. The Somerville Soil Zone and Seale Ranch volcanic ash samples contained enough volcanic glass shards for microprobe analysis, but not enough for NAA.

Element	Sam Rayburn	Conquista	South Somerville	Tarball	Claypits
Na	8290.19	17887.03	16521.96	11127.32	18729.77
Al	67526.60	61096.66	60686.55	62608.50	62362.00
K	32069.54	47644.32	46374.01	29226.15	42926.27
Ca	<3000	<2000	2789.64	2351.86	3278.13
Sc	5.13	1.85	2.25	3.84	4.49
Ti	<3000	<2000	<2000	<2000	<3000
V	<30	<30	<30	<30	<30
Cr	12.67	9.60	10.08	11.74	21.11
Mn	468.09	587.03	394.41	717.74	605.66
Fe	7198.34	6470.06	7430.28	5151.35	5758.20
Co	1.54	0.34	0.62	0.81	1.68
Zn	63.23	46.95	51.73	89.89	76.91
As	8.77	3.32	2.69	1.93	4.66
Rb	223.88	267.33	201.89	227.95	218.96
Zr	138.74	101.87	150.92	118.53	124.11
Sb	3.18	0.89	1.60	1.73	1.76
Cs	5.84	9.03	6.99	7.73	6.32
Ba	672.92	62.48	128.20	89.29	180.72
Hf	4.38	5.51	5.35	5.91	4.71
Ta	1.38	2.83	2.15	1.57	1.54
Th	16.82	34.56	22.18	17.61	23.22
U	5.56	9.74	5.20	4.05	7.45
La	22.36	29.68	50.17	25.64	25.41
Ce	54.60	71.50	102.66	58.32	55.97
Nd	18.80	22.83	33.43	26.49	23.45
Sm	6.02	8.02	7.06	5.65	5.40
Eu	0.41	0.11	0.20	0.60	0.41
Tb	0.87	1.29	0.89	0.90	1.03
Dy	6.13	8.27	5.42	4.46	7.25
Yb	3.63	6.51	4.69	3.83	4.99
Lu	0.46	1.07	0.63	0.47	0.57

Table 6. Raw NAA data of volcanic glass shards. <Number = below detection limit.

Trace element compositions of the volcanic glass samples are similar with Ba showing the most variation (Figure 13). Elements plotted to the left of La are more abundant than those to the right except for Ba. All of the samples are depleted in Ba, but the Sam Rayburn sample has a significantly higher level of Ba.

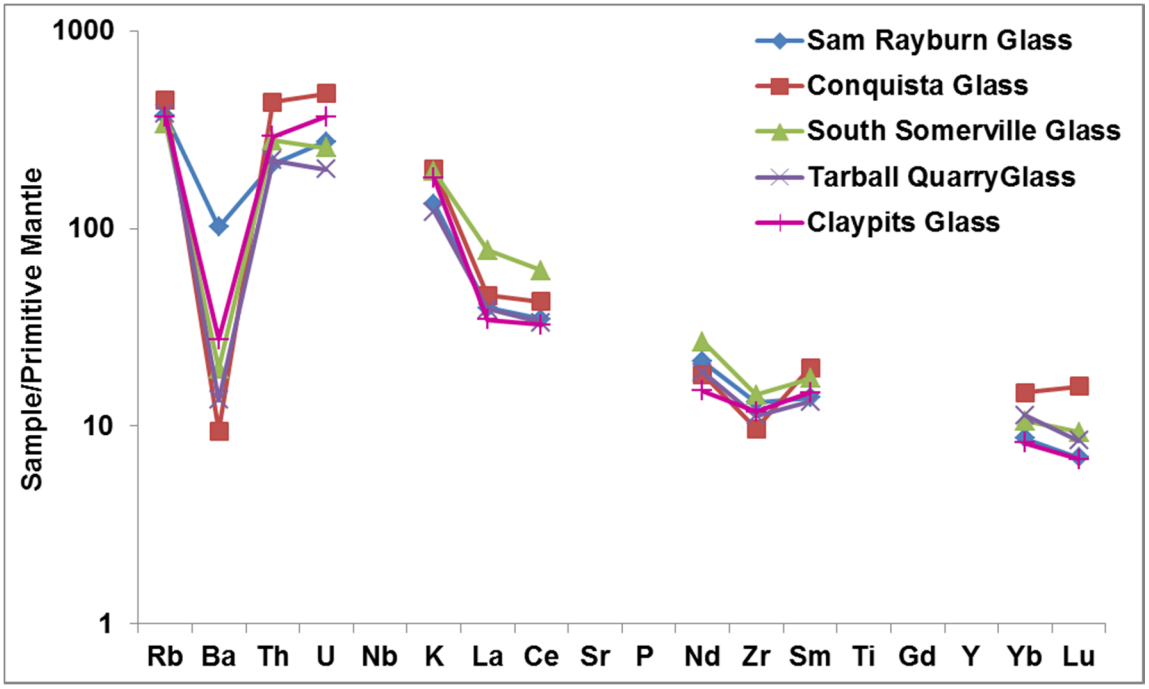

Figure 13. Trace element data from NAA of volcanic glass shards. All values are in ppm and normalized to the primitive mantle values of McDonough and Sun (1995).

REE compositions for the glass shard analysis are all very similar (Figure 14). Gd values were calculated using the slope of Sm to Tb to show the negative Eu anomaly and the values are normalized to the chondrite values of Sun and McDonough (1995). The samples show LREE enrichment with a moderate to large Eu anomaly and a flat HREE pattern.

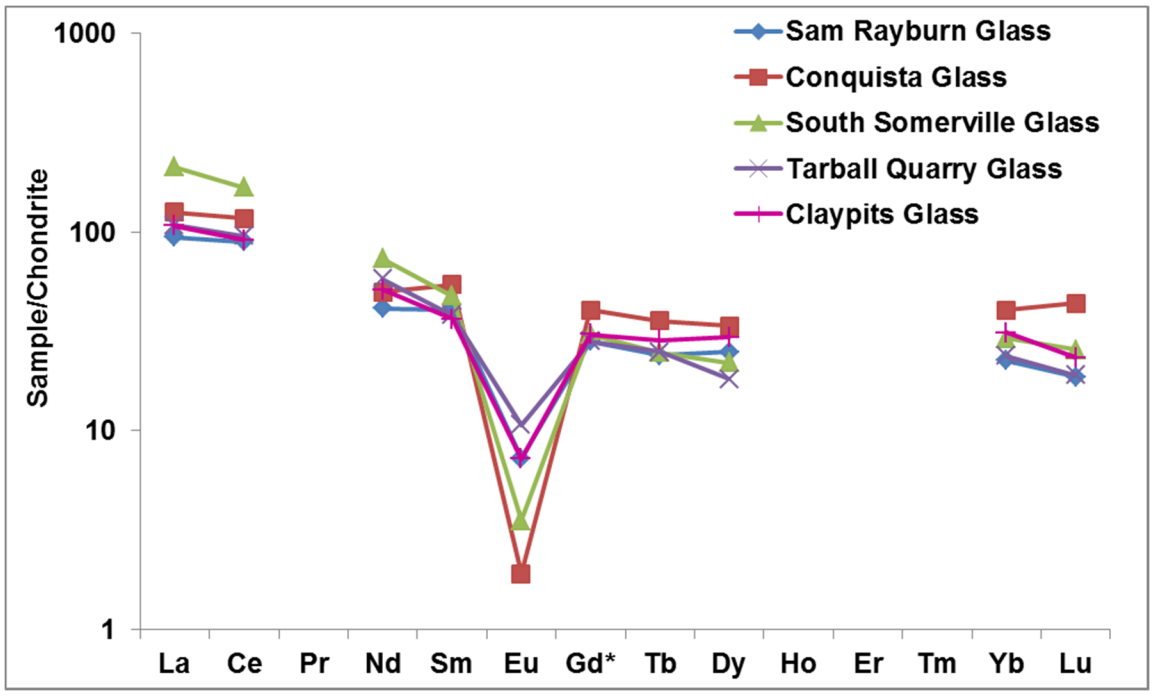

Figure 14. REE data from NAA of volcanic glass shards. Values are in ppm and normalized to the chondrite values of Sun and McDonough (1995).

Apatite Phenocryst Chemistry

Apatite phenocryst analysis provides an additional tool to support correlations identified by bulk volcanic ash analysis. Individual apatite phenocrysts from the four Crockett Formation ash samples were analyzed by electron microprobe (Table 7). Apatite analysis provided data on major element, trace element and REE reported in wt % oxide. Elements such as Mg, Cl, Mn, Fe, Ce and Y had sufficient variability to be efficient discriminators.

Element	Little Brazos	Alabama Ferry	Hurricane Bayou	Lower Little Brazos
Number Analyses	11	11	11	11
F (wt %)	2.502 (0.23)	2.431 (0.15)	2.429 (0.21)	3.287 (0.45)
MgO	0.113 (0.05)	0.094 (0.04)	0.115 (0.05)	0.186 (0.08)
P_2O_5	41.797 (0.38)	41.663 (0.25)	41.795 (0.53)	42.055 (0.31)
Cl	0.954 (0.11)	0.940 (0.08)	0.915 (0.11)	0.540 (0.10)
CaO	54.340 (0.25)	54.208 (0.22)	54.220 (0.15)	54.307 (0.23)
MnO	0.211 (0.02)	0.214 (0.01)	0.201 (0.03)	0.128 (0.04)
FeO	0.195 (0.05)	0.179 (0.04)	0.205 (0.06)	0.257 (0.07)
SrO	0.054 (0.01)	0.050 (0.01)	0.055 (0.01)	0.072 (0.02)
Y_2O_3	0.114 (0.04)	0.121 (0.03)	0.129 (0.02)	0.165 (0.05)
La_2O_3	0.174 (0.06)	0.207 (0.04)	0.209 (0.05)	0.157 (0.05)
Ce_2O_3	0.394 (0.11)	0.465 (0.11)	0.474 (0.08)	0.378 (0.12)
Nd_2O_3	0.200 (0.06)	0.227 (0.06)	0.224 (0.04)	0.242 (0.07)
Total (wt %)	100.339 (0.35)	100.146 (0.26)	100.330 (0.58)	100.480 (0.37)

Table 7. Raw data shown as average wt % from microprobe analysis of individual apatite phenocrysts. Values in parentheses are one standard deviation.

The Little Brazos, Alabama Ferry and Hurricane Bayou apatite analyses cluster closely together on a plot of Cl versus Mg versus Mn (Figure 15). The Lower Little Brazos sample is comparable to the other samples, but has lower levels of Cl and Mn. There are two outliers in the dataset, but two definitive groupings are shown in the plot.

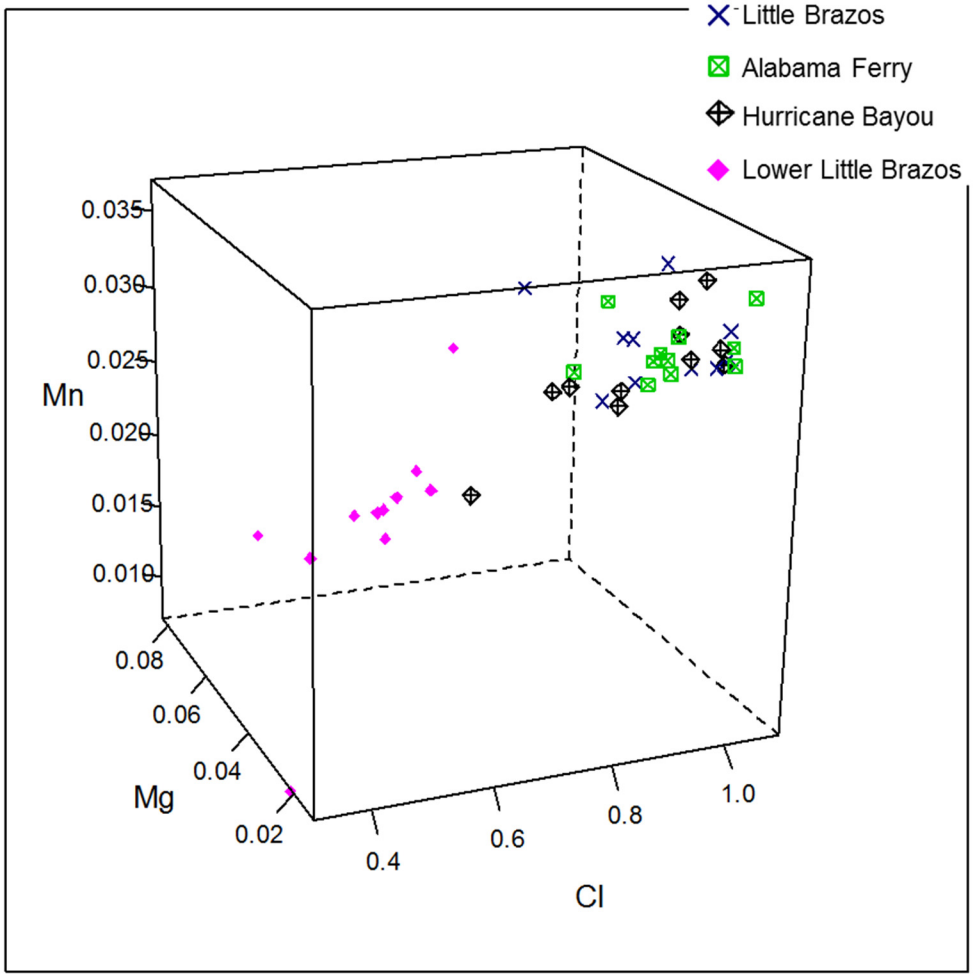

Figure 15. Plot of Mg versus Mn versus Cl (wt %) from individual apatite microprobe analysis. Plotted using GCDkit software (Janoušek et al. 2006).

$^{40}Ar/^{39}Ar$ Dating

Radiometric ages are available from $^{40}Ar/^{39}Ar$ dating of individual sanidine phenocrysts separated from the volcanic ash beds. Nine volcanic ash beds of the 16 submitted contained sanidine crystals large enough to be effectively dated using the single crystal method of analysis (Table 8). Detailed results are presented in Appendix A.

Sample	MSWD	n/n	Age(Ma)	2σ
Catahoula	1.5	17/26	30.65	±0.06
Conquista	11.1	26/29	34.07	±0.08
South Somerville	1.3	19/22	34.10	±0.02
Tarball Quarry	1.4	4/17	34.39	±0.10
Somerville Soil Zone	0.8	8/28	34.91	±0.20
Gibbons Creek	9.0	23/27	34.54	±0.03
Graham Road	2.1	7/11	35.83	±0.13
Easterwood	0.3	10/19	36.86	±0.07
Hurricane Bayou	1.3	9/24	41.79	±0.02

Table 8. Summary table of $^{40}Ar/^{39}Ar$ dating of individual sanidine phenocrysts. n/n = number grains providing preferred age/number of grains dated. MSWD = mean square of weighted deviates. All errors at 2σ and include error in J factor. Error in decay constant not included.

Sanidine phenocrysts in the samples are mostly about 125 μm in size, therefore yielding a low volume of argon, except for the Gibbons Creek and South Somerville sanidines that were significantly coarser at 350 μm. Each sanidine separate from a volcanic ash bed contained a cluster of sanidine grains with similar ages mixed with a variable amount of older grain ages. Weighted mean ages are calculated for the dominant age mode, correcting for the skew in age created by older grains. The uncertainty associated with the ages varies greatly, with the South Somerville ash having

the lowest uncertainty (±0.02) and the Somerville Soil Zone with the highest uncertainty (±0.20) (Figure 16). All of the determined ages agree with the in stratigraphic order of the ash beds except for the Somerville Soil Zone ash, the volcanic ash bed with the lowest level of accuracy.

The group of grain ages used to calculate each ash bed age is based upon culling older grains until the mean square of weighted deviates (MSWD) is between one and two, indicating that the ages are distributed normally. The Conquista and Gibbons Creek sanidines are two exceptions to this method, with the MSWD values between eight and twelve. The sanidine grains dated for these two samples do not have an obvious cutoff for older grains that could have been brought in by reworking or inherited by incorporation of older rock or magma at the eruption source, so the majority of grain ages were included in calculations to determine the age of eruption that produced the volcanic ash bed.

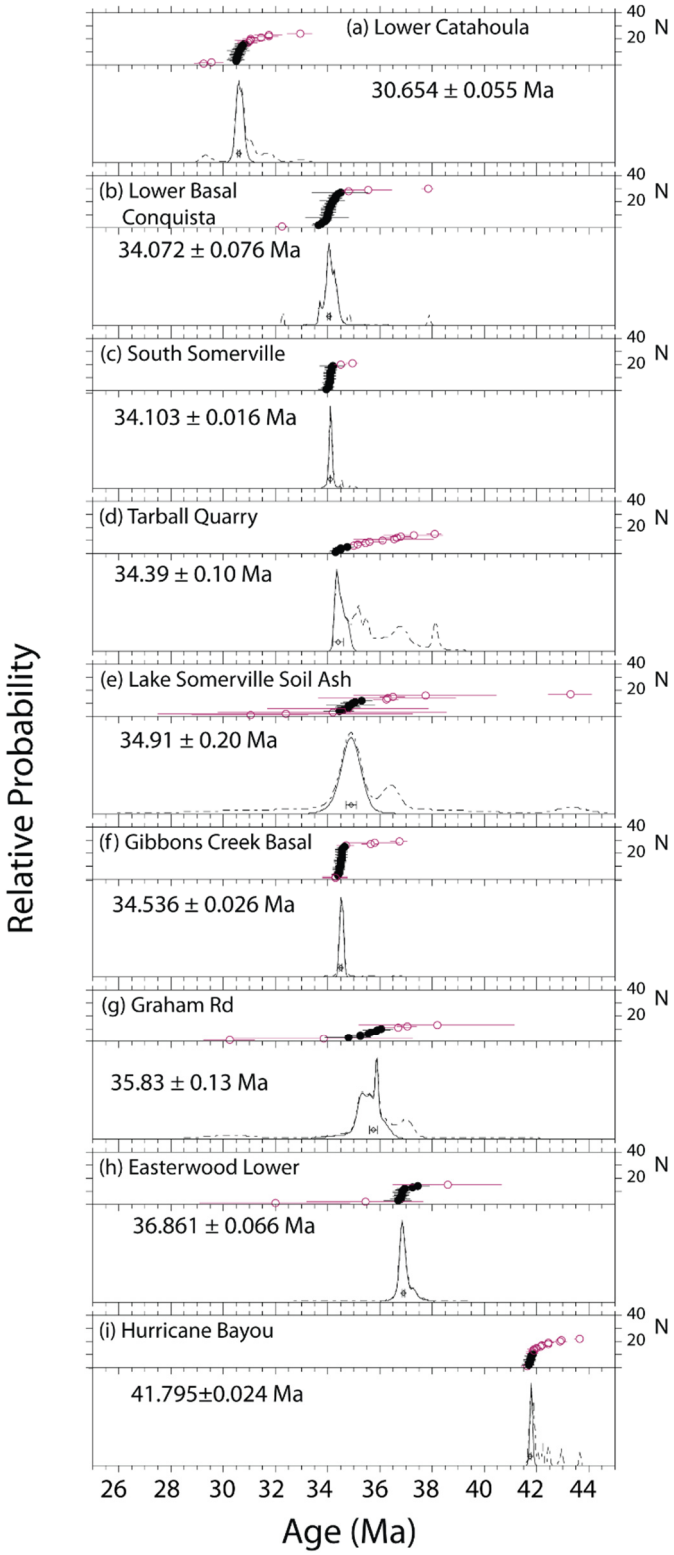

Figure 16. Summary of age probability data presented in stratigraphic order from youngest to oldest.

DISCUSSION

$^{40}Ar/^{39}Ar$ Dating

Five of the nine new age dates, from volcanic ash beds in Manning Formation strata, group with a published age date of 34.93 ±0.12 Ma for the Claypits ash bed (Guillemette and Yancey 1996), ranging in age from 34.93 ±0.12 Ma to 34.07 ±0.08 Ma. Four of the age dates come from volcanic ash beds 1 m or more in thickness, indicating a time of major eruptive activity with frequent large eruptions. The Somerville Soil Zone ash date of 34.91 ±0.20 is excluded from this discussion because it includes a significant population of inherited grains, with some of them as old as 1000 Ma. This volcanic ash bed also contains sponge spicules, small woody particles and rooting from overlying lignite that indicate that the ash could have been mixed at the time of deposition. For these reasons the Somerville Soil Zone ash radiometric date is considered invalid. An age date of 34.4 ±0.4 Ma for this same ash bed reported by Guillemette and Yancey (1996) and Yancey and Guillemette (1998) is dismissed for the same reason; mixing with older sanidines. This problematic condition is revealed with the new dating work.

Two dates are available for the Yegua Formation, having ages one million years older and two million years older than the Manning ages. This indicates less frequent times of major eruptive activity during the time of deposition of the Yegua Formation. The Crockett Formation date of 41.79 ±0.02 Ma is five million years older and is the oldest major eruptive event recorded in the east Texas section. Marine strata of the Crockett Formation contain at least four other thin volcanic ash beds bracketing the

dated ash bed, indicating frequent small scale eruptions but fewer major eruptions than during the Late Eocene.

Correlation of Volcanic Ash Beds

Plotting of bulk volcanic ash data on a TAS diagram (Figure 5; Figure 12) shows that the major element compositions of bulk volcanic ash is controlled primarily by the amount of diagenetic alteration the ash bed experiences after deposition. Therefore, the major element composition of volcanic glass shards (determined by microprobe analysis) is used to determine the potential for geochemical fingerprinting and correlation. The results obtained in this study are similar to those of Guillemette and Yancey (1996) and Yancey and Guillemette (1998) in showing that major element composition is very similar among glass shard-rich samples and major element data is of little use in correlation of individual volcanic ash beds. However, Guillemette and Yancey (1996) found that FeO levels proved to be an effective discriminator between middle and upper Manning Formation volcanic ashes. The Fe wt % content of glass shards is low, but the non-overlap of standard deviation on element abundance shows a real difference in composition. The new data obtained in this study supports that determination, except that the Seale Ranch sample has a high standard deviation value (0.18) and thus is not a reliable sample for use of the Fe wt % determinations in correlation. Among other Manning Formation samples there is a minor trend of changing Fe content through the section. The trend needs to be validated with sampling in other stratigraphic sections.

Three of the volcanic ash beds have definite or possible lateral occurrence in the Gulf coastal plains section: the Crockett, Caddell and South Somerville. The South Somerville and Plum bulk volcanic ash deposits Inductively Coupled Plasma Mass Spectrometry (ICPMS) analyses have similar rare earth element (REE) values (Figure 17). The Plum volcanic ash has been thought to be located in the basal Manning Formation by correlation of a resistant sandstone that resides below the ash bed (Stenzel 1953). Resistant sandstone beds become more common upward in the section, so it is possible that these two volcanic ashes are equivalent and located in the Upper Manning. Successful radiometric dating of the Plum sample would help test this correlation.

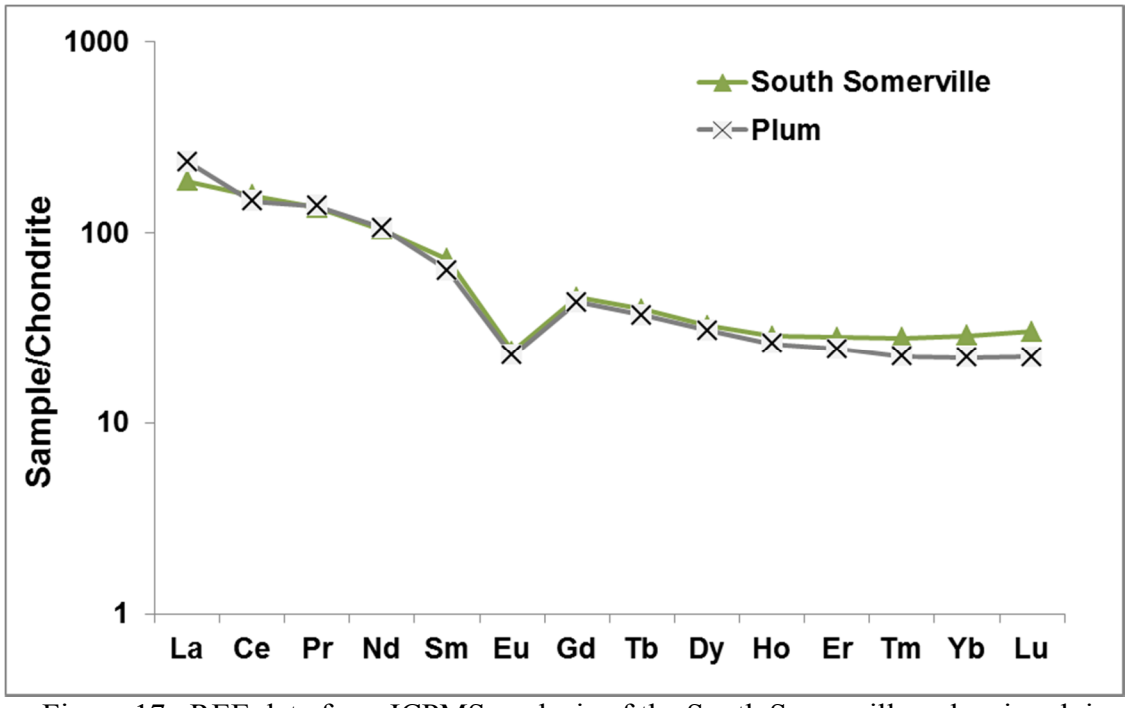

Figure 17. REE data from ICPMS analysis of the South Somerville volcanic ash in Brazos County and Plum volcanic ash in Fayette County. Values are in parts per million (ppm) and normalized to chondrite values of McDonough and Sun (1995).

Michaelides (2011) reported REE ICPMS data on a Caddell Formation volcanic ash that is stratigraphically equivalent to the Koppe Bridge ash (Figure 18). The McBA Gonzales County volcanic ash (of Michaelides 2011) is close in REE composition to the Koppe Bridge sample and the two deposits are thought to be stratigraphically equivalent (Chen 1968). It is possible that these two samples are deposits of the same volcanic ash. Palynology work on the Gonzales County samples would help to constrain this correlation.

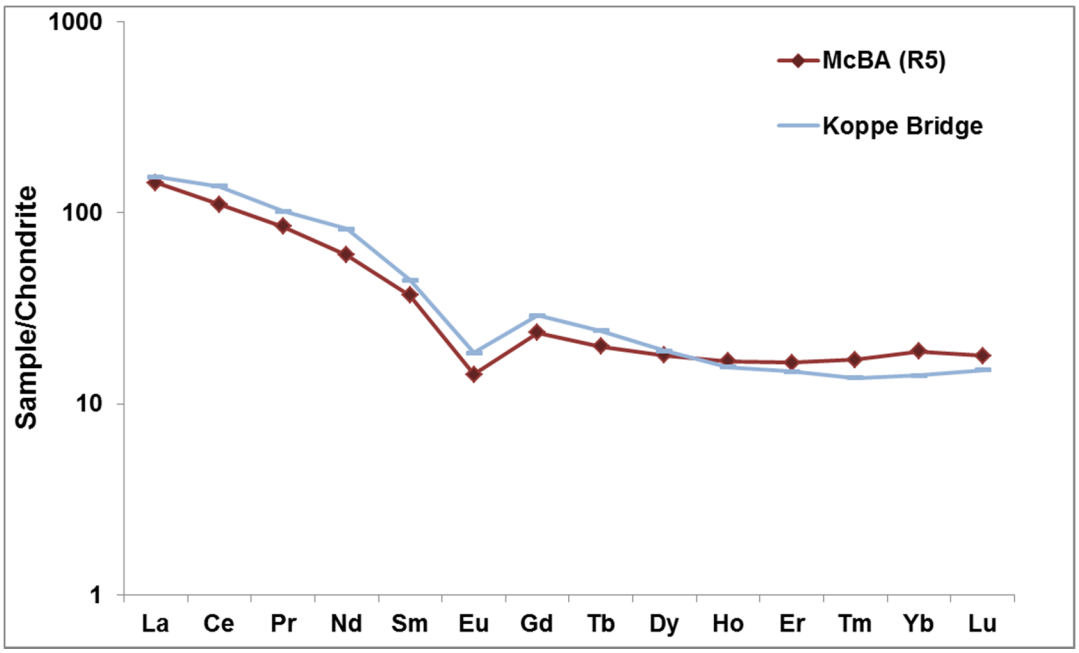

Figure 18. REE data from ICPMS analysis of the Koppe Bridge volcanic ash sample in Brazos County in comparison with the McBA (R5) volcanic ash sample from Gonzales County (Michaelides 2011). Values are in parts ppm and normalized to chondrite values of McDonough and Sun (1995).

Stratigraphic, paleontologic and mineralogical control indicate that the Little Brazos, Alabama Ferry and Hurricane Bayou volcanic ash bed occurrences are lateral exposures of the same thick volcanic ash bed. This conclusion is reinforced by the close similarity in elemental composition on bulk rock samples and on the high similarity of apatite phenocryst composition. There is an age date of 41.85 ±0.38 Ma for the Little Brazos ash exposure (Guillemette and Yancey 1996; Yancey and Guillemette 1998) and an age date of 42.0 ±0.8 Ma (Berggren et al. 1992) for the Alabama Ferry exposure as well as an unpublished age date of 41.66 ±0.52 Ma (John Obradovich to T. Yancey 1997) for the Alabama Ferry exposure. Although varied, these dates are within the assigned uncertainties of each other and the Obradovich dates have not been recalibrated to the new Heizler dates (New Mexico Tech). These are dates from different labs following different protocols and all could possibly be equivalent.

Data from the apatite analysis can be used to discriminate between the Little Brazos and Lower Little Brazos Crockett Formation ashes. Apatite analysis has proven to be an efficient method to correlate highly altered volcanic ash beds that are from a similar tectonic setting. The Little Brazos, Alabama Ferry and Hurricane Bayou bulk volcanic ash ICPMS data are very close in trace element and REE composition, whereas the Lower Little Brazos bulk volcanic ash is similar but slightly different (Figure 19; Figure 20). Minor variance in Rb, Ba, Nb, K, Sr and P could be caused by alteration mobilizing these elements. Studies have found that during the alteration of volcanic glass to clay, elements such as Zr, Nb and P can be mobilized (Zielinski 1982, 1985). Minor variation in Nb could also be caused by the fractionation of fergusonite or

ferrocolumbite in the melt that are known to concentrate Nb (Sheard et. al 2012). Biotite has also been found to fractionate Nb (Pearce and Norry 1979; Stepanov and Hermann 2013).

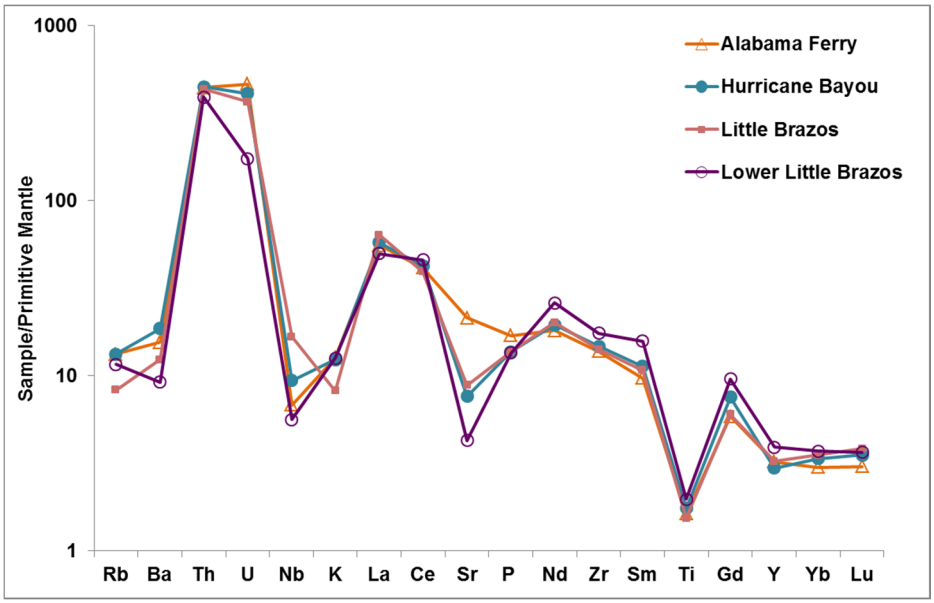

Figure 19. Trace element data from ICPMS analysis of bulk volcanic ash. All values are in ppm and normalized to the primitive mantle values of McDonough and Sun (1995).

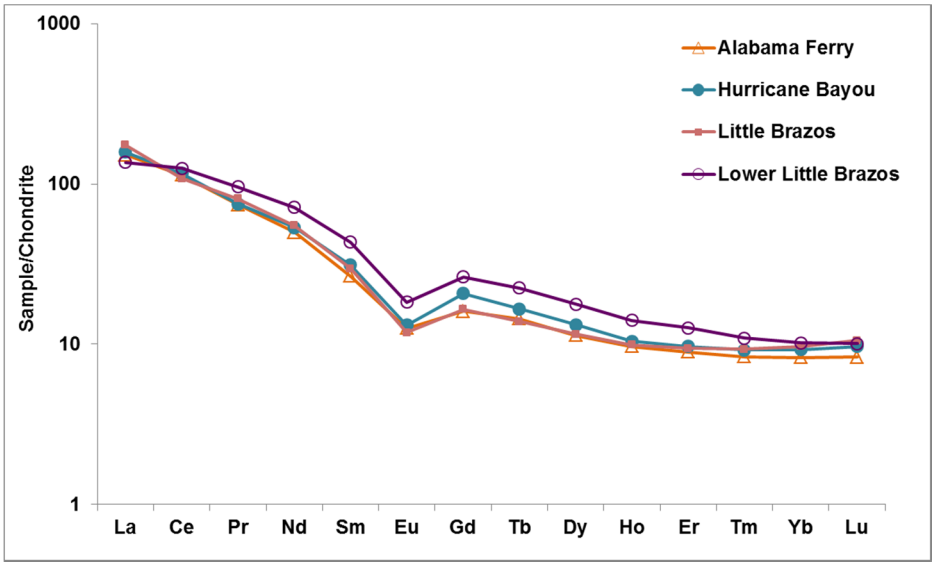

Figure 20. REE data from ICPMS analysis of bulk volcanic ash. Values are in ppm and normalized to primitive mantle values of McDonough and Sun (1995).

Trace element and REE data from the apatite phenocrysts provide additional evidence that the Little Brazos, Alabama Ferry and Hurricane Bayou deposits are part of the same volcanic ash bed. A plot of Mg versus Mn versus Fe shows they have the same range in composition. The Lower Little Brazos is lower in Mn and forms a distinct group, although there is some overlap between the two groups (Figure 21). The plots of Fe versus Mg versus Mn provide additional evidence to the plot of Cl versus Mg versus Mn (Figure 15) that the two clusters are distinct and apatites of the Lower little Brazos ash are compositionally different from the Little Brazos, Alabama Ferry and Hurricane Bayou samples.

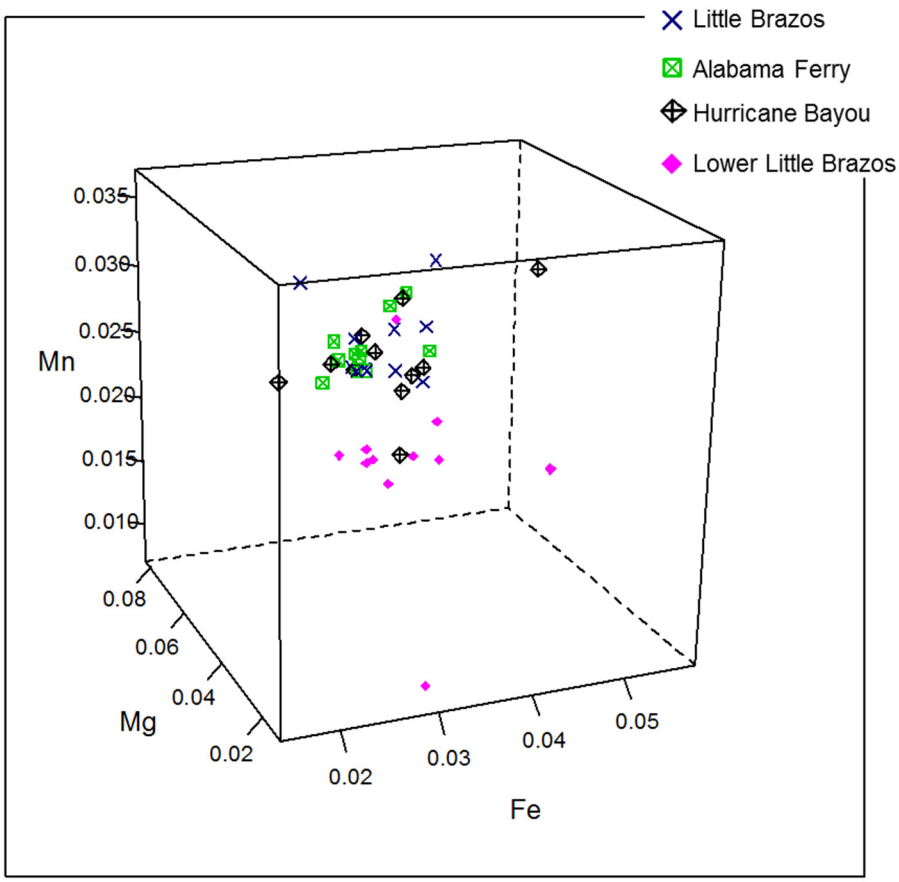

Figure 21. Plot of Fe versus Mg versus Mn (wt %) from individual apatite microprobe analysis. Plotted using GCDkit software (Janoušek et al. 2006).

The ratio of Ce/Y shows the degree of fractionation in the light rare earth elements (LREE) and the heavy rare earth elements (HREE) (Figure 22). The Little Brazos, Alabama Ferry and Hurricane Bayou ash samples are within the same range of each other, with the Lower Little Brazos sample being comparable, yet slightly lower in Ce content. The similar slope of the different analyses indicates that the apatites were crystallized from a similar source.

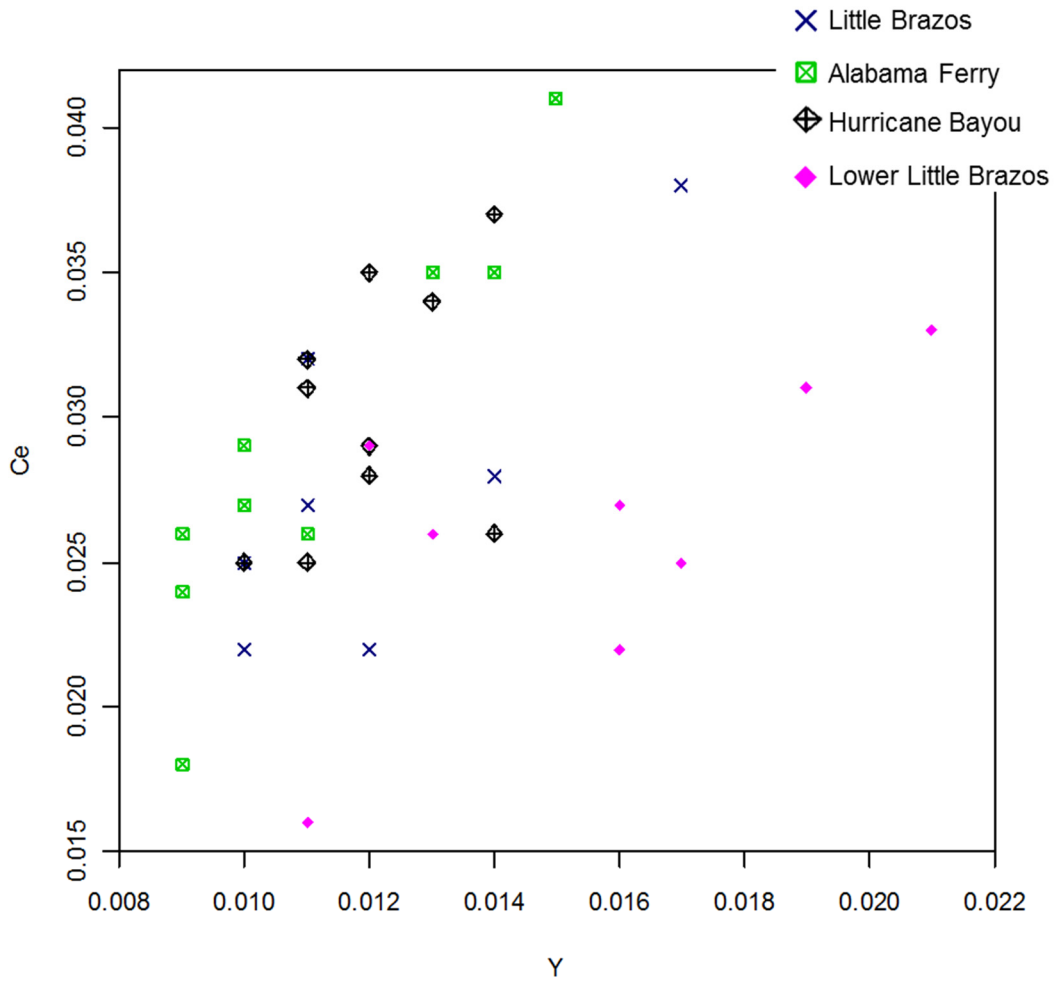

Figure 22. Plot of Ce versus Y (wt %) from microprobe analysis of individual apatite phenocrysts. Plotted using GCDkit software (Janoušek et al. 2006).

Grigsby (1999) reported REE data from ICPMS bulk ash analysis of Eocene volcanic ash beds located in northern Louisiana. He found the St. Johns volcanic ash bed of the Cook Mountain Formation to be equivalent to the Hurricane Bayou volcanic ash deposit. Data from Grigsby (personal communication) is plotted with data for the Hurricane Bayou sample showing the Crockett Formation bulk volcanic ash REE pattern is very similar to the St. Johns bentonite of Claiborne Parish, Louisiana (Figure 23). The St. Johns volcanic ash bed is possibly a lateral extension of the same ash deposit located in the Crockett Formation. This correlation to the St. Johns deposit is tentative and would be more definitive if there was microprobe apatite data available for the St. Johns bentonite.

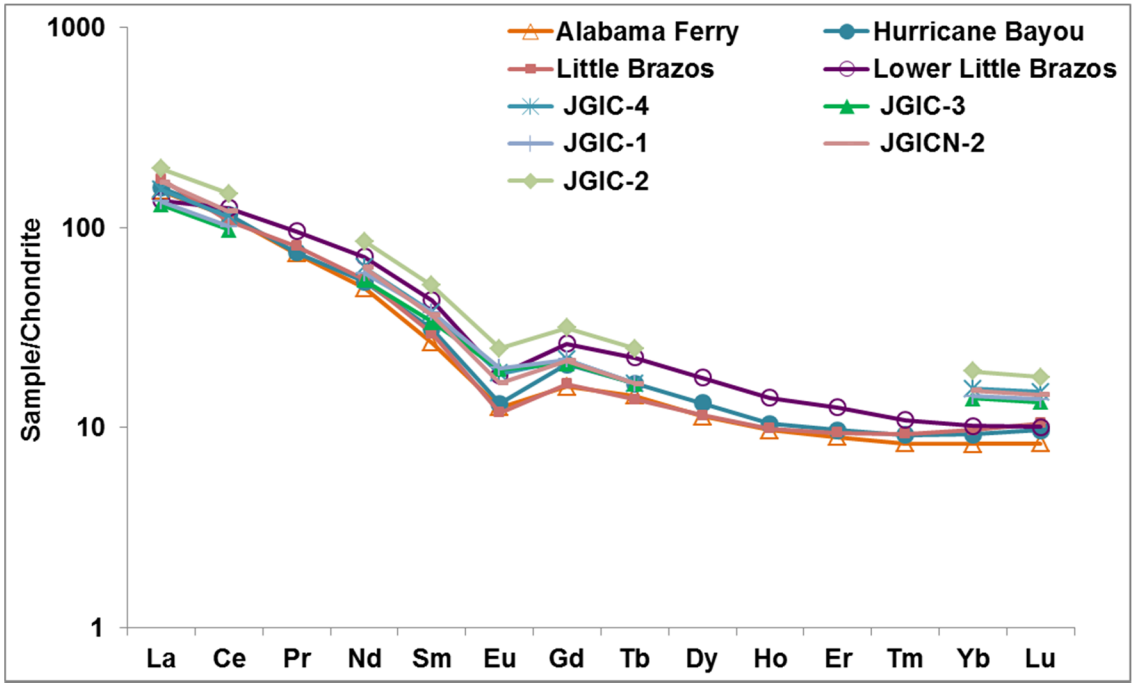

Figure 23. Comparison of ICPMS bulk volcanic ash data of Crockett and Cook Mountain Formation (JGIC) ash beds (Jeff Grigsby personal communication). Values are in ppm and normalized to chondrite values of McDonough and Sun (1995).

Patterns of Volcanic Ash Alteration

Comparison of bulk volcanic ash ICPMS data to microprobe-determined glass shard data reveal how diagenesis has altered the composition of volcanic ashes. The Chemical Index of Alteration (CIA) is a good measure of the degree of chemical alteration the ash has undergone (Nesbitt and Young 1982). The values can range from 0-100 with 100 being the most altered. For example, kaolinite has a CIA of 100, illite falls in the range of 75-90 and feldspars are at 50 (Nesbitt and Young 1982; Fedo et al. 1995).

$$CIA = [Al_2O_3/(Al_2O_3 + CaO + Na_2O + K_2O)]*100$$

The glass-dominated samples of Sam Rayburn, South Somerville, Tarball Quarry, Somerville Soil Zone and Claypits all have lower bulk volcanic ash CIA levels with the Conquista being an outlier with approximately 10% higher values (Table 9). The Gibbons Creek, Plum, Koppe Bridge, Graham Road, Easterwood, Alabama Ferry, Hurricane Bayou, Little Brazos and Lower Little Brazos, which are dominated by smectite and kaolinite, show higher levels of alteration. The glass shard analyses show much lower levels of alteration, although Sam Rayburn has a higher CIA than the others. The Conquista glass is on trend with the rest of the glass analyses CIA.

Sample	Bulk ash CIA	Glass Shard CIA
Sam Rayburn	72	66
Conquista	85	57
South Somerville	75	57
Tarball Quarry	76	57
Somerville Soil Zone	78	
Gibbons Creek	91	
Claypits	74	59
Plum	90	
Koppe Bridge	92	
Graham Road	91	
Easterwood	88	
Alabama Ferry	86	
Hurricane Bayou	85	
Little Brazos	89	
Lower Little Brazos	91	

Table 9. Chemical Index of Alteration (CIA) values of raw bulk volcanic ash ICPMS data and microprobe glass shard analysis (Nesbitt and Young 1982; Fedo et al. 1995).

When major elements are plotted on a total alkali versus silica (TAS) diagram the loss in Na_2O, K_2O, and SiO_2 is illustrated (Figure 24). The bulk volcanic ash samples have undergone different levels of alteration depending on their depositional setting and that is reflected in the mobility of the major elements. These changes in composition increase with greater alteration of the bulk volcanic ash. The REE profiles of all of the volcanic ashes are consistent with rhyolitic volcanism and this supports the interpretation that the major element data is showing alteration trends (Figure 7).

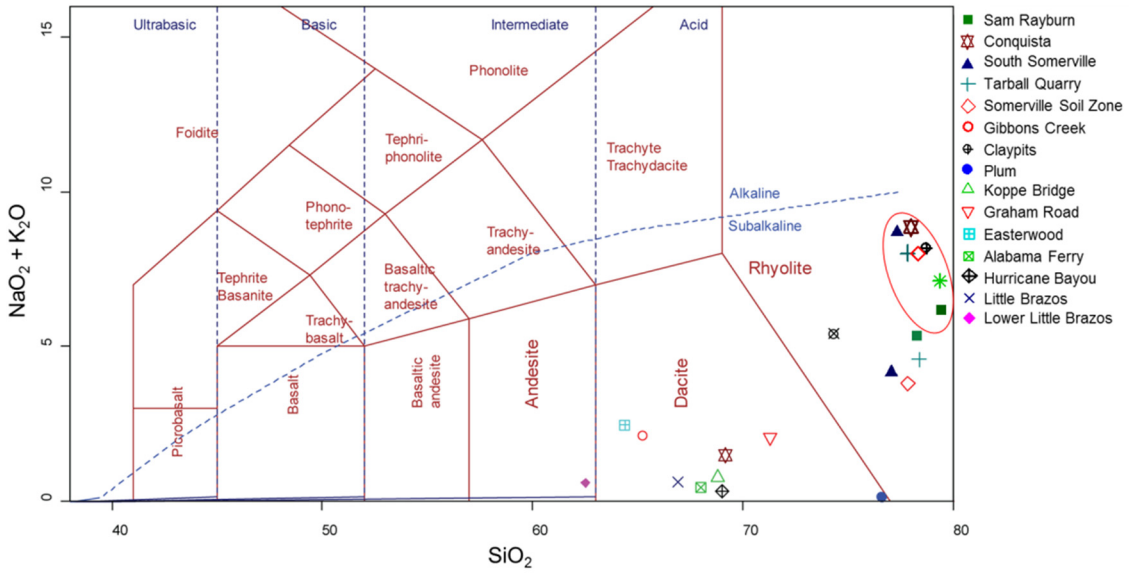

Figure 24. Total Alkali versus Silica (TAS) diagram (Le Bas 1986) showing Na_2O + K_2O versus SiO_2 in wt %. Volcanic glass shard microprobe data are circled and the bulk ICPMS data is plotted for comparison. The microprobe data is normalized to 100 total wt % and the ICPMS data is corrected for loss on ignition (LOI). Claypits, Somerville Soil Zone and Sam Rayburn volcanic glass shard data are from Yancey and Guillemette (1998). Plotted using GCDkit software (Janoušek et al. 2006).

When data from NAA of bulk volcanic ash and volcanic glass shards are compared, the two data sets show the same general trends but there is either enrichment or depletion in some of the elements (Figure 25). Al, Sc, Fe, Hf and Ta show consistent enrichment in the bulk volcanic ash data that could be caused by elements being concentrated in an insoluble residue, and Fe is easily incorporated into clay minerals (Zielinski 1982; dos Muchangos 2006). Na, K, Mn, Rb, Cs, and Cr are depleted in the bulk volcanic ash data due to the leaching of soluble ions. Co, Zn, As, Zr and Ba show variable behavior between the bulk volcanic ash and volcanic glass shard data. The REE show an inconsistent behavior regarding enrichment and depletion, yet are comparable between the two datasets. The bulk volcanic ash data shows higher levels of Eu, due to the bulk volcanic ash containing feldspar phenocrysts that exhibit a positive Eu anomaly (Rollinson 1993). Contamination of foreign grains by reworking could alter the bulk volcanic ash data although these volcanic ash beds show no sign of major reworking.

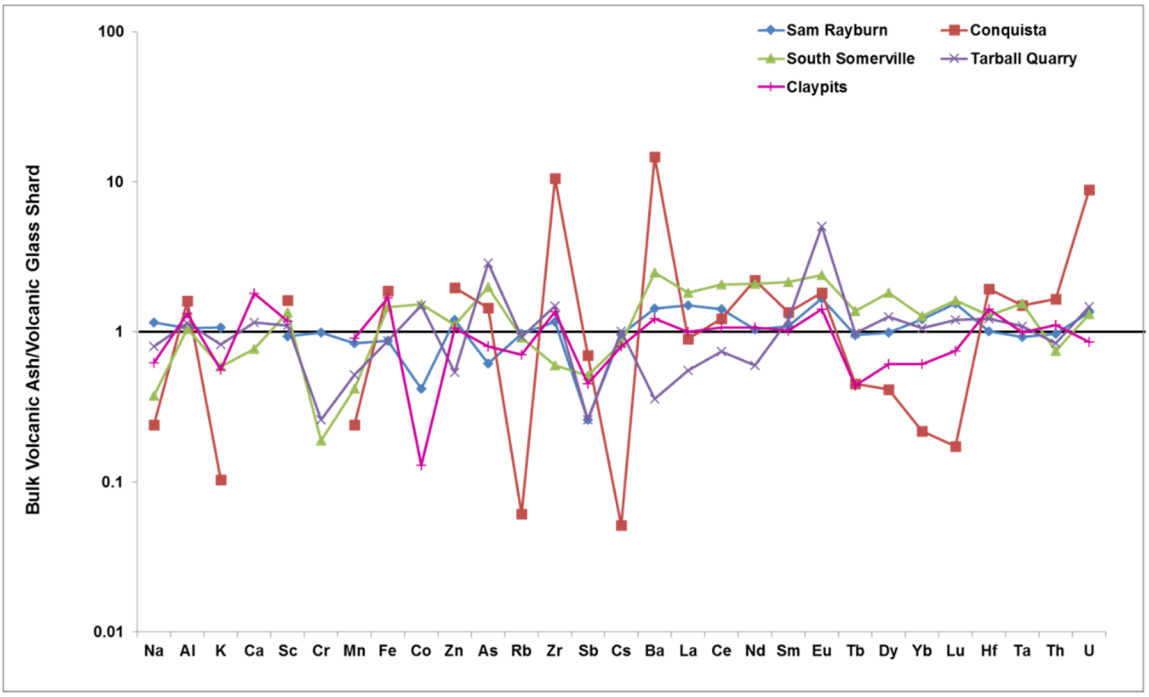

Figure 25. Relative enrichment or depletion of selected elements from NAA in bulk volcanic ash compared to volcanic glass shard data. All values are in ppm.

The Conquista sample shows the greatest difference in between the bulk volcanic ash and glass shard data with major variation in many of the elements (Figure 25). There is not only variation in the more mobile elements (Rb, Ba and K) but there is also variation in some elements that are thought to be immobile through low temperature alteration (HREE). The Conquista bulk volcanic ash also stands out with higher levels of U and Th in the ICPMS data as well (Figure 6). The Conquista volcanic ash is located in a uranium mine in Karnes County, Texas and has been exposed to U-rich groundwater during the U transport process (Fisher et al. 1970).

Possible Source of Volcanic Ash

Previous studies have suggested that the Sierra Madre Occidental of Mexico, the Trans-Pecos volcanic province of west Texas, or the Mogollon-Datil volcanic field of New Mexico could be the source of these volcanic ash beds (Guillemette and Yancey 1996, Yancey and Guillemette 1998; Grigsby 1999; Michaelides 2011). Volcanism during the Eocene was related to volcanic intrusion at the continental margin during subduction, whereas the Oligocene volcanic activity consists mostly of a large outpouring of felsic ash flow tuffs that erupted during a shift in tectonic setting from subduction to intraplate extension (Aguirre-Diaz and McDowell 1991). The Sierra Madre Occidental and Trans-Pecos actively erupted rhyolitic volcanics through the Eocene and the activity increased into the Oligocene, with a period of high intensity volcanism extending from 46 Ma to 27.5 Ma (McDowell and Mauger, 1994). The Sierra Madre Occidental volcanism is mostly calc-alkaline and is dominated by rhyolite (Henry et al. 1991; Ferrari et al. 2007). The Trans-Pecos of west Texas produced strictly alkaline volcanism nearly continuously from 48 to 17 Ma, although the degree of alkalinity varies (Nelson et al. 1987). The Mogollon-Datil erupted calc-alkalic rocks ranging from basalt to rhyolite with high K content from approximately 40 to 18 Ma (Bornhorst 1980).

Major elements can be useful as a classification method that can help to identify possible source regions. All seven glass shard-bearing volcanic ash samples from the Catahoula and Manning Formations have the geochemical signature of sub-alkaline, rhyolitic volcanism (Figure 12), and are within TAS diagram ranges of volcanic rocks

from the Sierra Madre Occidental and Trans-Pecos reported in Webber and others (1994), Ferrari and others (2007) and Parker and White (2008).

CIPW Norm calculations are done using GDCkit software (Janoušek et al. 2006) to calculate the normative mineralogy of the whole rock composition (Table 10). This calculation takes the volcanic glass shard chemistry and estimates what the ideal mineralogy of the whole volcanic ash would be based on those values. The Sam Rayburn and Seale Ranch samples have the highest amount of normative quartz. The presence of quartz in the normative mineralogy and no other silica containing minerals, such as leucite or sodalite, classifies the ideal whole rock composition as oversaturated with silica. The presence of corundum in the normative mineralogy is from an excess of Al_2O_3. All samples contain normative corundum, so they are classified as peraluminous.

Mineral	Sam Rayburn	Conquista	South Somerville	Tarball Quarry	Somerville Soil Zone	Seale Ranch	Claypits
Quartz	47.315	34.062	33.655	34.631	37.332	42.983	36.107
Corundum	4.004	0.249	0.39	0.879	1.272	2.865	0.984
Orthoclase	25.412	34.808	35.99	37.05	34.276	26.594	30.73
Albite	13.539	21.324	19.631	17.757	18.023	17.77	22.847
Anorthite	1.935	1.637	1.885	1.77	2.034	1.935	1.488
Hypersthene	1.065	1.451	1.708	1.17	1.322	1.524	0.973
Sum	93.27	93.53	93.26	93.257	94.26	93.67	93.13

Table 10. CIPW Norm calculations done using GDCkit software for the volcanic glass shard analyses (Janoušek et al. 2006).

When major element data is plotted on an $Al_2O_3/CaO+Na_2O+K_2O$ versus Al_2O_3/Na_2O+K_2O (A/CNK-A/NK) plot the levels of Al, Ca, Na and K in the volcanic glass shards determined whether the sample is classified as meta/peraluminous or peralkaline. The samples plot in a linear alignment showing increasingly peraluminous values on the A/CNK-A/NK plot (Figure 26).

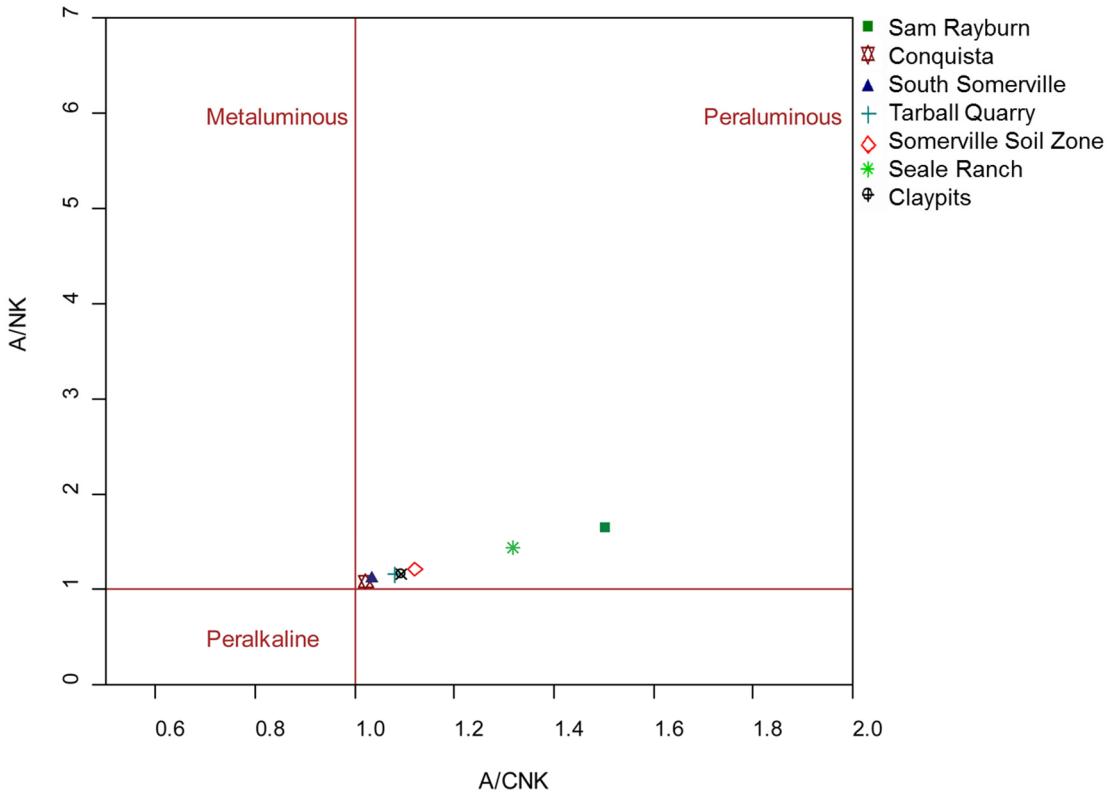

Figure 26. A/CNK-A/NK plot showing $Al_2O_3/CaO+Na_2O+K_2O$ versus Al_2O_3/Na_2O+K_2O (Shand 1943). Plotted using GCDkit software (Janoušek et al. 2006).

When trace element data from bulk volcanic ash and volcanic glass shards are normalized to primitive mantle values the elements to the left of La are more abundant than those to the right and this indicates that these beds are the product of subduction related volcanism (Gill 2010) (Figure 6; Figure 13). The bulk volcanic ash data also shows depletion in Nb, P and Ti values and supports the interpretation that the ashes are products of subduction related volcanism. The enrichment of LREE and moderate Eu anomaly exhibited by the bulk volcanic ash data and volcanic glass shard data is indicative of rhyolitic volcanism (Gill 2010) (Figure 7; Figure 14). The negative Eu anomaly is caused by fractionation of plagioclase from the melt prior to the eruption of the volcanic ash (Rollinson 1993).

Depletion of the HREE in comparison to the LREE can be caused by the fractionation of garnet from the melt. All of the bulk volcanic ash samples show similar REE concentrations and, therefore, they may be derived from a similar source. The REE fractionation shown by the La/Yb ratios displays two trends (Figure 8). Increasing REE fractionation loosely correlates to increasing age of the samples. Alternatively, increasing La/Yb ratios correlate with progressively greater alteration levels in the samples from different depositional environments. La/Yb ratios could either be showing a progressive change in magma composition over time, or the trend could be from the alteration causing REE fractionation. It is more likely that the trend is caused by a change in magma composition because the REE may undergo some fractionation in alteration, but they usually retain close to their original pattern (Zielinski 1982, 1985; dos Muchangos 2006).

CONCLUSIONS

This study shows that bulk volcanic ash trace element and rare earth element (REE) compositions, combined with the existing paleontology and lithostratigraphy, supports the idea that the Little Brazos, Alabama Ferry and Hurricane Bayou samples are deposits of the same volcanic ash deposit. The Lower Little Brazos volcanic ash is from an earlier eruption of the same source. The new radiometric date from Hurricane Bayou of 41.79 ±0.02 Ma is within the assigned uncertainties of previous age dating and supports this correlation. Correlation of the Little Brazos, Alabama Ferry and Hurricane Bayou samples establishes this bed as a regional marker for 120 km along strike. The possible extension of this correlation to the St. Johns volcanic ash would extend this marker to over 480 km. A volcanic ash of the same approximate age as the upper Crockett Formation has been reported as far east as North Carolina (Harris and Fullagar 1987). This presents the possibility of the upper Crockett Formation volcanic ash being a regional marker bed through the United States Gulf Coast and beyond. The tentative correlation of the Caddell Formation volcanic ashes in Gonzales and Brazos Counties of Texas could establish a marker bed that over a distance of 120 km. The correlation of the South Somerville and Plum volcanic ashes from Fayette to Brazos County would have implications for locating the Plum ash bed higher in the Manning Formation. Further radiometric dating and geochemical fingerprinting would test these correlations and possibly enable them to be extended further.

These volcanic ashes appear to have originated from the same magmatic province and some of them possibly even the same volcanic source. Major element data from seven Catahoula and Manning Formation samples indicate that they are the product of sub-alkaline rhyolitic volcanism. CIPW Norm calculations indicate that the glass bearing samples are peraluminous. Trace element data from both the Neutron Activation Analysis (NAA) and the Inductively Coupled Plasma Mass Spectrometry (ICPMS) analysis indicate that these ashes are deposits of volcanism related to subduction zone tectonics. REE profiles from the NAA and ICPMS analysis are consistent with those of felsic rocks. The timing, frequency and type of volcanic ash deposits make the Sierra Madre Occidental of Mexico the likely source, but the Trans-Pecos of Texas and Mogollon-Datil of New Mexico cannot be definitively ruled out. Further radiometric dating and geochemical characterization of the source regions would enable the volcanic source to be better constrained.

The nine radiometric dates obtained by this study serve to better constrain the ages of the Claiborne and Jackson Groups and the Catahoula Formation of Texas. The Conquista volcanic ash has potential to become a calibration point for the Eocene/Oligocene boundary with further analysis and the Hurricane Bayou volcanic ash has the potential to become a calibration point for the Lutetian-Bartonian boundary.

REFERENCES

Aguirre-Diaz, G.J, and McDowell, F.W., 1991, The volcanic section at Nazas, Durango, Mexico, and the possibility of widespread Eocene volcanism within the Sierra Madre Occidental, Journal of Geophysical Research, v. 96, n. B8, p. 13373-13388

Atlee, W.A., Loep, K.J., Elsik, W.C., Pointer, G.N., Zingula, R.P., and Ogden, J.C., 1967, Selected Cretaceous and Tertiary depositional environments, Society for Sedimentary Geology, Gulf Coast Section, Field Trip Guidebook, 50 p.

Bailey, T.L., 1926, The Gueydan, a new middle Tertiary formation from the southwestern coastal plain of Texas, The University of Texas Bulletin, v. 2645, p. 187

Berg, R.R., 1970, Outcrops of the Claiborne group in the Brazos Valley, Southeast Texas, Geological Society of America, 4th Annual Meeting of the South-Central Section, p. 79

Berggren, W.A., Kent, D.V., Obradovich, J.D., and Swisher, C.C., III, 1992, Toward a revised Paleogene geochronology, *in* Prothero, D.E. and Berggren, W.A., eds., Eocene-Oligocene climatic and biotic evolution, Princeton University Press, Princeton, New Jersey, p. 29-45

Bornhorst, T.J., 1980, Major and trace element geochemistry and mineralogy of Upper Eocene to Quaternary volcanic rocks of the Mogollon-Datil volcanic field,

southwestern New Mexico, [Ph.D. thesis]: Albuquerque, The University of New Mexico, 426 p.

Callender, D.L., and Folk, R.L., 1958, Idiomorphic zircon, key to volcanism in the lower Tertiary sands of central Texas, American Journal of Science, v. 256, p. 257-269

Carey, A., Samson, S.D., and Sell, B.K., 2009, Utility and limitations of apatite phenocryst chemistry for continent-scale correlation of Ordovician K bentonites, Journal of Geology, v. 117, n. 1, p. 1-14

Chen, P.Y., 1968, Geology and mineralogy of the white bentonite beds of Gonzales County, Texas, [Ph.D. thesis]: Austin, The University of Texas, 193 p.

dos Muchangos, A.C., 2006, The mobility of rare earth and other elements in the process of alteration of rhyolitic rocks to bentonite (Lebombo volcanic mountainous chain, Mozambique), Journal of Geochemical Exploration, v. 88, p. 300-303

Fedo, C.M., Nesbitt, H.W., and Young, G.M., 1995, Unraveling the effects of potassium metasomatism in sedimentary rocks and paleosols, with implications for paleoweathering conditions and provenance, Geology, v. 23, p. 921-924

Ferrari, L., Valencia-Moreno, M., and Bryan, S., 2007, Magmatism and tectonics of the Sierra Madre Occidental and its relation with the evolution of the western margin of North America, *in* Alaniz-Alvarez, S.A., and Nieto-Samaniego, A.F., eds., Geology of Mexico: Celebrating the Centenary of the Geological Society of Mexico: Geological Society of America Special Paper 422, p. 1-39

Fisher, W.L., Proctor, C.V., Galloway, W.E., and Nagle, J.S., 1970, Depositional systems in the Jackson Group of Texas their relationship to oil, gas and Uranium,

Transactions of the Gulf Coast Association of Geological Societies, v. XX, p. 234-261

Gill, R., 2010, Igneous rocks and processes a practical guide: Chichester, England, Wiley-Blackwell, 428 p.

Gimbrede, L.A., 1951, Hurricane Lentil, Cook Mountain Eocene in East Texas, [M.S. thesis]: Austin, University of Texas, 40 p.

Gowan, S.W., 1985, Depositional environment of the San Miguel lignite deposit in Atascosa and McMullen Counties, Texas, [Ph.D. thesis]: College Station, Texas A&M University, 199 p.

Gray, D.M., 1953, Geology of the Porter Springs Area, western Houston County, Texas [M.S. Thesis]: Austin, University of Texas, 124 p.

Grigsby, J.D., 1999, Source and correlation of Eocene-Oligocene bentonites of the Gulf Coastal Plain, Geological Society of America Abstracts with Programs, A298

Grigsby, J.D., and Dennis, R.K., 1991, Recognition and implications of volcanic glass detritus in the fluvial deposits of the Middle Frio Formation, South Texas, Gulf Coast Association of Geological Societies, Transactions, vol. XLI, p. 353-358

Guillemette, R. and Yancey, T.E., 1996, Composition and provenance of volcanic glass in Late Eocene Manning Formation, east-central Texas, Gulf Coast Association of Geological Societies, Transactions, v. 46, p. 159-166

Harris, W.B., and Fullagar P.D., 1989, Comparison of Rb-Sr and K-Ar dates of the middle Eocene bentonite and glauconite, southeastern Atlantic Coastal Plain, Geological Society of America Bulletin, v. 101, p. 573-577

Henry, C.D., Price, J.G., and James, E.W., 1991, Mid-Cenozoic stress evolution and magmatism in the southern Cordillera, Texas and Mexico: transition from continental arc to intraplate extension, Journal of Geophysical Research, v. 96, p. 13545-13560

Janoušek, V., Farrow, C.M., and Erban, V., 2006, Interpretation of whole-rock geochemical data in igneous geochemistry: introducing Geochemical Data Toolkit (GCDkit), Journal of Petrology 47 v. 6 p. 1255-1259

Jarosewich, E., and Boatner, L., 1991, Rare-earth element reference samples for electron microprobe analysis, Geostand Newsletter v. 15, p. 307-309

Jarosewich, E., and White, J.S., 1987, Strontianite reference samples for electron microprobe and SEM analyses, Journal Sedimentary Petrology 57 v. 4, p. 762- 763

Jarosewich, E., and MacIntyre, I.G., 1983, Carbonate reference samples for electron microprobe and scanning electron microscope analyses, Journal Sedimentary Petrology 52 v. 2, p. 677-678

Kersey, D.G., and Stanton, R.J., Jr., 1979, Lower Tertiary of the Brazos River Valley, Houston Geological Society Guidebook, 126 p.

Le Bas, M.J., Le Maitre, R.W., Streckeisen, A. and Zanettin, B. 1986, A chemical classification of volcanic rocks based on the total alkali-silica diagram, Journal of Petrology, v. 27, p. 745-750

Ledger, E.B., 1988, The Catahoula Formation; A volcaniclastic unit in east Texas, *in* Geological Society of America, Centennial Field Guide, South Central Section, p. 383-385

McBride, E.F., Lindemann, W.L., and Freeman, P.S., 1968, Lithology and petrology of the Gueydan (Catahoula) Formation in south Texas, Bureau of Economic Geology Report of Investigations, n. 63

McDonough, W.F., and Sun, S.S., 1995, The composition of the Earth, Chemical Geology, v. 120, p. 223-253

McDowell, F.W., and Mauger, R.L, 1994, K-Ar and U-Pb zircon chronology of Late Cretaceous and Tertiary magmatism in central Chihuahua State, Mexico, Geological Society of America Bulletin, January, v. 106, n. 1, p. 118-132

Michaelides, M.N., 2011, Depositional and diagenetic processes in the formation of the Eocene Jackson Group bentonites, Gonzales County, Texas, [M.S. thesis]: Austin, University of Texas, 173 p.

Nelson, D.O., Nelson K.L., Reeves, K.D., and Mattison, G.D., 1987, Geochemistry of Tertiary alkaline rocks of the Eastern Trans-Pecos Magmatic Province, Texas, Contributions to Mineralogy and Petrology, v. 97, p. 72-92

Nesbitt, H.W., and Young, G.M., 1982, Early Proterozoic climates and plate motions inferred from major element chemistry of lutites, Nature, v. 299, p. 715-717

Obradovich, J.O., Dockery, D.D., and Swisher III, C.C., 1993, $^{40}Ar/^{39}Ar$ ages of bentonites in the upper part of the Yazoo Formation (upper Eocene), West-Central Mississippi, Mississippi Geology, v. 14, p. 1-9.

Parker, D.F., and White, J.C., 2008, Large scale silicic alkalic magmatism associated with the Buckhorn Caldera, Trans-Pecos Texas, USA: comparison with Pantelleria, Italy, Bulletin of Volcanology, v. 70, p. 403-415

Pearce, J.A., and Norry, M.J., 1979, Petrogenetic implications of Ti, Zr, Y, and Nb. Variations in volcanic rocks, Contributions to Mineralogy and Petrology, v. 69, p. 33-37

Renick, B.C., 1936, The Jackson Group and the Catahoula and Oakville formations in a part of the Texas Gulf Coastal Plain, University of Texas Bulletin, n. 3619, 104 p.

Roberson, H.E., 1964, Petrology of Tertiary bentonites of Texas, Journal of Sedimentary Petrology, v. 34, n. 2, p. 401-411

Rollinson, H.R., 1993, Using geochemical data: evaluation, presentation, interpretation, New York, Longman Scientific and Technical, 352 p.

Ross, C.S., and Kerr, P.F., 1930, The Kaolin minerals, United States Geological Survey, Professional Paper 165, p. 151-176

Sell, B.K, and Samson, S.D., 2011, A tephrochronologic method based on apatite trace-element chemistry, Quaternary Research, v. 76, p. 157-166

Sell, B.K, and Samson, S.D., 2011, Apatite phenocryst compositions demonstrate a miscorrelation between the Millbrig Kinnekulle K-bentonites of North American and Scandinavia, Geological Society of America, v. 39, n. 4, p. 303-306

Senkayi, A.L., Dixon, J.B., Hossner, L.R., Abder-Ruhman, M., and Fanning, D.S., 1984, Mineralogy and genetic relationships of tonstein, bentonite, and lignitic strata in the Eocene Yegua Formation of east-central Texas, Clays and Clay Minerals, August, v. 32, p. 259-271

Shand, S.J., 1943, Eruptive rocks: their genesis, composition, and classification, with a chapter on meteorites: New York, J. Wiley and sons, 444 p.

Sheard, E.R., Williams-Jones, A.E, Heiligmann, M., Pederson, C., and Trueman, D.L., 2012, Controls on the concentration of zirconium, niobium, and the rare earth elements in the Thor Lake Rare Metal Deposit, Northwest Territories, Canada, Economic Geology, v. 107, n. 1, p. 81-104

Stenzel, H.B., 1938, The geology of Leon County, Texas, University of Texas-Austin, Bureau of Economic Geology Publication, n. 3818, 295 p.

Stenzel, H.B., 1940, New zone in Cook Mountain Formation, the *Crassatella texalta* Harris *Turritella cortezi* Bowles zone, Bulletin of American Association of Petroleum Geologists, v. 24, p. 1663-1675

Stenzel, H.B., 1940, The Yegua Problem, The University of Texas Bulletin 3945, p. 847-911

Stenzel, H.B., 1953, Field Trip #5 to Austin: American Association of Petroleum Geologists Guidebook Field Trips, Houston Meeting, p. 43-60

Stepanov, A.S., and Hermann, J., 2013, Fractionation of Nb and Ta by biotite and phengite: Implications for the "missing Nb paradox," Geology, v. 41, i.3, p. 303

Webber, K.L., Fernandez, L.A., and Simmons, W.B., 1994, Geochemistry and mineralogy of the Eocene-Oligocene volcanic sequence, Southern Sierra Madre Occidental, Juchipila, Zacatecas, Mexico, Geofisica Internacional, v. 33, p. 77-89

Yancey, T.E., 1997, Depositional environments of Late Eocene lignite-bearing strata, east-central Texas, International Journal of Coal Geology, v. 34, p. 261-275

Yancey, T.E. and Guillemette, R., 1998, Major volcanic ash units in the Late Eocene of east Texas; Gulf Coast Association of Geological Societies Transactions, v. 48, p. 511-516

Zielinski, R.A, 1982, The mobility of uranium and other elements during alteration of rhyolite ash to montmorillonite: a case study in the Troublesome Formation, Colorado, Chemical Geology, v. 35, p. 185-204

Zielinski, R.A, 1985, Element mobility during alteration of silicic ash to kaolinite – a study of tonstein, Sedimentology, v. 32, p. 567-579

APPENDIX A

The New Mexico Geochronology Research Laboratory completed $^{40}Ar/^{39}Ar$ radiometric dating of single crystals of sanidine from nine samples from the Crockett, Yegua, Manning, and Catahoula Formations. Dr. Matt Heizler included the following report with the raw data from the radiometric dating that provides insight into the dating method that will support different interpretations.

$^{40}Ar/^{39}Ar$ Analytical Methods and Results

Of the samples provided, 9 yielded sanidine separates that were typically mixed with some inherited K-feldspar grains that are milky in appearance compared to the clear sanidine grains. The separates were irradiated for 40 hours at the UGGS TRIGA reactor in Denver, CO along with the standard Fish Canyon tuff sanidine as a neutron flux monitor. Fish Canyon sanidine is assigned an age of 28.201 Ma using a total ^{40}K decay constant of 5.463e-10 /a following the recommendations of Kuiper et al. (2008) and Min et al. (2000). Irradiation was conducted in Al-trays with three concentric rings of holes with standards and unknowns alternated between every other hole. In total, 13 monitor positions were used to determine fluence values for the 9 unknowns thereby providing precise (ca. ±0.003%) and accurate determination of the J-factor. Following irradiation, visibly clear individual crystals were loaded into copper trays, evacuated in an ultra-high vacuum chamber and baked at 150°C for 2-8 hours before single crystal laser fusion (SCLF) analyses (Table A1.) Flux monitor sanidine crystals were also fused in a single step using the CO_2 laser. All isotope measurements were performed using an ARGUS VI mass spectrometer operated in multicollector mode that utilized faraday detectors for masses 40-37 and an ion counter for mass 36 (Table A1). Additional methodology specific to this report and summary age data are provided in Table A1 and general operational details for the NMGRL can be found at internet site http://geoinfo.nmt.edu/publications/openfile/argon/home/html.

Twenty-five to 30 individual crystals were dated for each sample and the age results are presented on probability diagrams (Figures A1-9) and the isotopic data are

compiled in Table A2. Crystals were typically about 125 microns and thus yielded low argon concentrations (~1e-15 and 2e-15 moles ^{39}Ar and ^{40}Ar, respectively). However because system blanks and backgrounds are exceptionally low (Table A1) measured argon intensities were typically 50-100x (^{40}Ar) and 1000x (^{39}Ar) above blank levels. The Lower Basal Conquista sample was an exception as it contained relatively coarse sanidine (45 mesh) with correspondingly higher argon concentrations (Table A2). Analyses that yielded very low and/or non-detectable ^{39}Ar are considered to represent quartz or Na-rich plagioclase and these will not be reported or considered further.

The age distribution diagrams share common features that include a dominant population of ages and outliers that skew to ages older than the primary population (Figs. A1-9). Weighted mean ages were determined for each dominant population and range between 30.64±0.03 Ma and 41.79±0.01 Ma with 7 of the 9 samples falling between about 34 and 37 Ma (Table A1; Figs. A1-9). Two probability diagrams are shown for each sample; figure 'a' plots a narrow age range to reveal details of the grains that comprise the ages used for weighted mean age determination, whereas figure 'b' reports the full distribution of ages that were measured for each sample. In addition K/Ca and radiogenic yield diagrams are provided to visually aid in age interpretation. With some exception most individual grains have high (>95%) radiogenic argon values and K/Ca values were highly variable (~0.1 – 500). The K/Ca ratio is determined from the $^{39}Ar/^{37}Ar$ ratio and when significantly less the 1 it indicates analysis of plagioclase. In many cases, ^{37}Ar is not above detection level and this could indicate a grain with

exceptionally low Ca (likely an inherited plutonic or metamorphic crystal) or a relatively low Ca-content sanidine that is fine-grained that did not produce measureable ^{37}Ar.

Discussion

In general the preferred population of analyses to determine the weighted mean ash deposition age was based on deleting relatively old ages until an MSWD value was obtained (usually between 1-2) that indicated a normal distribution of ages. This method assumes that older grains are not accurate and likely are inherited either at the source of the eruption and/or during post-deposition reworking. Samples Lower Basal Conquista and Gibbons Creek are exceptions in that weighted mean ages are calculated from populations with MSWD values of 11.1 and 8.9, respectively. The age data for these samples (Figs. A2; A5) have probability diagrams that do not reveal an obvious truncation point for eliminating old (i.e. outlier) points and thus we take a conservative approach to age estimation by including the majority of results from each sample to obtain an eruption age.

The assignment of eruption age was conducted without knowledge of stratigraphic ordering of the samples and only after reporting the data was the stratigraphy revealed. A summary diagram of probability plots arranged in stratigraphic order reveals that 8 of the 9 reported eruption ages fall in correct stratigraphic order (Figure A10). The stratigraphy-violating sample is Lake Somerville Soil Ash with an assigned age of 34.91±0.20 Ma (Figure A6, Table A1). Based on comparison of the underlying Gibbons Creek sample (34.54±0.026 Ma) and overlying Tarball Quarry sample (34.39±0.10 Ma) the Lake Somerville date is about 400 ka too old. Detailed

scrutiny of the Lake Somerville Soil Ash data and comparison to stratigraphically similar samples is shown in Figure A11. The Lake Somerville Soil Ash sample has an overall complex dataset that record a significant inherited population (as old as 1000 Ma) and are the least precise because of very small grain size and low radiogenic yields (Figure A11). Because of the complexity of the Lake Somerville Soil Ash data and the inability to objectively assign a stratigraphically acceptable eruption age the argon analysis of the individual grains does not best constrain the Lake Somerville Soil Ash eruption age. However, because this sample lies between the Gibbons Creek and Tarball Quarry samples it can be inferred to have been deposited between 34.54±0.026 and 34.39±0.10 Ma and thus indirectly the Lake Somerville Soil Ash can be assigned an accurate and precise eruption age.

In summary, the $^{40}Ar/^{39}Ar$ data provide a detailed chronology of volcanism and associated ash deposition of samples located along the Texas Coastal Plain. Results span mid Eocene to early Oligocene and are in accord with expected results. The ARGUS VI multicollector mass spectrometer proved uniquely suited to provide precise and accurate data that could not have been achieved at this level with older generation mass spectrometers such as the MAP-215-50 or VG5400. A potentially useful sample for time scale calibration is Lower Basal Conquista that yielded an age very near the Oligocene/Eocene boundary. If biostratigraphy and/or paleomagnetic data can constrain the epoch that this sample is collected from then additional geochronology on this sample could prove to be an excellent time scale calibration point.

References cited

Kuiper K. F., Deino A., Hilgen F. J., Krijgsman W., Renne P. R., and Wijbrans J. R. (2008) Synchronizing the rock clocks of Earth history. Science 320, 500–504.

Min K., Mundil R., Renne P. R. and Ludwig K. R. (2000) A test for systematic errors in $^{40}Ar/^{39}Ar$ geochronology through comparison with U–Pb analysis of a 1.1 Ga rhyolite. Geochim. Cosmochim. Acta 64, 73–98.

Steiger, R.H., and Jäger, E., 1977. Subcommission on geochronology: Convention on the use of decay constants in geo- and cosmochronology. Earth and Planet. Sci. Lett., 36, 359-362.

Taylor, J.R., 1982. An Introduction to Error Analysis: The Study of Uncertainties in Physical Measurements,. Univ. Sci. Books, Mill Valley, Calif., 270 p.

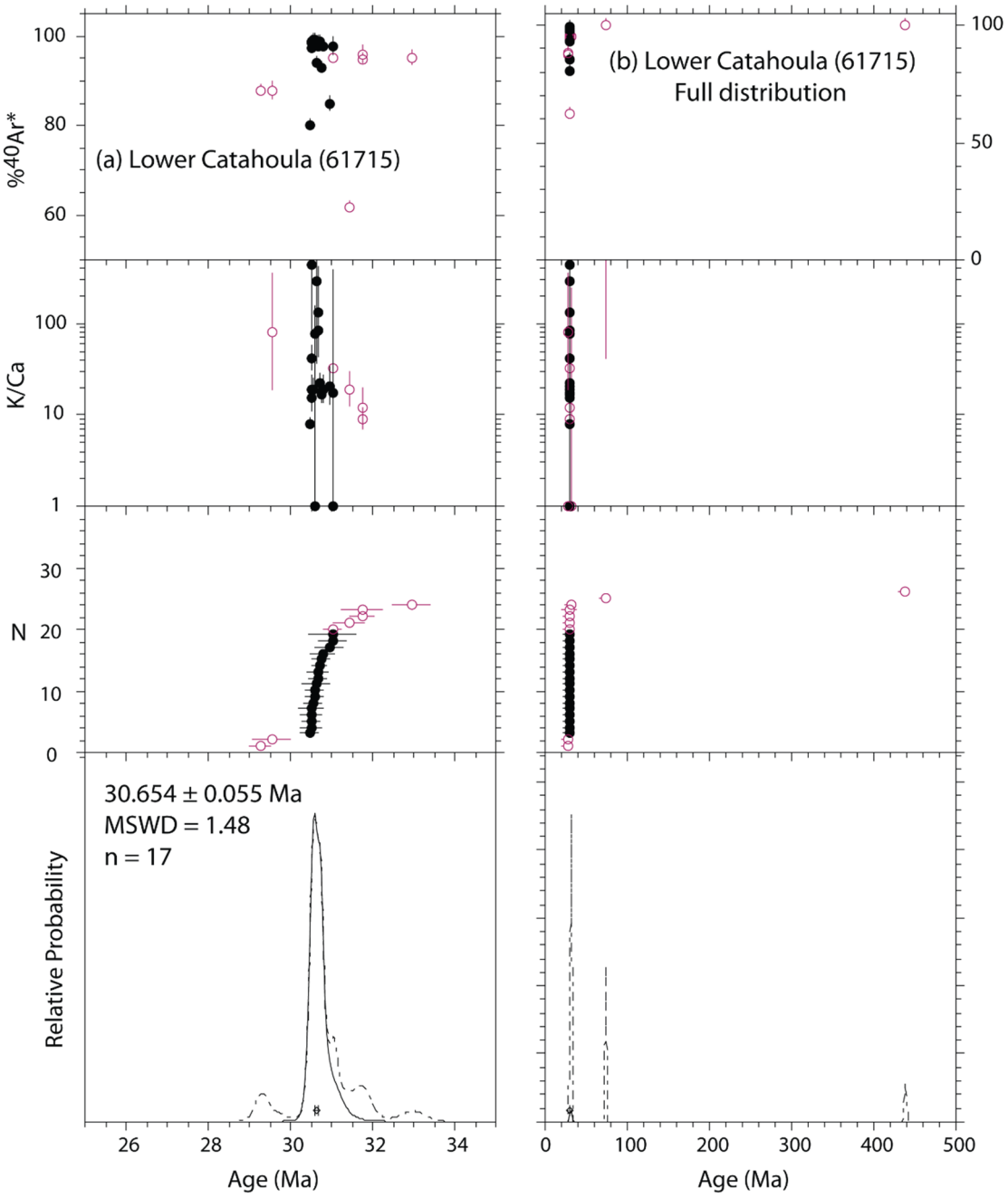

Figure A1. Age, K/Ca and radiogenic yield diagram for single crystal laser fusion results. (a) Diagram with scales chosen to best visualize the population of crystals used to determine the preferred ash deposition age. (b) Diagram with scales chosen to display the full distribution of results.

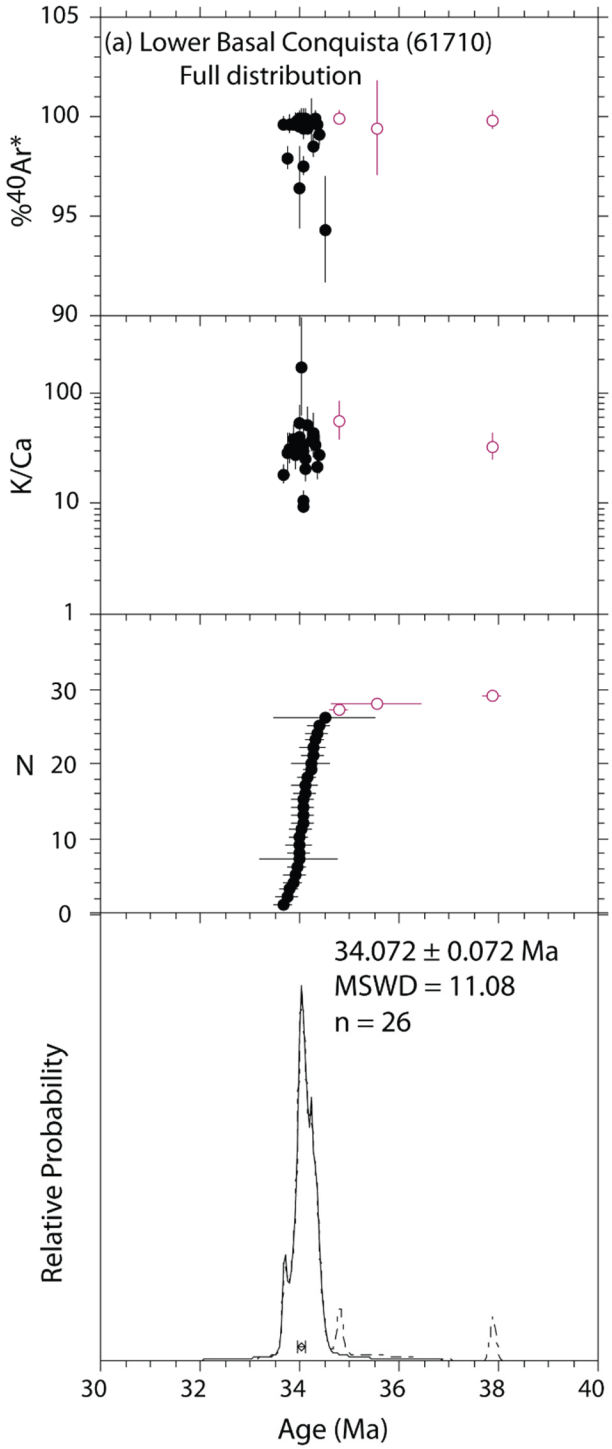

Figure A2. Age, K/Ca and radiogenic yield diagram for single crystal laser fusion results. (a) Diagram with scales chosen to best visualize the population of crystals used to determine the preferred ash deposition age.

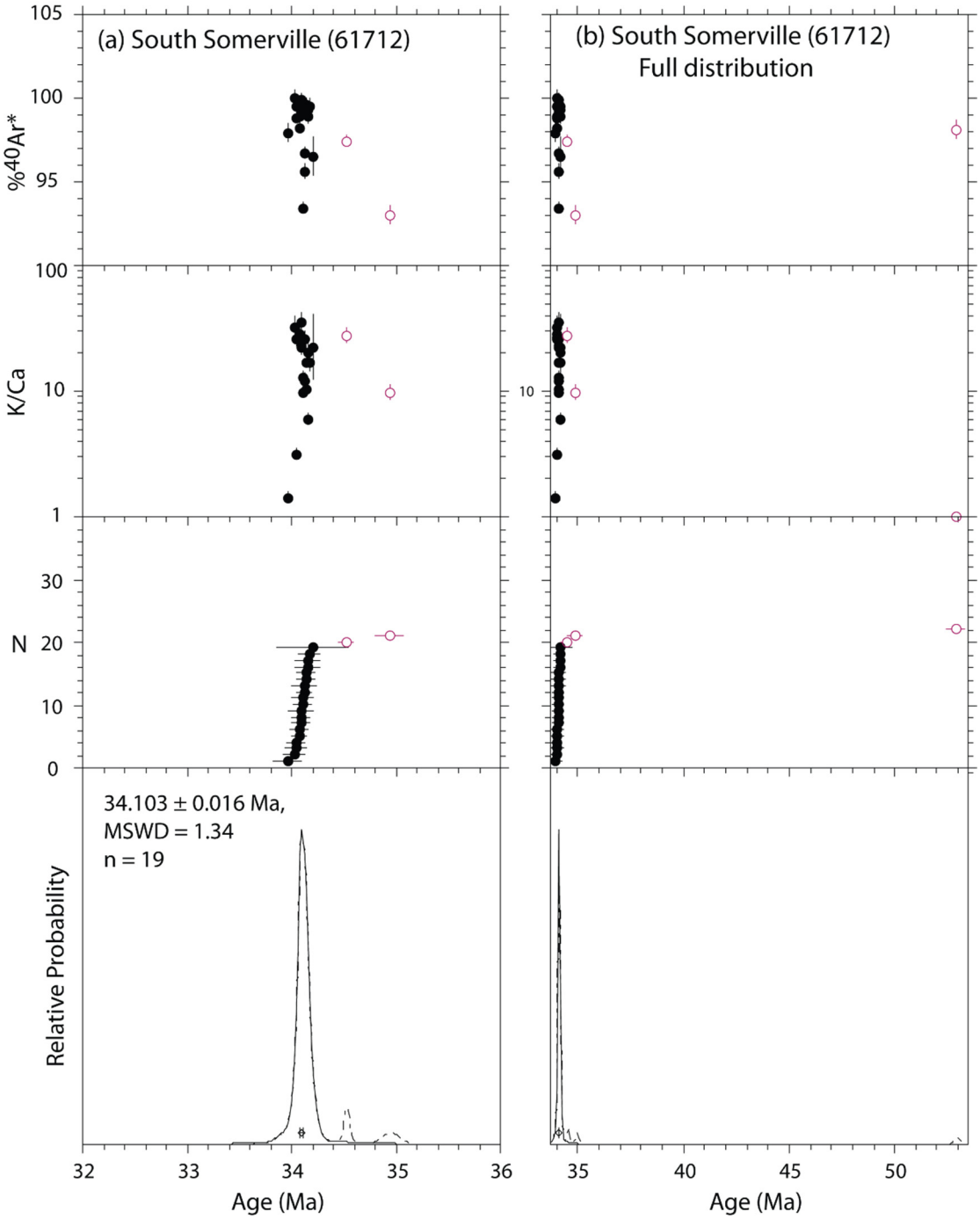

Figure A3. Age, K/Ca and radiogenic yield diagram for single crystal laser fusion results. (a) Diagram with scales chosen to best visualize the population of crystals used to determine the preferred ash deposition age. (b) Diagram with scales chosen to display the full distribution of results.

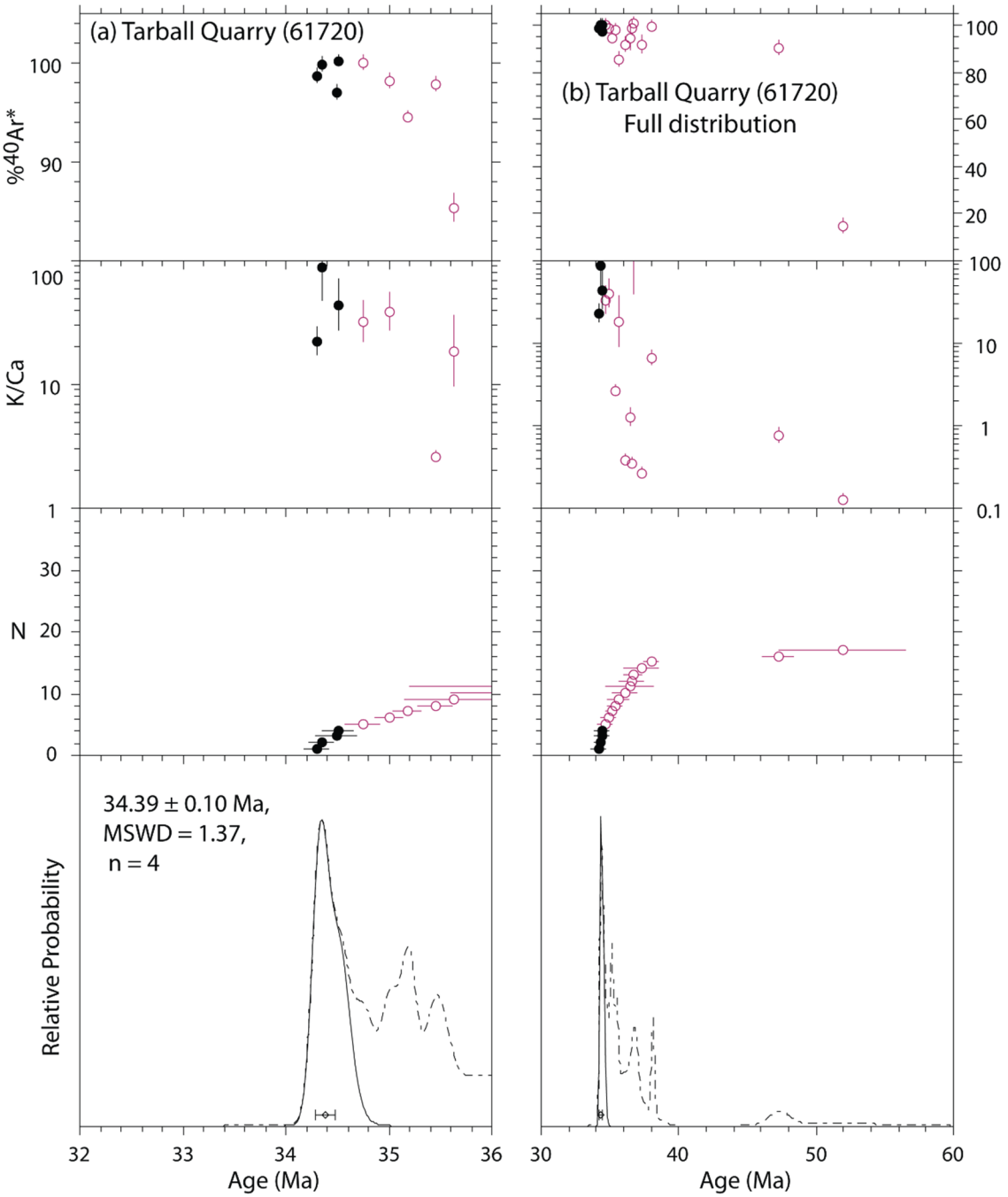

Figure A4. Age, K/Ca and radiogenic yield diagram for single crystal laser fusion results. (a) Diagram with scales chosen to best visualize the population of crystals used to determine the preferred ash deposition age. (b) Diagram with scales chosen to display the full distribution of results.

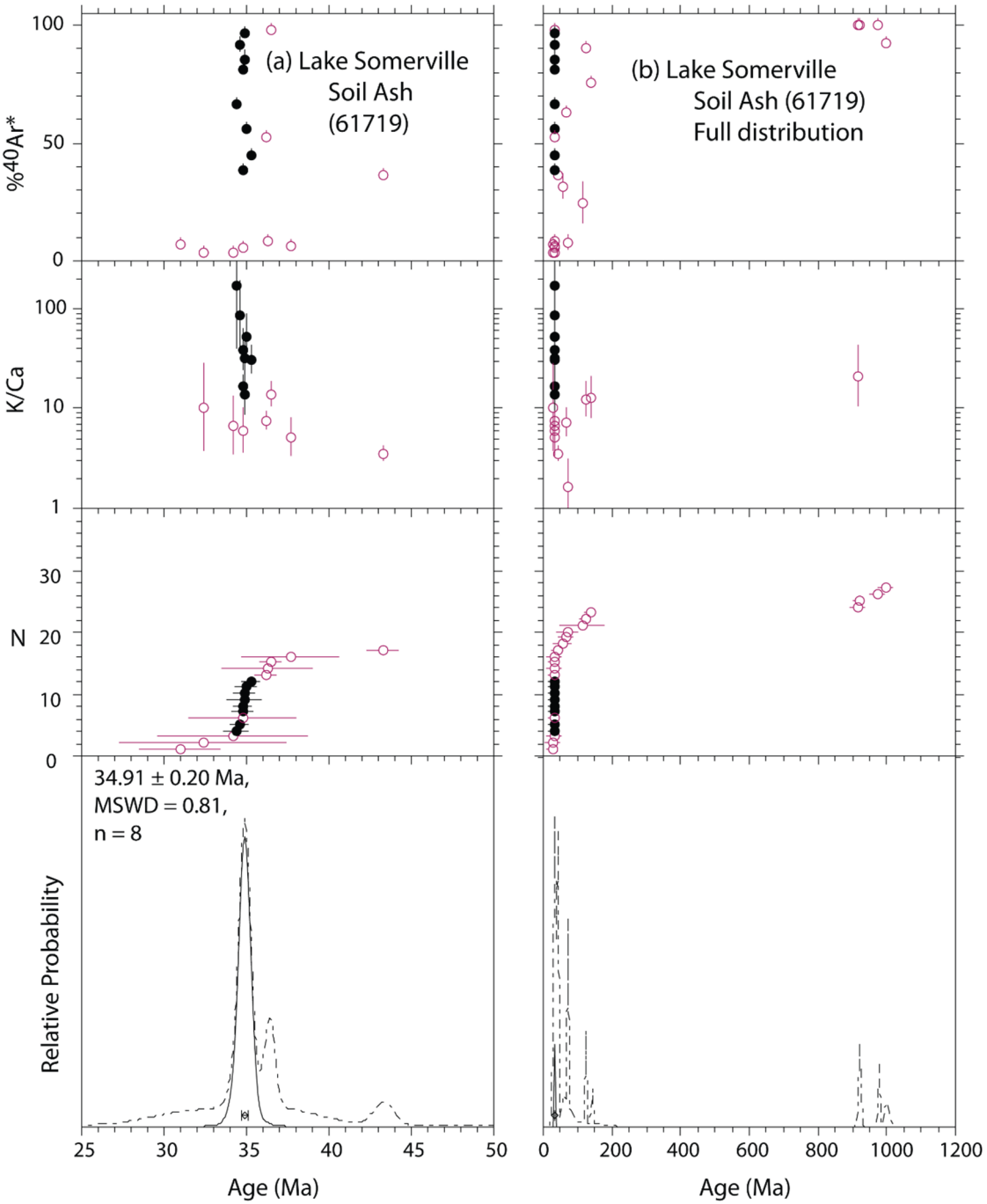

Figure A5. Age, K/Ca and radiogenic yield diagram for single crystal laser fusion results. (a) Diagram with scales chosen to best visualize the population of crystals used to determine the preferred ash deposition age. (b) Diagram with scales chosen to display the full distribution of results.

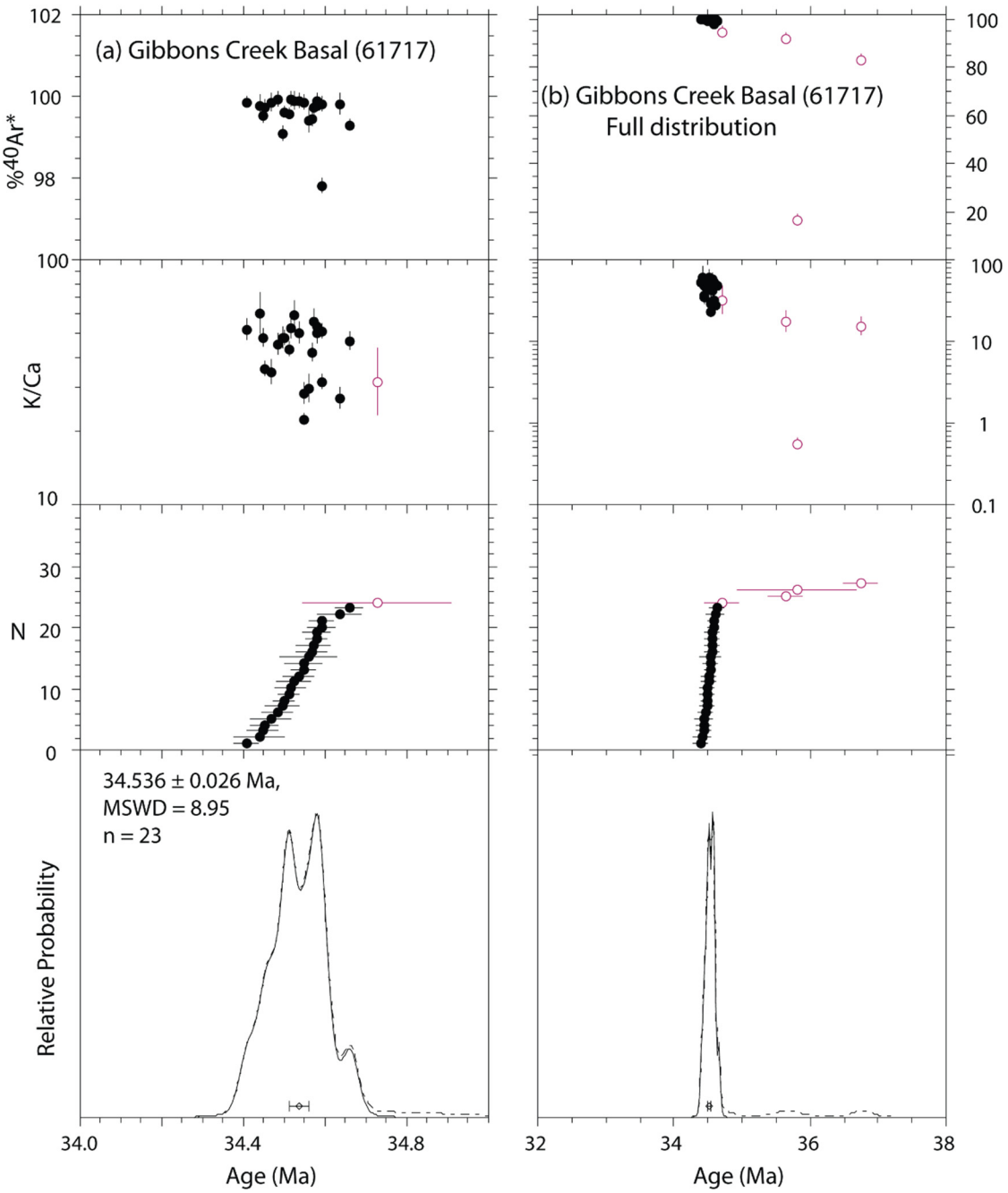

Figure A6. Age, K/Ca and radiogenic yield diagram for single crystal laser fusion results. (a) Diagram with scales chosen to best visualize the population of crystals used to determine the preferred ash deposition age. (b) Diagram with scales chosen to display the full distribution of results.

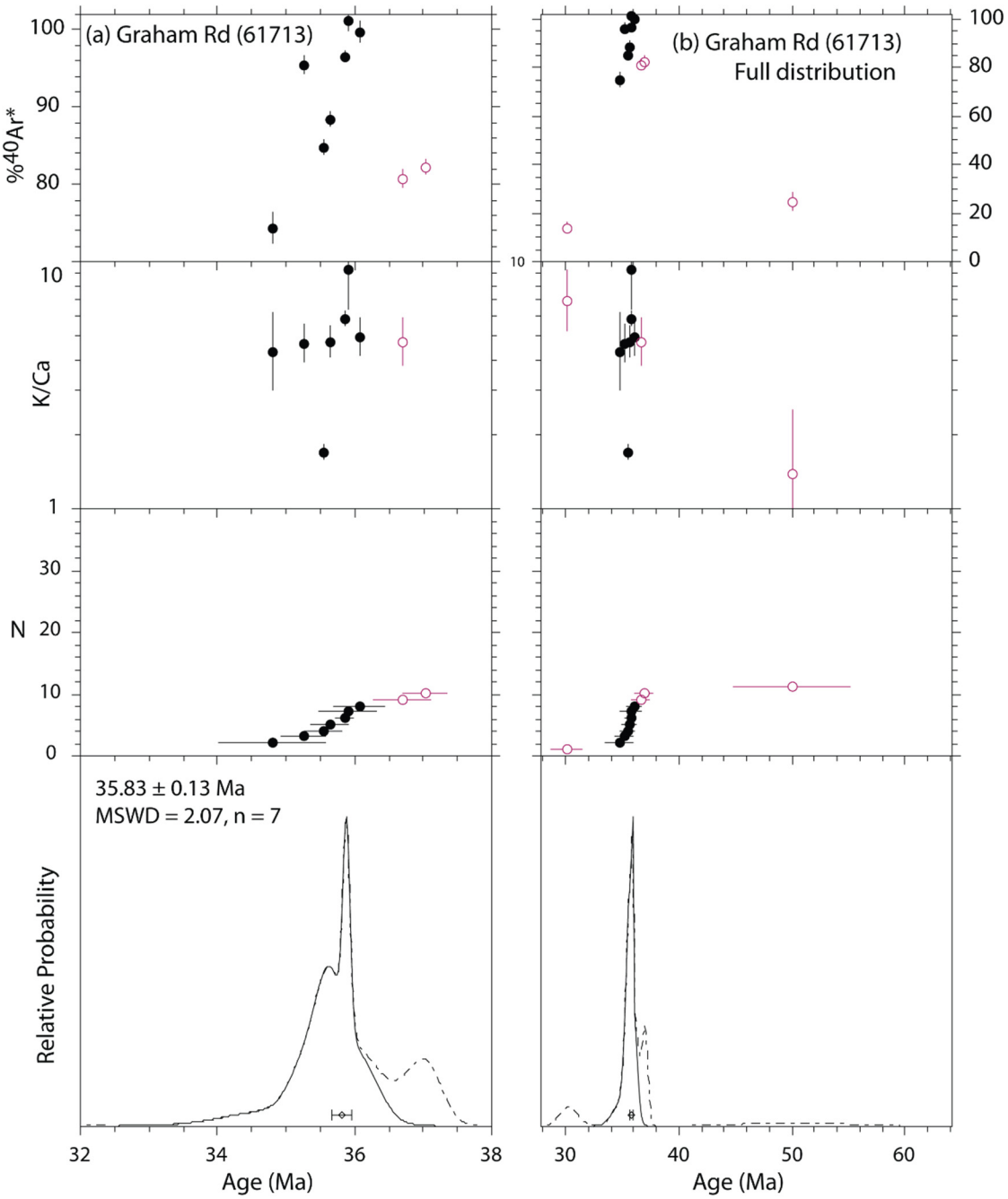

Figure A7. Age, K/Ca and radiogenic yield diagram for single crystal laser fusion results. (a) Diagram with scales chosen to best visualize the population of crystals used to determine the preferred ash deposition age. (b) Diagram with scales chosen to display the full distribution of results.

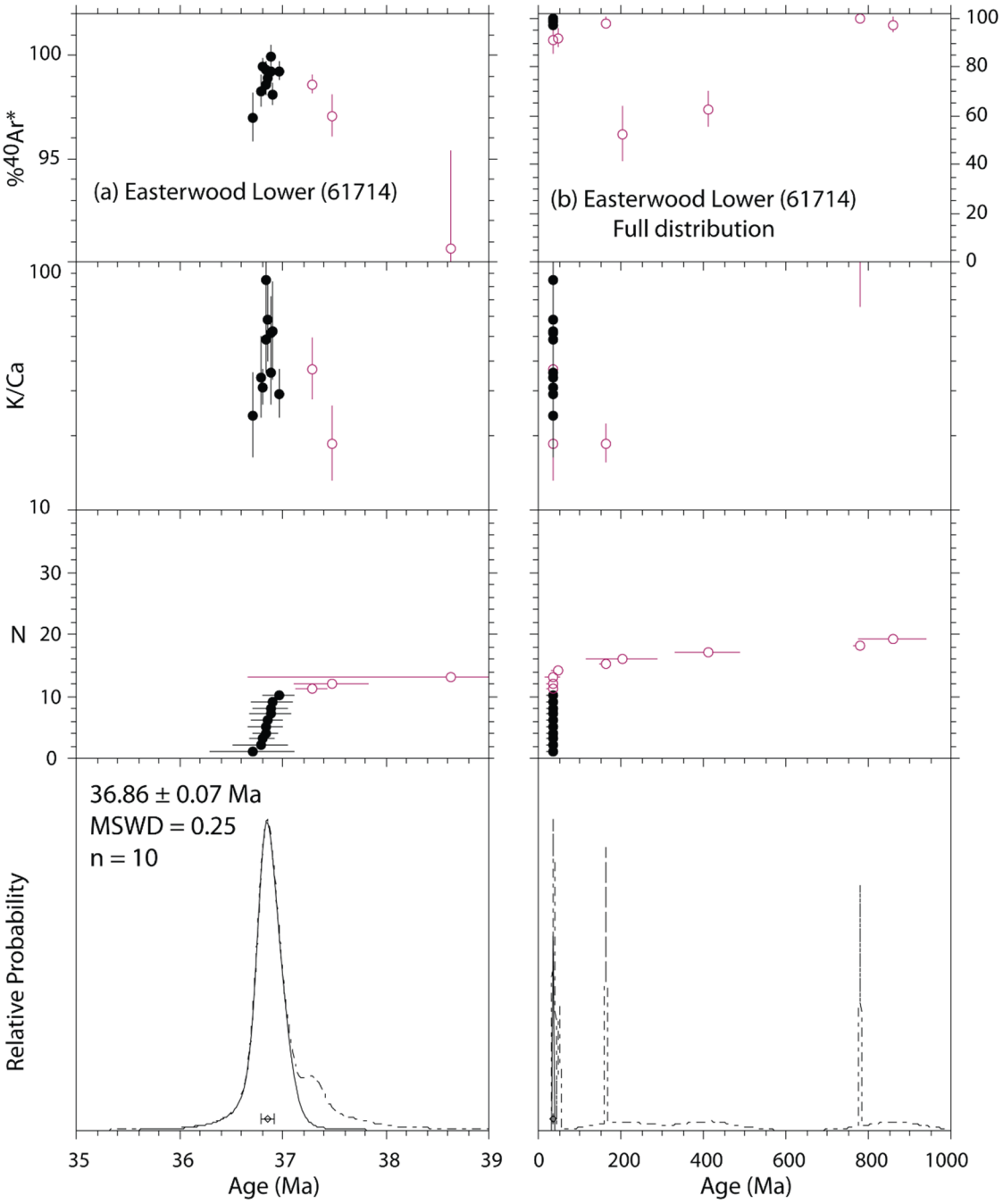

Figure A8. Age, K/Ca and radiogenic yield diagram for single crystal laser fusion results. (a) Diagram with scales chosen to best visualize the population of crystals used to determine the preferred ash deposition age. (b) Diagram with scales chosen to display the full distribution of results.

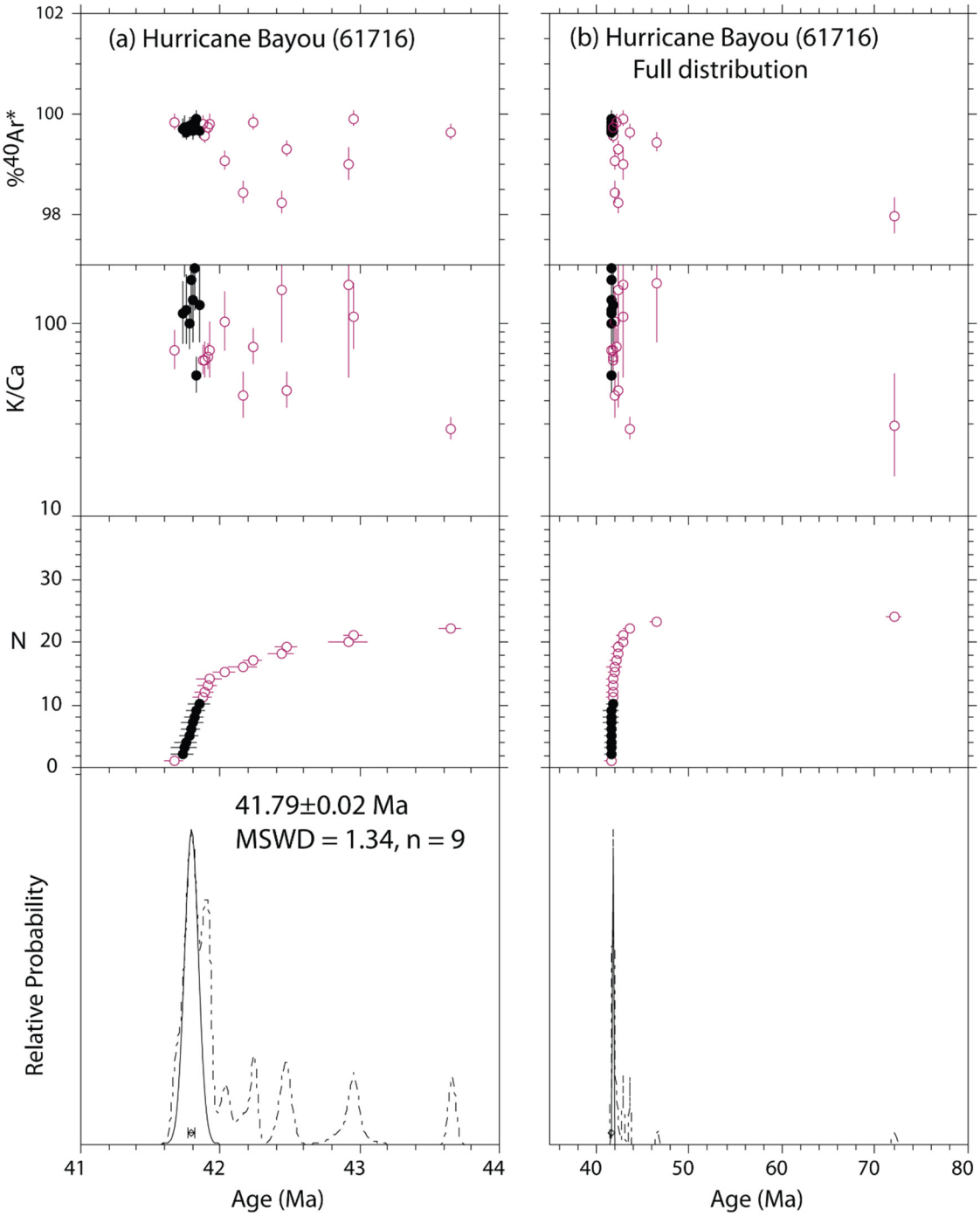

Figure A9. Age, K/Ca and radiogenic yield diagram for single crystal laser fusion results. (a) Diagram with scales chosen to best visualize the population of crystals used to determine the preferred ash deposition age. (b) Diagram with scales chosen to display the full distribution of results.

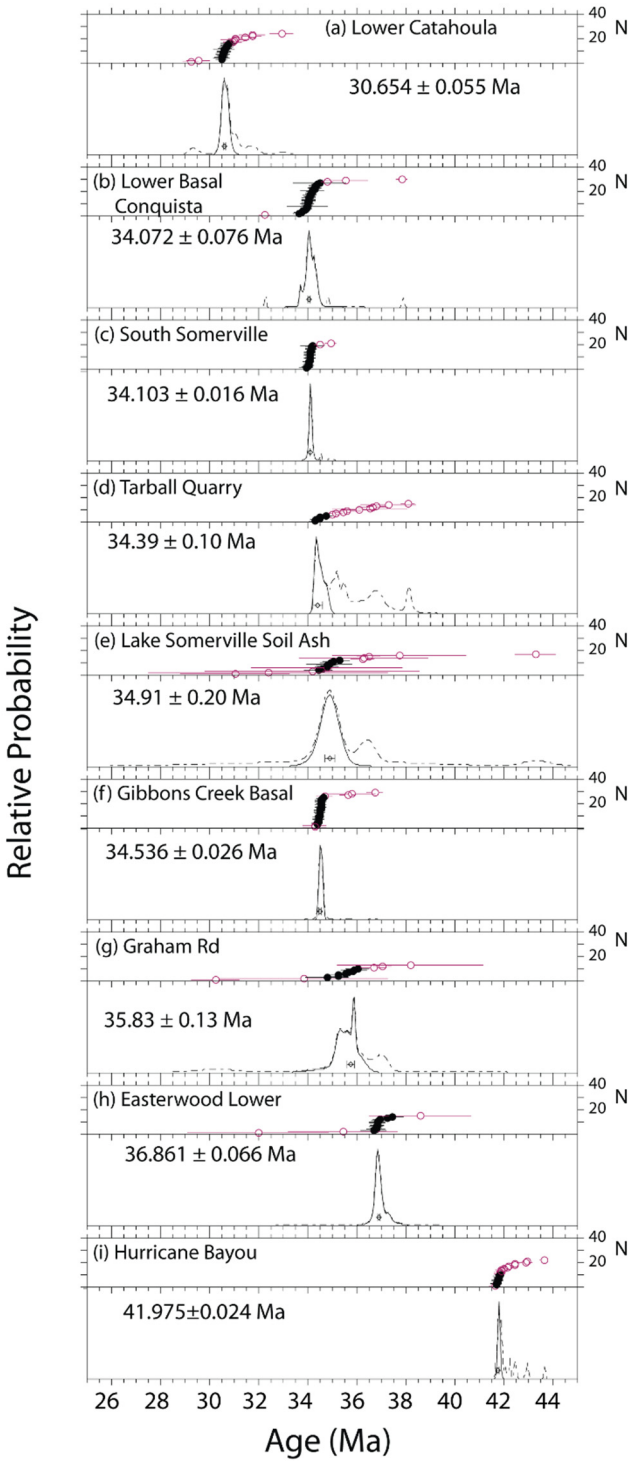

Figure A10. Summary of age probability data presented in stratigraphic order. All samples yield stratigraphically age order with the exception of Lake Somerville Soil Ash.

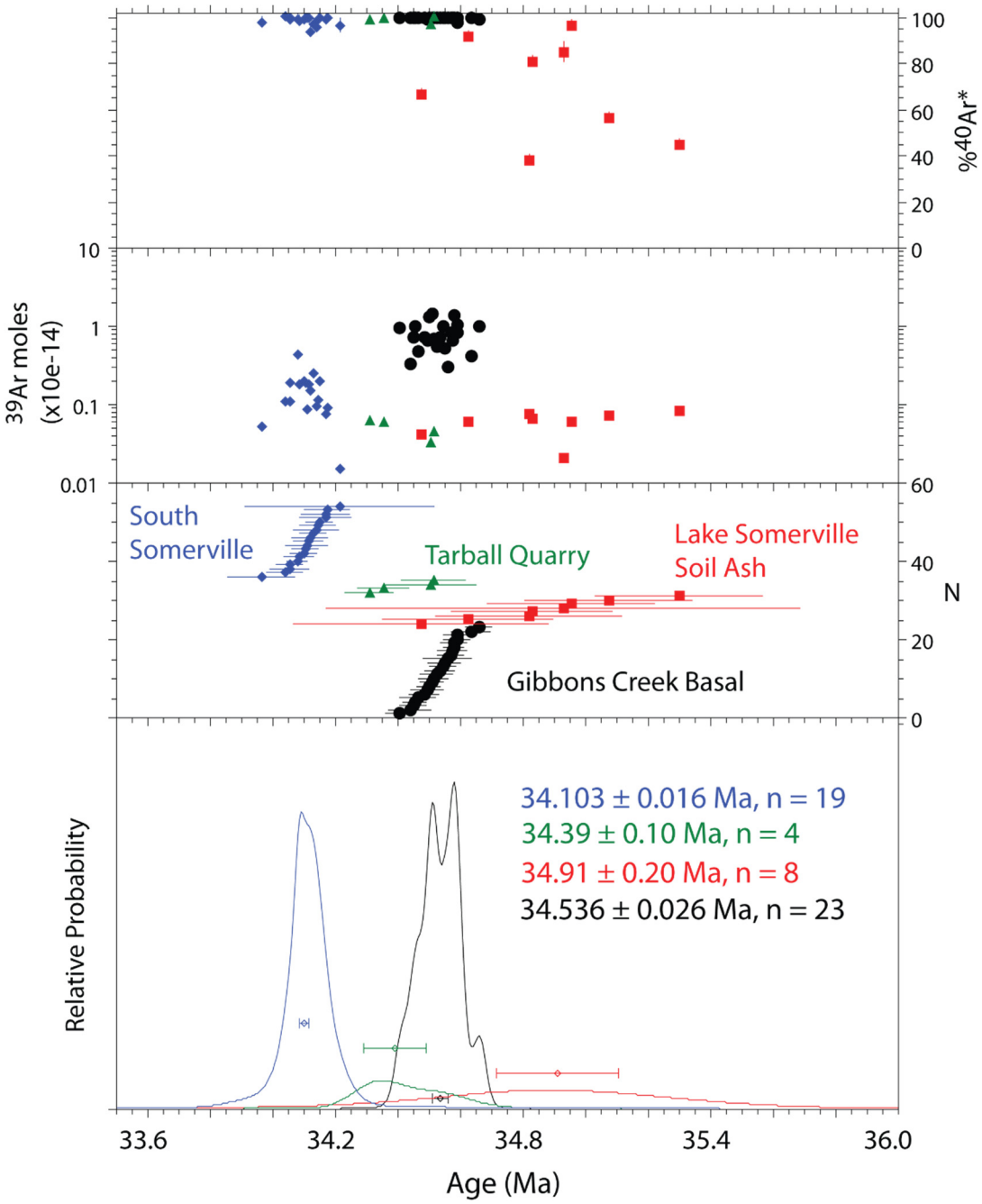

Figure A11. Comparison of age results documenting the complexity of Lake Somerville Soil Ash with respect to stratigraphically similar samples. The Lake Somerville Soil Ash sample is relatively imprecise and significantly less radiogenic. This sample is not ideal for dating and perhaps small systematic errors in overall data corrections contribute to an apparently inaccurate result.

Sample	MSWD	n/n	Age(Ma)	2σ
Catahoula	1.5	17/26	30.65	±0.06
Conquista	11.1	26/29	34.07	±0.08
South Somerville	1.3	19/22	34.10	±0.02
Tarball Quarry	1.4	4/17	34.39	±0.10
Somerville Soil Zone	0.8	8/28	34.91	±0.20
Gibbons Creek	9.0	23/27	34.54	±0.03
Graham Road	2.1	7/11	35.83	±0.13
Easterwood	0.3	10/19	36.86	±0.07
Hurricane Bayou	1.3	9/24	41.79	±0.02

Table A1. Summary table of $^{40}Ar/^{39}Ar$ dating of individual sanidine phenocrysts. n/n = number grains providing preferred age/number of grains dated. MSWD = mean square of weighted deviates. All errors at 2σ and include error in J factor. Error in decay constant not included.

Analytical Methods and Instrumentation

Sample preparation and irradiation:
Light density fraction provided by Mindi Heintz. Sanidine concentrated by heavy liquid and hand-picking. Samples were loaded into machined Al discs and irradiated for 40 hours, USGS TRIGA Reactor, Denver, CO Neutron flux monitor Fish Canyon Tuff sanidine (FC-2). Assigned age = 28.201 Ma (Kuiper et al., 2008). Decay constant 5.463e-10 /a (Min et al., 2000).

Instrumentation:
Thermo-Fisher Scientific ARGUS VI mass spectrometer on line with automated all-metal extraction system.
System = Jan
Multi-collector configuration: 40Ar-H1, 39Ar-Ax, 38Ar-L1, 37Ar-L2, 36Ar-L3
Amplification: H1, L1, L2 all 1E12 Ohm Faraday, AX 1E13 Ohm Faraday, L3 - CDD ion counter, deadtime 14 nS.
Laser single crystal total fusion.
Samples fused for 30 seconds at 4 W using a 75W Photon-Machines CO2 laser.
Reactive gases removed by 60 second reaction with 1 SAES NP-10 getter operated at 1.6 A.

Analytical parameters:
Mass spectrometer sensitivity = 5E-17 mol/fA
Typical total system blank and background: 5±2%, 0.08±20%, 0.04±30%, 0.10±15%, 0.02±5%, x 10-17 moles for masses 40, 39, 38, 37, 36, respectively.
J-factors determined to a precision of ~± 0.01% by CO2 laser-fusion of 6 single crystals from each of 13 radial positions around the irradiation tray.
Correction factors for interfering nuclear reactions were determined using K-glass and CaF2 and are as follows:
(40Ar/39Ar)K = 0.0072±0.00002; (36Ar/37Ar)Ca = 0.0002724±0.0000002; and (39Ar/37Ar)Ca = 0.000690±0.000002.

	ID	$^{40}Ar/^{39}Ar$	$^{37}Ar/^{39}Ar$	$^{36}Ar/^{39}Ar$ (x 10^{-3})	$^{39}Ar_K$ (x 10^{-15} mol)	K/Ca	$^{40}Ar^*$ (%)	Age (Ma)	±1σ (Ma)
Lower Catahoula, sanidine J=0.0092432±0.00%, IC=1.05±0.001, NM-258B, Lab#=61715									
x	21	2.002	-0.0134	0.8432	0.456	-	87.5	29.29	0.15
x	28	2.016	0.0064	0.8380	0.209	79.3	87.7	29.56	0.32
	03	2.281	0.0656	1.562	0.981	7.8	79.9	30.504	0.090
	14	1.884	0.0276	0.2010	0.538	18.5	97.0	30.53	0.12
	25	1.851	0.0127	0.0830	1.070	40.1	98.7	30.544	0.061
	26	1.864	0.0012	0.1230	0.710	434	98.0	30.550	0.095
	24	1.855	0.0332	0.1003	0.463	15.3	98.5	30.55	0.14
	19	1.851	0.0274	0.0757	0.884	18.6	98.9	30.594	0.075
	06	1.869	-0.0042	0.1260	0.635	-	98.0	30.613	0.100
	17	1.848	0.0068	0.0565	0.688	75.2	99.1	30.616	0.094
	02	1.957	0.0018	0.4174	0.306	287	93.7	30.65	0.21
	23	1.883	0.0061	0.1601	0.909	83.0	97.5	30.684	0.077
	04	1.865	0.0039	0.0934	0.538	129.3	98.5	30.70	0.11
	11	1.868	0.0229	0.1004	1.367	22.3	98.5	30.746	0.050
	27	1.988	0.0305	0.5060	0.943	16.7	92.6	30.770	0.081
	12	1.895	0.0278	0.1787	0.478	18.4	97.3	30.83	0.13
	22	2.185	0.0250	1.127	0.344	20.4	84.8	30.99	0.21
	20	1.903	-0.0039	0.1506	0.288	-	97.6	31.04	0.22
	09	1.908	0.0304	0.1740	0.154	16.8	97.4	31.06	0.42
x	18	1.957	0.0161	0.3359	0.849	31.6	95.0	31.068	0.083
x	15	3.052	0.0274	3.962	0.349	18.7	61.6	31.47	0.25
x	16	2.013	0.0578	0.3899	0.392	8.8	94.5	31.78	0.17
x	07	1.985	0.0433	0.2912	0.183	11.8	95.8	31.80	0.34
x	01	2.079	-0.0055	0.3539	0.209	-	94.9	32.99	0.30
x	05	4.489	0.0007	0.0428	0.785	759	99.7	74.10	0.33
x	08	29.35	-0.0052	0.1789	0.845	-	99.8	438.5	1.3
	Mean age ± 2 σ		n=17	MSWD=1.48		80 ±229		30.654	0.055

Table A2. $^{40}Ar/^{39}Ar$ analytical data.

Notes:

Isotopic ratios corrected for blank, radioactive decay, and mass discrimination, not corrected for interfering reactions.

Errors quoted for individual analyses include analytical error only, without interfering reaction or J uncertainties.

Mean age is weighted mean age of Taylor (1982). Mean age error is weighted error of the mean (Taylor, 1982), multiplied by the root of the MSWD where MSWD>1, and also incorporates uncertainty in J factors and irradiation correction uncertainties.

Isotopic abundances after Steiger and Jäger (1977).

Decay constants after Min et al.

x preceding sample ID denotes analyses excluded from mean age calculations.

Ages calculated relative to FC-2 Fish Canyon Tuff sanidine interlaboratory standard at 28.201 Ma

Decay Constant (LambdaK (total)) = 5.543e-10/a

Correction factors:

$(^{39}Ar/^{37}Ar)_{Ca}$ = 0.00069 ± 2e-06

$(^{36}Ar/^{37}Ar)_{Ca}$ = 0.0002724 ± 0

$(^{38}Ar/^{39}Ar)_{K}$ = 0.01077

$(^{40}Ar/^{39}Ar)_{K}$ = 0.0072 ± 2e-05

	ID	$^{40}Ar/^{39}Ar$	$^{37}Ar/^{39}Ar$	$^{36}Ar/^{39}Ar$ (x 10^{-3})	$^{39}Ar_K$ (x 10^{-15} mol)	K/Ca	$^{40}Ar^*$ (%)	Age (Ma)	±1σ (Ma)
	Lower Basal Conquista, sanidine, J=0.0091748±0.00%, IC=1.05±0.001, NM-258B, Lab#=61710								
	25	2.041	0.0284	0.0386	1.922	17.9	99.6	33.698	0.035
	27	2.081	0.0181	0.1567	0.612	28.2	97.8	33.77	0.10
	09	2.047	0.0168	0.0342	1.017	30.4	99.6	33.803	0.067
	08	2.054	0.0139	0.0353	1.431	36.8	99.5	33.911	0.048
	03	2.055	0.0187	0.0289	1.042	27.3	99.7	33.957	0.066
	04	2.056	0.0158	0.0240	1.774	32.3	99.7	33.998	0.038
	15	2.128	0.5318	0.4067	0.099	0.96	96.3	34.02	0.65
	16	2.064	0.0097	0.0423	1.377	52.4	99.4	34.032	0.049
	19	2.058	0.0142	0.0213	0.745	35.8	99.7	34.037	0.085
	07	2.057	0.0132	0.0161	1.695	38.8	99.8	34.040	0.040
	18	2.058	0.0031	0.0104	0.780	163.6	99.9	34.078	0.082
	05	2.068	0.0562	0.0583	0.884	9.1	99.4	34.081	0.080
	29	2.062	0.0178	0.0231	0.861	28.7	99.7	34.093	0.073
	20	2.060	0.0154	0.0158	0.861	33.2	99.8	34.097	0.076
	30	2.110	0.0484	0.1932	0.973	10.5	97.5	34.108	0.068
	11	2.063	0.0249	0.0212	0.826	20.5	99.8	34.139	0.081
	24	2.064	0.0206	0.0175	0.721	24.8	99.8	34.156	0.089
	06	2.075	0.0101	0.0494	1.352	50.3	99.3	34.178	0.052
	14	2.071	0.0140	0.0249	2.524	36.5	99.7	34.242	0.027
	23	2.070	0.5017	0.1525	0.251	1.0	99.8	34.25	0.26
	01	2.078	0.0119	0.0311	1.023	42.8	99.6	34.317	0.067
	13	2.101	0.0130	0.1099	0.786	39.2	98.5	34.318	0.084
	10	2.074	0.0155	0.0173	1.409	33.0	99.8	34.323	0.048
	02	2.082	0.0242	0.0389	0.795	21.1	99.5	34.365	0.088
	21	2.095	0.0186	0.0731	0.649	27.5	99.0	34.401	0.099
	22	2.209	0.6611	0.6102	0.071	0.77	94.2	34.53	0.89
x	28	2.104	0.0092	0.0146	1.213	55.2	99.8	34.818	0.054
x	17	2.157	1.774	0.5294	0.087	0.29	99.4	35.58	0.75
x	26	2.292	0.0161	0.0214	1.167	31.7	99.8	37.891	0.056
	Mean age ± 2 σ	n=26	MSWD=11.08		32.4	±60.4		34.072	0.076

Table A2 Continued

	ID	$^{40}Ar/^{39}Ar$	$^{37}Ar/^{39}Ar$	$^{36}Ar/^{39}Ar$ (x 10^{-3})	$^{39}Ar_K$ (x 10^{-15} mol)	K/Ca	$^{40}Ar^*$ (%)	Age (Ma)	±1σ (Ma)
	South Somerville, sanidine, J=0.0091943±0.00%, IC=1.05±0.001, NM-258B, Lab#=61712								
	08	2.089	0.3751	0.2545	0.522	1.4	97.8	33.969	0.091
	06	2.049	0.0162	0.0051	1.068	31.5	100.0	34.042	0.041
	05	2.076	0.1681	0.1349	1.053	3.0	98.7	34.058	0.047
	22	2.061	0.0201	0.0439	1.896	25.4	99.5	34.059	0.023
	21	2.076	0.0183	0.0891	4.335	27.8	98.8	34.084	0.013
	15	2.090	0.0191	0.1347	1.803	26.7	98.2	34.087	0.028
	10	2.070	0.0145	0.0625	1.975	35.1	99.2	34.105	0.025
	04	2.060	0.0231	0.0318	1.889	22.1	99.6	34.107	0.026
	18	2.057	0.0228	0.0197	0.833	22.4	99.8	34.112	0.053
	14	2.063	0.0399	0.0449	1.809	12.8	99.5	34.120	0.027
	19	2.199	0.0542	0.5061	1.503	9.4	93.4	34.123	0.040
	13	2.125	0.0199	0.2454	2.472	25.7	96.7	34.131	0.024
	02	2.150	0.0431	0.3324	0.923	11.8	95.6	34.141	0.058
	12	2.078	0.0510	0.0905	1.125	10.0	98.9	34.147	0.041
	09	2.064	0.0307	0.0373	1.938	16.6	99.6	34.154	0.024
	01	2.072	0.0254	0.0599	0.741	20.1	99.2	34.171	0.064
	11	2.080	0.0864	0.1038	0.745	5.9	98.9	34.171	0.061
	07	2.068	0.0303	0.0438	0.873	16.8	99.5	34.179	0.052
	17	2.134	0.0230	0.2586	0.149	22.2	96.5	34.22	0.29
x	20	2.135	0.0189	0.1960	2.072	27.0	97.4	34.531	0.027
x	16	2.262	0.0535	0.5495	0.667	9.5	93.0	34.955	0.084
x	03	3.265	-0.0097	0.2122	0.296	-	98.0	52.99	0.16
	Mean age ± 2 σ		n=19	MSWD=1.34		18.3 ±19.3		34.103	0.016

Table A2 Continued

	ID	$^{40}Ar/^{39}Ar$	$^{37}Ar/^{39}Ar$	$^{36}Ar/^{39}Ar$ (x 10^{-3})	$^{39}Ar_K$ (x 10^{-15} mol)	K/Ca	$^{40}Ar^*$ (%)	Age (Ma)	±1σ (Ma)
	Tarball Quarry, sanidine J=0.0092039±0.00%, IC=1.05±0.001, NM-258B, Lab#=61720								
	04	2.091	0.0232	0.1008	0.606	22.0	98.7	34.311	0.072
	12	2.069	0.0059	0.0142	0.590	85.9	99.8	34.357	0.074
	15	2.142	-0.0093	0.2255	0.327	-	96.8	34.51	0.14
	16	2.075	0.0119	0.0018	0.448	42.9	100.0	34.519	0.092
x	13	2.093	0.0161	0.0126	0.461	31.7	99.9	34.77	0.10
x	02	2.145	0.0133	0.1376	0.561	38.3	98.1	35.016	0.086
x	03	2.240	0.0002	0.4172	0.713	2086	94.5	35.195	0.070
x	19	2.181	0.1999	0.2199	0.392	2.6	97.7	35.46	0.10
x	07	2.514	0.0280	1.261	0.119	18.2	85.2	35.65	0.40
x	05	2.369	1.396	1.052	0.083	0.37	91.6	36.13	0.52
x	20	2.328	0.4240	0.5504	0.032	1.2	94.4	36.6	1.3
x	10	2.235	1.474	0.5019	0.103	0.35	98.7	36.70	0.42
x	14	2.208	0.0011	-0.0212	0.212	471	100.3	36.81	0.21
x	08	2.456	1.941	1.248	0.047	0.26	91.3	37.34	0.91
x	01	2.317	0.0777	0.1007	0.529	6.6	99.0	38.120	0.097
x	17	3.166	0.6762	1.252	0.058	0.75	90.0	47.32	0.77
x	18	21.65	4.233	63.82	0.014	0.12	14.4	52.0	4.2
	Mean age ± 2 σ	n=4	MSWD=1.37		50.3	±56.5		34.39	0.10

Table A2 Continued

	ID	$^{40}Ar/^{39}Ar$	$^{37}Ar/^{39}Ar$	$^{36}Ar/^{39}Ar$ (x 10^{-3})	$^{39}Ar_K$ (x 10^{-15} mol)	K/Ca	$^{40}Ar^*$ (%)	Age (Ma)	±1σ (Ma)
	Lake Somerville, sanidine J=0.009222±0.00%, IC=1.05±0.001, NM-258B, Lab#=61719								
x	19	27.14	-0.0036	85.53	0.104	-	6.8	31.1	2.1
x	30	66.80	0.0512	219.5	0.047	10.0	2.9	32.4	4.7
x	13	72.08	0.0773	237.0	0.064	6.6	2.8	34.2	4.2
	29	3.115	0.0031	3.541	0.409	166	66.3	34.48	0.39
	02	2.267	0.0062	0.6416	0.599	82.4	91.6	34.63	0.25
x	32	38.32	0.0876	122.6	0.076	5.8	5.4	34.8	2.9
	27	5.485	0.0310	11.50	0.737	16.4	38.0	34.82	0.28
	35	2.585	0.0135	1.676	0.642	37.9	80.8	34.83	0.24
	33	2.466	0.0377	1.261	0.200	13.5	85.0	34.93	0.74
	36	2.187	0.0166	0.3058	0.592	30.7	95.9	34.96	0.25
	21	3.757	0.0101	5.593	0.693	50.4	55.9	35.08	0.25
	20	4.731	0.0172	8.844	0.823	29.7	44.7	35.30	0.25
x	34	4.172	0.0686	6.769	0.558	7.4	52.1	36.27	0.32
x	18	27.88	-0.0092	86.97	0.085	-	7.8	36.3	2.4
x	23	2.251	0.0370	0.2062	0.531	13.8	97.4	36.54	0.28
x	17	39.35	0.0995	125.5	0.104	5.1	5.7	37.8	2.5
x	06	7.157	0.1510	15.44	0.293	3.4	36.3	43.35	0.61
x	25	11.65	1.283	27.46	0.040	0.40	31.2	60.4	7.4
x	14	6.966	0.0722	8.871	0.668	7.1	62.4	71.89	0.93
x	05	63.68	0.3212	200.0	0.046	1.6	7.2	76	13
x	01	237.8	-0.3326	786.0	0.019	-	2.3	91	44
x	22	29.41	-1.8415	74.80	0.015	-	24.3	117	49
x	04	8.602	0.0425	3.011	0.773	12.0	89.7	125.72	0.61
x	03	11.64	0.0410	9.799	0.529	12.4	75.1	141.9	1.3
x	24	70.96	0.0246	0.1990	0.645	20.7	99.9	920.9	3.6
x	26	71.51	-0.0192	1.030	1.479	-	99.6	923.9	1.5
x	15	76.57	-0.0053	0.1085	1.772	-	100.0	977.5	1.8
x	31	85.99	-0.0072	23.92	0.347	-	91.8	1000.9	6.9
	Mean age ± 2 σ		n=8	MSWD=0.81		53.3 ±100.6		34.91	0.20

Table A2 Continued

	ID	$^{40}Ar/^{39}Ar$	$^{37}Ar/^{39}Ar$	$^{36}Ar/^{39}Ar$ (x 10^{-3})	$^{39}Ar_K$ (x 10^{-15} mol)	K/Ca	$^{40}Ar^*$ (%)	Age (Ma)	±1 σ (Ma)
	Gibbons Creek Basal, coarse sanidine J=0.0092479±0.00%, IC=1.05±0.001, NM-258B, Lab#=61717								
	01	2.063	0.0099	0.0167	9.248	51.7	99.8	34.408	0.019
	26	2.066	0.0085	0.0214	3.186	59.8	99.7	34.441	0.049
	04	2.072	0.0108	0.0385	7.114	47.3	99.5	34.451	0.024
	09	2.068	0.0144	0.0245	9.618	35.5	99.7	34.455	0.018
	12	2.067	0.0147	0.0173	4.597	34.7	99.8	34.470	0.035
	11	2.066	0.0113	0.0115	6.940	45.0	99.9	34.487	0.024
	24	2.084	0.0108	0.0683	6.483	47.2	99.1	34.499	0.026
	10	2.073	0.0108	0.0315	12.871	47.3	99.6	34.502	0.014
	02	2.075	0.0119	0.0371	14.399	42.7	99.5	34.515	0.013
	05	2.067	0.0098	0.0087	6.827	52.0	99.9	34.518	0.024
	27	2.069	0.0087	0.0120	5.316	58.5	99.9	34.525	0.030
	14	2.069	0.0103	0.0116	6.952	49.6	99.9	34.539	0.024
	08	2.071	0.0233	0.0185	9.878	21.9	99.8	34.550	0.017
	20	2.071	0.0180	0.0182	5.191	28.4	99.8	34.551	0.031
	13	2.081	0.0172	0.0472	2.909	29.6	99.4	34.563	0.055
	07	2.081	0.0124	0.0447	8.138	41.2	99.4	34.572	0.021
	18	2.076	0.0092	0.0248	6.376	55.4	99.7	34.576	0.026
	16	2.075	0.0097	0.0222	13.757	52.6	99.7	34.581	0.013
	22	2.072	0.0102	0.0118	7.623	49.9	99.9	34.581	0.021
	06	2.117	0.0162	0.1624	8.221	31.5	97.8	34.592	0.022
	21	2.074	0.0102	0.0173	10.147	50.1	99.8	34.594	0.017
	28	2.077	0.0188	0.0197	4.072	27.1	99.8	34.637	0.039
	25	2.090	0.0110	0.0566	9.569	46.3	99.2	34.662	0.018
x	03	2.202	0.0162	0.4233	0.934	31.4	94.4	34.73	0.17
x	23	2.326	0.0300	0.6583	0.915	17.0	91.7	35.66	0.18
x	30	13.30	0.9302	38.01	0.407	0.55	16.1	35.84	0.78
x	19	2.672	0.0340	1.604	1.121	15.0	82.3	36.77	0.16
	Mean age ± 2 σ		n=23	MSWD=8.95		43.7 ±21.2		34.536	0.026

Table A2 Continued

	ID	$^{40}Ar/^{39}Ar$	$^{37}Ar/^{39}Ar$	$^{36}Ar/^{39}Ar$ (x 10^{-3})	$^{39}Ar_K$ (x 10^{-15} mol)	K/Ca	$^{40}Ar^*$ (%)	Age (Ma)	±1 σ (Ma)
	Graham Rd, sanidine, J=0.0092118±0.00%, IC=1.05±0.001, NM-258B, Lab#=61713								
x	02	13.89	0.0739	40.89	0.215	6.9	13.0	30.25	0.82
	16	2.817	0.1190	2.486	0.105	4.3	74.2	34.81	0.70
	14	2.224	0.1107	0.3850	0.303	4.6	95.3	35.27	0.23
	18	2.524	0.3061	1.396	0.417	1.7	84.6	35.56	0.20
	19	2.427	0.1084	0.9912	0.436	4.7	88.3	35.67	0.18
	01	2.238	0.0881	0.3019	1.592	5.8	96.3	35.883	0.052
	07	2.136	0.0559	-0.0609	0.212	9.1	101.0	35.92	0.33
	03	2.177	0.1050	0.0560	0.266	4.9	99.6	36.09	0.28
x	11	2.738	0.1083	1.826	0.233	4.7	80.6	36.73	0.33
x	08	2.716	-0.0080	1.649	0.356	-	82.0	37.06	0.23
x	10	12.59	0.3701	32.48	0.017	1.4	24.0	50.2	4.7
	Mean age ± 2 σ	n=7	MSWD=2.07		5.0	±4.4		35.83	0.13

Table A2 Continued

	ID	$^{40}Ar/^{39}Ar$	$^{37}Ar/^{39}Ar$	$^{36}Ar/^{39}Ar$ (x 10^{-3})	$^{39}Ar_K$ (x 10^{-15} mol)	K/Ca	$^{40}Ar^*$ (%)	Age (Ma)	±1 σ (Ma)
	Easterwood Lower, sanidine J=0.0092295±0.00%, IC=1.05±0.001, NM-258B, Lab#=61714								
	25	2.272	0.0214	0.2403	0.388	23.9	96.9	36.72	0.35
	05	2.248	0.0151	0.1395	0.566	33.7	98.2	36.81	0.20
	11	2.222	0.0166	0.0507	1.468	30.8	99.4	36.816	0.065
	08	2.228	0.0061	0.0614	1.413	83.3	99.2	36.844	0.072
	20	2.244	0.0107	0.1150	1.032	47.9	98.5	36.85	0.11
	17	2.237	0.0088	0.0914	1.008	57.9	98.8	36.859	0.099
	23	2.232	0.0143	0.0665	0.897	35.8	99.2	36.89	0.14
	21	2.216	0.0099	0.0101	1.023	51.3	99.9	36.90	0.11
	10	2.259	0.0099	0.1532	0.695	51.7	98.0	36.91	0.14
	09	2.237	0.0175	0.0700	0.954	29.1	99.1	36.98	0.10
x	14	2.271	0.0140	0.1186	0.901	36.5	98.5	37.29	0.11
x	19	2.318	0.0280	0.2423	0.346	18.3	97.0	37.49	0.30
x	18	2.555	2.488	1.489	0.053	0.21	90.6	38.6	1.9
x	13	3.276	7.209	2.909	0.087	0.071	91.4	50.1	1.2
x	04	10.44	0.0278	0.7890	2.279	18.4	97.8	164.67	0.37
x	07	25.05	5.063	42.17	0.004	0.10	51.9	208	71
x	22	44.39	1.760	57.73	0.003	0.29	61.9	414	64
x	03	57.73	0.0046	0.2116	3.316	111	99.9	781.09	0.71
x	12	67.08	0.4392	6.716	0.022	1.2	97.1	862	69
	Mean age ± 2 σ		n=10	MSWD=0.25		44.5 ±35.6		36.861	0.066

Table A2 Continued

	ID	$^{40}Ar/^{39}Ar$	$^{37}Ar/^{39}Ar$	$^{36}Ar/^{39}Ar$ (x 10^{-3})	$^{39}Ar_K$ (x 10^{-15} mol)	K/Ca	$^{40}Ar^*$ (%)	Age (Ma)	±1 σ (Ma)
	Hurricane Bayou, sanidine J=0.0092498±0.00%, IC=1.05±0.001, NM-258B, Lab#=61716								
x	18	2.502	0.0072	0.0182	1.778	71.1	99.8	41.681	0.026
	23	2.508	0.0046	0.0273	1.468	110	99.7	41.740	0.032
	04	2.508	0.0001	0.0234	0.926	-	99.7	41.747	0.047
	03	2.512	0.0044	0.0336	1.484	116	99.6	41.765	0.031
	06	2.510	0.0052	0.0233	1.693	98.3	99.7	41.781	0.027
	10	2.510	0.0031	0.0214	1.657	166	99.8	41.792	0.028
	09	2.513	0.0039	0.0301	1.241	131	99.7	41.808	0.036
	21	2.510	0.0027	0.0177	1.722	191	99.8	41.817	0.027
	20	2.510	0.0097	0.0136	1.521	52.6	99.9	41.833	0.030
	17	2.517	0.0041	0.0323	1.260	124	99.6	41.859	0.036
x	07	2.515	0.0081	0.0197	2.564	63.1	99.8	41.885	0.019
x	01	2.521	0.0081	0.0402	1.937	63.1	99.6	41.898	0.024
x	24	2.519	0.0077	0.0275	3.375	66.6	99.7	41.922	0.015
x	05	2.518	0.0072	0.0213	1.186	71.3	99.8	41.932	0.040
x	16	2.542	0.0051	0.0818	1.606	101	99.1	42.038	0.030
x	11	2.567	0.0123	0.1408	0.809	41.5	98.4	42.170	0.056
x	25	2.536	0.0069	0.0175	2.011	73.9	99.8	42.244	0.022
x	13	2.590	0.0035	0.1563	0.989	147	98.2	42.452	0.048
x	14	2.564	0.0115	0.0653	1.329	44.4	99.3	42.478	0.035
x	02	2.598	0.0033	0.0888	0.441	156	99.0	42.927	0.096
x	19	2.578	0.0048	0.0126	1.502	107	99.9	42.956	0.032
x	12	2.627	0.0182	0.0399	1.894	28.0	99.6	43.663	0.026
x	15	2.812	0.0032	0.0567	0.840	159	99.4	46.619	0.055
x	22	4.441	0.0176	0.3139	0.205	29.0	97.9	72.09	0.23
	Mean age ± 2 σ	n=9	MSWD=1.34		123.6 ±79.0			41.795	0.024

Table A2 Continued